NON-PERTURBATIVE METHODS: HQET AND LATTICE GAUGE THEORY

A Dissertation

Presented to the Faculty of the Graduate School

of Cornell University

in Partial Fulfillment of the Requirements for the Degree of

Doctor of Philosophy

by

William C. Dimm

May 1995

NON-PERTURBATIVE METHODS:

HQET AND LATTICE GAUGE THEORY

William C. Dimm, Ph.D.

Cornell University 1995

Although Quantum Chromodynamics (QCD) is considered to be the correct description of the strong interaction it is difficult to extract predictions for many processes from the theory because perturbation theory often cannot be applied. In this dissertation two approaches for extracting non-perturbatives predictions from QCD are used. The Heavy Quark Effective Theory (HQET) is combined with chiral symmetry to make predictions for the decays $\bar{B} \to (D, D^*)\pi\ell\bar{\nu}$. It is found that the branching ratio for $\bar{B} \to D\pi\ell\bar{\nu}$ is about $(0.5 - 1)\%$. The branching ratio for $\bar{B} \to D^*\pi\ell\bar{\nu}$ is found to be about $10^{-4} - 10^{-5}$ but this does not include possible contributions from diagrams involving an intermediate D^{**}. The second approach is lattice gauge theory. Here, the connection between Monte Carlo results and lattice perturbation theory is examined. It is shown that 2-loop perturbative coefficients for the quark mass renormalization can be extracted from Monte Carlo data for both Wilson and NRQCD quarks. Such a procedure is important for understanding the relationship between bare lattice parameters and the physical parameter values which determine the meaning of a simulation. Understanding such relationships is crucial to the program of constructing improved lattice actions which allow efficient computation of non-perturbative physical quantities.

BIOGRAPHICAL SKETCH

William C. Dimm was born on April 27, 1969. He entered Lehigh University in the Fall of 1987 and completed a B.S. in Engineering Physics in the Fall of 1989. He worked at the Intense Pulsed Neutron Source Division of Argonne National Lab during the Spring and Summer of 1990 before entering Cornell University in the Fall of 1990. He received his master's degree in 1993 and his Ph.D. in Theoretical Physics in May of 1995 from Cornell University.

ACKNOWLEDGMENTS

I would like to thank Tung-Mow Yan and G. Peter Lepage for the opportunity to learn from them and for their patience. I would also like to express my appreciation for the financial support of the Cornell Physics Department and the National Science Foundation through the LNS theory grant. I am grateful for the interactions that I have had with the other graduate students at Cornell including Lisa Angelos, Costas Efthimiou, Janet Finch, Yakov Kanter, Craig Keller, Patrick LaBelle, Greg Mahlon, Lev Nayvelt, Makiko Nio, Ragu Raghavan, Cliff Richardson, Thomas Roos, Mark Scheel, and Todd Ward. I would also like to thank Pam Morehouse for her help.

I would like to express my gratitude to Jerome Licini for his guidance in my undergraduate research. Finally, I would like to thank my mother and brother for their support.

TABLE OF CONTENTS

LIST OF TABLES

LIST OF FIGURES

1 HQET and Chiral Symmetry – Introduction

While the perturbative (in the coupling constant) predictions of Quantum Chromodynamics (QCD) agree well with experiment, there is a large class of experimental quantities where perturbation theory cannot be applied. To test QCD in such circumstances, other methods must be used in order to extract predictions from the theory. One such approach is to write down the most general effective theory applicable to a problem and then use the symmetries of QCD to remove some of the parameters from the effective theory. Some unknown parameters will be left in such a theory, but once they are measured in a particular experiment, they can be used to make predictions about other experiments. One example of such an approach is the Heavy Quark Effective Theory (HQET) which makes predictions for processes involving hadrons containing a single heavy quark ($m_Q \gg \Lambda_{\rm QCD}$). Another example is chiral symmetry which makes predictions for processes involving light quarks ($m_q \ll \Lambda_{\rm QCD}$) at low energies. Heavy quark symmetry and chiral symmetry can be combined to give predictions for decays such as $\bar{B} \to D\pi\ell\bar{\nu}$ and $\bar{B} \to D^*\pi\ell\bar{\nu}$. In this dissertation, we study the predictions for these decays.

2 Heavy Quark Effective Theory

2.1 Intuitive Picture

To see how simplifications arise when dealing with hadrons containing a single heavy quark (c,b,t), consider a simpler system – the hydrogen atom. Since the proton in the hydrogen atom is so much heavier than the electron, the momenta exchanged between the two due to their interactions will not significantly affect the velocity of the proton. The velocity of the proton is very nearly equal to the velocity of the hydrogen atom. In the rest frame of the atom, the electron moves as if the proton is a static source of the electric field. If we increase the mass of the nucleus (by adding a neutron, for example), the wavefunction for the electron is almost completely unchanged in the rest frame of the atom. This is because the nucleus is nearly stationary so the electron isn't sensitive to the dynamics of the nucleus – it only sees the electric charge. In the hydrogen atom, the spin of the proton only arises in the hyperfine splitting, i.e. at $\mathcal{O}(1/m_P)$, so the wavefunction of the electron is nearly independent of the spin of the proton and the spin of the proton is nearly conserved.

Hadrons containing a single heavy quark are very similar to the hydrogen atom. Typical strong interactions involve momentum transfers of order $\Lambda_{\rm QCD}$ between the heavy and light quarks. If $m_Q \gg \Lambda_{\rm QCD}$ these interactions will have very little affect on the heavy quark's velocity. The hadron moves with nearly the same velocity as the heavy quark, and the light quark(s) see the heavy quark as a static source of the color field. The light quark is not sensitive to the mass of the heavy quark (as long as it is large) or its spin. In scattering or decay processes, it will be the change in 4-velocity of the hadron that is relevant (rather than the momentum) since the light quark is only sensitive to the change in the reference frame that contains the static color source.

We can simplify the Feynman rules for a heavy quark as follows. We write the momentum of the heavy quark as

$$p_\mu = m_Q v_\mu + k_\mu \tag{1}$$

where v is the velocity of the hadron and k is the "residual momentum" which is of order $\Lambda_{\rm QCD}$. Now look at the heavy quark propagator:

$$i\frac{\not p + m_Q}{p^2 - m_Q^2} = i\frac{m_Q \not v + \not k + m_Q}{2m_Q v\cdot k + k^2} = \frac{\not v + 1}{2}\frac{i}{v\cdot k} + \mathcal{O}(k/m_Q). \tag{2}$$

To see how the QCD vertex $-ig\gamma_\mu T^C$ behaves between heavy quark propagators, we look at

$$\frac{\not v + 1}{2}\gamma_\mu \frac{\not v + 1}{2}. \tag{3}$$

Using $(\not v + 1)\not v = 1 + \not v$, we see that we can insert factors of $\not v$ between the propagators without changing anything, so we can write (3) as:

$$\frac{\not v + 1}{2}\left[\frac{\not v \gamma_\mu + \gamma_\mu \not v}{2}\right]\frac{\not v + 1}{2}. \tag{4}$$

The quantity in brackets is just the anticommutator $\{\not v, \gamma_\mu\}/2$ which is equal to v_μ. So for low momentum QCD interactions we have the effective Feynman rules for heavy quarks:

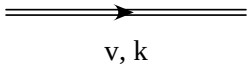

$$= \frac{\not v + 1}{2}\frac{i}{v\cdot k} \tag{5}$$

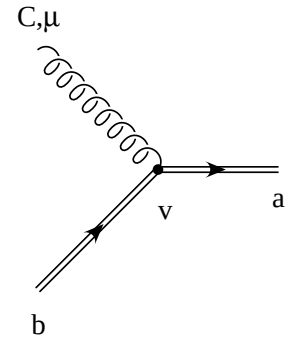

$$= -igv_\mu T^C_{ab} \tag{6}$$

Since there are no gamma matrices in the vertex, the heavy quark spin is unaffected by low momentum gluon interactions. This tells us that the heavy quark spin is a good quantum number (i.e. it is approximately conserved). Since the total angular momentum of a hadron is also a good quantum number, the total angular momentum of the light degrees of freedom in the hadron must also be a good quantum number (by "light degrees of freedom" we mean light quarks, gluons, etc. – often referred to as "brown muck").

The HQET formalism was created by Isgur and Wise [1] in 1989 based on ideas which had been known to several people for some time. Several good reviews of the subject exist, such as [2, 3, 4].

2.2 Matrix Elements

Now we examine the implications of heavy quark symmetry for the calculation of the matrix elements involved in heavy hadron decays. First we note that the operator which measures the heavy quark's spin in its rest frame can be used to connect spin-0 and spin-1 mesons whose light degrees of freedom have zero orbital angular momentum:

$$|P_Q\rangle = \frac{1}{\sqrt{2}}\left[|\Uparrow\downarrow\rangle - |\Downarrow\uparrow\rangle\right], \quad J = 0, \tag{7}$$

$$|P_Q^*\rangle = \frac{1}{\sqrt{2}}\left[|\Uparrow\downarrow\rangle + |\Downarrow\uparrow\rangle\right], \quad J = 1, J_z = 0, \tag{8}$$

$$S_z^Q|P_Q\rangle = \frac{1}{2}|P_Q^*\rangle, \tag{9}$$

where the last equation arises because S_z^Q acting on a state with a $\Downarrow$ gives a $-1/2$ causing the sign of the second term to flip. Note that we needed heavy quark symmetry in this procedure to tell us that the spins of the heavy and light degrees of freedom were good quantum numbers. Relation (9) combined with the commutation relations between various currents (evaluated at the origin)

and S_z^Q allows us to relate matrix elements. For example,

$$\begin{aligned}\langle 0|A^0(0)|P\rangle &= 2\langle 0|A^0(0)S_z^Q|P^*\rangle \\ &= 2\langle 0|\left[A^0(0),S_z^Q\right]|P^*\rangle \\ &= \langle 0|V^3(0)|P^*\rangle. \end{aligned} \tag{10}$$

One can write down the most general expressions allowed by parity and the Lorentz structure for vector and axial-vector current matrix elements between P and P^* states. Then, relationships like the one above allow the form factors which arise to be related to each other. It turns out that the $V-A$ interaction matrix elements responsible for the weak decays:

$$\begin{aligned} P_i &\to P_j + \ell\bar{\nu}, \\ P_i &\to P_j^* + \ell\bar{\nu}, \\ P_i^* &\to P_j + \ell\bar{\nu}, \\ P_i^* &\to P_j^* + \ell\bar{\nu}, \end{aligned} \tag{11}$$

can all be described by a single form factor, $\xi(v\cdot v')$, when heavy quark symmetry is used. Without HQET, 17 independent form factors would be needed. HQET also tells us the normalization of the form factor: $\xi(1)=1$. So, an experiment on a single decay process such as $\bar{B}\to D^*\ell\bar{\nu}$ can determine the decay rates for all of the processes above. Similar relationships arise for baryons which will not be considered here.

To compute matrix elements, we begin by constructing an effective Lagrangian for heavy quark fields. We write the heavy quark field, $Q(x)$, as:

$$Q(x) = e^{-im_Q v\cdot x}\left[h_v(x) + H_v(x)\right] \tag{12}$$

where

$$h_v(x) \equiv e^{im_Q v\cdot x}\frac{1+\not{v}}{2}Q(x), \quad H_v(x) \equiv e^{im_Q v\cdot x}\frac{1-\not{v}}{2}Q(x), \tag{13}$$

which satisfy

$$\not{v} h_v = h_v, \quad \not{v} H_v = -H_v. \tag{14}$$

h_v annihilates a heavy quark with velocity v and H_v creates a heavy antiquark with velocity v. The spatial dependence of $h_v(x)$ gives the residual momentum fluctuations of the field about the case of an on-shell heavy quark with velocity v. The heavy quark part of the QCD Lagrangian in terms of these fields is:

$$\mathcal{L} = \bar{h}_v iv \cdot D h_v - \bar{H}_v (iv \cdot D + 2m_Q) H_v + \bar{h}_v i\not{D}_\perp H_v + \bar{H}_v i\not{D}_\perp h_v, \tag{15}$$

where

$$D^\mu_\perp \equiv D^\mu - v^\mu v \cdot D, \tag{16}$$

and $v \cdot D^\mu_\perp = 0$. In deriving (15) we make use of $\bar{h}_v \not{D}_\perp h_v = \bar{H}_v \not{D}_\perp H_v = 0$ (the proof of this is similar to (4)) and $\bar{h}_v H_v = 0$. We see that the field H_v has mass $2m_Q$ while the h_v field is massless. For large m_Q we can compute matrix elements of the h_v field by integrating out the H_v field to obtain an effective Lagrangian. This was examined in [5] and they found that the resulting non-local action is:

$$S_{\text{eff}} = \int d^4x \mathcal{L}_{\text{eff}} - \frac{1}{2} \text{Tr} \left\{ \ln(iv \cdot D + 2m_Q - i\epsilon) \right\} \tag{17}$$

where $\mathcal{L}_{\text{eff}}$ is the Lagrangian that one gets classically from the equation of motion. The extra term in the action can be shown [5, 6] to be an irrelevant constant in axial gauge: $v \cdot A = 0$. Now we compute $\mathcal{L}_{\text{eff}}$ starting with the equation of motion $(i\not{D} - m_Q)Q = 0$ which gives:

$$i\not{D} h_v + (i\not{D} - 2m_Q) H_v = 0. \tag{18}$$

If we multiply this by $\not{v}$ and make use of (14) along with $\not{v}\not{D} H_v = (\not{D} + 2v \cdot D) H_v$, we get:

$$i\not{v}\not{D} h_v + i(\not{D} + 2v \cdot D) H_v + 2m_Q H_v = 0. \tag{19}$$

Subtracting (18) from this and using $(\not{v}\not{D} - \not{D})h_v = -2\not{D}_\perp h_v$ gives

$$-2i\not{D}_\perp h_v + (2iv \cdot D + 4m_Q)H_v = 0. \tag{20}$$

Finally, we have

$$H_v = \frac{1}{iv \cdot D + 2m_Q - i\epsilon} i\not{D}_\perp h_v \tag{21}$$

for the classical relationship between the fields. Notice that the H part of the Q field is suppressed by a factor of $1/m_Q$ relative to the h part of the field. We can plug this into (15) to compute the $\mathcal{L}_{\text{eff}}$ which appears in (17) as an expansion in $1/m_Q$. We get:

$$\mathcal{L}_{\text{eff}} = \bar{h}_v iv \cdot D h_v + \frac{1}{2m_Q} \bar{h}_v \left[\frac{g}{2} \sigma_{\mu\nu} F^{\mu\nu} - D_\perp^2 \right] h_v + \mathcal{O}(1/m_Q^2), \tag{22}$$

where $F^{\mu\nu}$ is the gluon field strength. Notice that the first term in $\mathcal{L}_{\text{eff}}$ gives the Feynman rules (5) and (6) which we found earlier. In this dissertation we will work to lowest order in $1/m_Q$ and we will deal with tree-level processes. For details on higher order corrections the reader is referred to [2].

To compute rates for weak decays, we are interested in matrix elements of the vector and axial currents evaluated at the origin (the translation properties of the states allow the value at the origin to be related to the value at any point x). We write these currents in terms of the fields above as:

$$V_\mu^{ji}(0) = \bar{h}_{v'}^j(0) \gamma_\mu h_v^i(0) + \mathcal{O}(1/m_Q), \quad A_\mu^{ji}(0) = \bar{h}_{v'}^j(0) \gamma_\mu \gamma_5 h_v^i(0) + \mathcal{O}(1/m_Q) \tag{23}$$

and we neglect the $\mathcal{O}(1/m_Q)$ terms. First we look at the matrix element for the decay of a spin zero meson into another spin zero meson containing a (generally) different heavy quark, $P_i(v) \to P_j(v') + \ell\bar{\nu}$. Note that we parameterize the states by the heavy quark 4-velocity rather than the momentum since velocity is the more natural quantity to use. The most general form for the hadronic matrix

element with the right Lorentz and parity transformation properties is:

$$\langle P_j(v')|V_\mu^{ji}(0)|P_i(v)\rangle/\sqrt{M_{P_j}M_{P_i}} = (v+v')_\mu f_+(v\cdot v') + (v-v')_\mu f_-(v\cdot v'), \quad (24)$$

where f_+ and f_- are scalar form factors and all quantities on the right hand side are dimensionless. From (23) and (14), we know that

$$(v-v')^\mu V_\mu^{ji} = \bar{h}_{v'}^j(\not{v}-\not{v}')h_v^i = 0, \quad (25)$$

and

$$(v+v')^\mu A_\mu^{ji} = \bar{h}_{v'}^j(\not{v}\gamma_5 + \not{v}'\gamma_5)h_v^i = \bar{h}_{v'}^j(-\gamma_5\not{v} + \not{v}'\gamma_5)h_v^i = 0. \quad (26)$$

Applying (25) to (24) gives

$$0 = 2(1-v\cdot v')f_-(v\cdot v') \quad (27)$$

for all v and v'. We conclude that $f_-(v\cdot v') = 0$. The matrix element for the axial current is trivially zero since there is no way to construct a pseudovector from just v and v':

$$\langle P_j(v')|A_\mu^{ji}(0)|P_i(v)\rangle = 0. \quad (28)$$

We can now compute the decay rate for $P_i(v) \to P_j(v') + \ell\bar{\nu}$ in terms of a single form factor $f_+(v\cdot v')$ for all pairs of heavy quarks i and j. We can think of $f_+(v\cdot v')$ as describing the overlap between the light degrees of freedom moving about a heavy quark with velocity v and those moving about a heavy quark with velocity v'.

To find the normalization of $f_+(v\cdot v')$, we note that $J^\mu = \bar{h}_v\gamma^\mu h_v$ is conserved in the effective theory, and it has the associated charge

$$N_Q = \int d^3x J^0(x) = \int d^3x h_v^\dagger(x)h_v(x), \quad (29)$$

which counts the number of heavy quarks Q. If we put N_Q between two identical states we get

$$\langle P(v)|N_Q|P(v)\rangle = \langle P(v)|P(v)\rangle = 2M_P v^0(2\pi)^3\delta^3(\vec{0}). \quad (30)$$

Now we compare this to (24) with $i = j$, $\mu = 0$ and $v' = v$ and we see that $f_+(1) = 1$. It turns out that this same form factor arises in all vector and axial-vector matrix elements between mesons without orbital excitations, so the form factor is "universal", and is normally denoted by $\xi(v \cdot v') \equiv f_+(v \cdot v')$.

In order to relate the form factors for the decays $P_i(v) \to P_j^*(v') + \ell\bar{\nu}$ and $P_i^*(v) \to P_j^*(v') + \ell\bar{\nu}$ to $\xi(v \cdot v')$, we must use the commutation relation between S_z^Q and the currents so we derive it now. We start with the equal time commutation relation:

$$\begin{aligned}\Big[\psi^\dagger(x)\Gamma\psi(x), \psi^\dagger(y)\Gamma'\psi(y)\Big] = \\ \psi^\dagger(x)\Gamma\{\psi(x), \psi^\dagger(y)\}\Gamma'\psi(y) - \psi^\dagger(y)\Gamma'\{\psi(y), \psi^\dagger(x)\}\Gamma\psi(x).\end{aligned} \tag{31}$$

We generically write a current evaluated at the origin as

$$J_\mu^{ji} = \bar{h}_{v'}^j(0)\Gamma_\mu h_v^i(0), \tag{32}$$

where i and j are quark flavors and Γ_μ is some gamma matrix. The spin operator for a heavy quark with flavor Q is given by

$$S_z^Q = \frac{i}{2}\int d^3x h_{v''}^{Q\dagger}(x)\gamma^1\gamma^2 h_{v''}^Q(x). \tag{33}$$

The equal time anti-commutator for $h(x)$ is derived from the canonical anticommutation relation for the $Q(x)$ field and (12) and (21). It is

$$\{h_v(t,\vec{x}), h_{v'}^\dagger(t,\vec{y})\} = \delta^3(\vec{x}-\vec{y})\delta^{v,v'} + \mathcal{O}(1/m_Q). \tag{34}$$

Putting this all together we find

$$\Big[J_\mu^{ji}, S_z^Q\Big] = \frac{i}{2}\bar{h}_v^j(0)\Gamma_\mu\gamma^1\gamma^2 h_v^Q(0)\delta^{iQ}\delta^{v'',v} - \frac{i}{2}\bar{h}_v^Q(0)\gamma^1\gamma^2\Gamma_\mu h_v^i(0)\delta^{jQ}\delta^{v'',v'}. \tag{35}$$

Now we are prepared to relate the matrix elements for $P_i(v) \to P_j^*(v') + \ell\bar{\nu}$ to those for $P_i(v) \to P_j(v') + \ell\bar{\nu}$. The most general form allowed by parity and Lorentz transformation properties is:

$$\langle P_j^*(v',\varepsilon)|V_\mu^{ji}|P_i(v)\rangle/\sqrt{M_{P_j^*}M_{P_i}} = i\epsilon_{\mu\nu\lambda\sigma}\varepsilon^{*\nu}v'^\lambda v^\sigma g(v\cdot v') \tag{36}$$

where ε is the polarization vector for the spin-1 P^* and the form factor g is independent of ε because the right hand side must be linear in ε (recall the form of an amplitude when Feynman rules are used). We look at this matrix element in the frame where the P^* is at rest so $v' = (1, \vec{0})$, $\varepsilon^\nu = (0, 0, 0, 1)$ (zero spin along z-axis), and we take $v^\sigma = (y, \sqrt{y^2-1}, 0, 0)$. The only non-zero matrix element is $\mu = 2$. Using the convention $\epsilon_{0123} = +1$ we have

$$\langle P_j^*(v', \varepsilon)|V_2^{ji}|P_i(v)\rangle / \sqrt{M_{P_j^*} M_{P_i}} = i\sqrt{y^2-1}\, g(y). \tag{37}$$

Now we relate this to a matrix element which we have already computed

$$\begin{aligned} \langle P_j^*(v', \varepsilon)|V_2^{ji}|P_i(v)\rangle &= 2\langle P_j(v')|S_z^j V_2^{ji}|P_i(v)\rangle \\ &= 2\langle P_j(v')|\left[S_z^j, V_2^{ji}\right]|P_i(v)\rangle \\ &= -i\langle P_j(v')|V_1^{ji}|P_i(v)\rangle, \end{aligned} \tag{38}$$

where we have made use of (35). The matrix element on the right hand side was computed before (24) so we have

$$\langle P_j^*(v', \varepsilon)|V_2^{ji}|P_i(v)\rangle = -i\sqrt{M_{P_j} M_{P_i}}(v+v')_1 \xi(v\cdot v') = i\sqrt{M_{P_j} M_{P_i}}\sqrt{y^2-1}\,\xi(y). \tag{39}$$

Comparing this to (37) and noting that $M_{P_j^*} = M_{P_j}$ in the $m_Q \to \infty$ limit, we find that $g(v\cdot v') = \xi(v\cdot v')$. As stated before, the same form factor arises in both $P_i(v) \to P_j^*(v') + \ell\bar{\nu}$ and $P_i(v) \to P_j(v') + \ell\bar{\nu}$. A similar calculation for the axial current again shows that all form factors are functions of $\xi(v\cdot v')$.

2.3 Interpolating Fields

We could continue with the procedure above to determine the $V-A$ matrix elements for $P_i^*(v) \to P_j^*(v') + \ell\bar{\nu}$. Instead, we introduce the method of interpolating fields which makes the calculation of matrix elements more efficient.

The idea is to represent the hadrons by operators which have the right quantum numbers to describe the hadrons. For example, the (properly normalized) interpolating fields which destroy the ground state 0^- and 1^- mesons are:

$$P(v) = \bar{q}_v \gamma_5 h_v \sqrt{M_P}, \quad P^*(v,\varepsilon) = \bar{q}_v \not{\varepsilon} h_v \sqrt{M_{P^*}}, \tag{40}$$

where q_v is a dirac spinor representing the state of the "brown muck" (light quarks and gluons) which has $j = 1/2$. Here we have assumed that the polarization vector ε is real – if it is not we must use its complex conjugate in the equation above. The subscript v on q_v indicates that the spinor describes the dynamics for the "brown muck" moving around a heavy quark that has velocity v – it does not mean that the light quark has velocity v (it does not). q_v is a complicated object which we do not understand beyond its Lorentz transformation properties. The interpolating fields for creating mesons are:

$$P(v)^\dagger = -\sqrt{M_P}\bar{h}_v \gamma_5 q_v, \quad P^*(v,\varepsilon)^\dagger = \sqrt{M_{P^*}}\bar{h}_v \not{\varepsilon} q_v. \tag{41}$$

Interpolating field representations of states with arbitrary spin have been derived in [7]. To examine the formalism, we start by computing the matrix element of a generic current (32) between pseudoscalar states:

$$\langle P_j(v')|J_\mu^{ji}|P_i(v)\rangle = -\sqrt{M_{P_i} M_{P_j}}\langle 0|\bar{q}_{v'}\gamma_5 h^j_{v'}\bar{h}^j_{v'}\Gamma_\mu h^i_v \bar{h}^i_v \gamma_5 q_v|0\rangle. \tag{42}$$

We make the replacement

$$h^i_v \bar{h}^i_v \to \frac{\not{v}+1}{2} \tag{43}$$

and we get

$$\langle P_j(v')|J_\mu^{ji}|P_i(v)\rangle = \sqrt{M_{P_i} M_{P_j}}\mathrm{Tr}\left\{\gamma_5 \frac{\not{v}'+1}{2}\Gamma_\mu \frac{\not{v}+1}{2}\gamma_5 \mathcal{M}\right\}, \tag{44}$$

where

$$\mathcal{M} = \langle 0|q_v \bar{q}_{v'}|0\rangle = A + B\not{v} + C\not{v}' + D\not{v}\not{v}' \tag{45}$$

with the last equality given by the Lorentz structure of the matrix element and the fact that we can't write down any more terms since $\not{v}\not{v} = 1$. Given the cyclic property of the trace, and $(\not{v}+1)\gamma_5\not{v} = -\gamma_5(\not{v}+1)$ and $\not{v}'\gamma_5(\not{v}'+1) = -\gamma_5(\not{v}'+1)$, we can effectively replace $\mathcal{M}$ in (44) with

$$\mathcal{M} \to A - B - C + D \equiv \xi(v \cdot v'). \tag{46}$$

These results with $\Gamma_\mu = \gamma_\mu$ and $\Gamma_\mu = \gamma_\mu\gamma_5$ yield

$$\langle P_j(v')|V_\mu^{ji}|P_i(v)\rangle = \sqrt{M_{P_i}M_{P_j}}(v+v')_\mu\xi(v\cdot v'), \tag{47}$$

and

$$\langle P_j(v')|A_\mu^{ji}|P_i(v)\rangle = 0, \tag{48}$$

as we found before. Now we proceed to the matrix element of a general current between a vector and pseudoscalar:

$$\begin{aligned}\langle P_j^*(v',\varepsilon')|J_\mu^{ji}|P_i(v)\rangle &= -\sqrt{M_{P_i}M_{P_j^*}}\langle 0|\bar{q}_{v'}\not{\varepsilon}'h^j_{v'}\bar{h}^j_{v'}\Gamma_\mu h^i_v\bar{h}^i_v\gamma_5 q_v|0\rangle \\ &= \sqrt{M_{P_i}M_{P_j^*}}\mathrm{Tr}\left\{\not{\varepsilon}'\frac{\not{v}'+1}{2}\Gamma_\mu\frac{\not{v}+1}{2}\gamma_5\mathcal{M}\right\}. \end{aligned}\tag{49}$$

We note that $\not{v}'\not{\varepsilon}'(\not{v}'+1) = -\not{\varepsilon}'(\not{v}'+1)$ since $\varepsilon'\cdot v' = 0$. So we can again make the replacement (46). Taking the appropriate traces, we get

$$\langle P_j^*(v',\varepsilon')|V_\mu^{ji}|P_i(v)\rangle = \sqrt{M_{P_i}M_{P_j^*}}i\xi(v\cdot v')\epsilon_{\mu\nu\lambda\sigma}\varepsilon'^\nu v'^\lambda v^\sigma, \tag{50}$$

and

$$\langle P_j^*(v',\varepsilon')|A_\mu^{ji}|P_i(v)\rangle = \sqrt{M_{P_i}M_{P_j^*}}\xi(v\cdot v')\left[(1+v\cdot v')\varepsilon'_\mu - (\varepsilon'\cdot v)v'_\mu\right], \tag{51}$$

where ε' must be replaced with its complex conjugate if the polarization vector is not real. Matrix elements of currents between vector meson states are computed in a similar way. A summary of various matrix elements is given in [8].

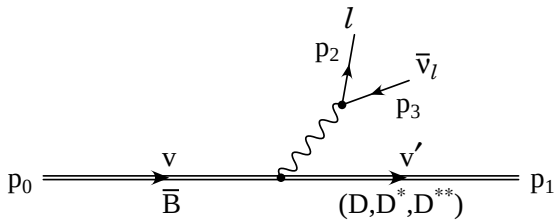

Figure 1: Feynman diagram for $\bar{B} \to (D, D^*, D^{**})\ell\bar{\nu}$.

2.4 $\bar{B} \to (D, D^*, D^{**})\ell\bar{\nu}$

2.4.1 General Aspects of $\bar{B} \to (D, D^*, D^{**})\ell\bar{\nu}$

To compute the decay rate for a $\bar{B}$-meson into a D-meson (or D^* or D^{**}) with a lepton and neutrino, we start with the amplitude

$$T = V_{cb}\frac{G_F}{\sqrt{2}}\bar{u}(p_2)\gamma^\alpha(1-\gamma_5)v(p_3)\langle D|V_\alpha - A_\alpha|\bar{B}\rangle. \tag{52}$$

Now we square T and sum over the lepton and neutrino spins giving

$$\sum_{\text{spin}}|T|^2 = \frac{V_{cb}^2 G_F^2}{2}H_{\alpha\beta}L^{\alpha\beta}, \tag{53}$$

where

$$H_{\alpha\beta} = \langle D|V_\alpha - A_\alpha|\bar{B}\rangle\left(\langle D|V_\beta - A_\beta|\bar{B}\rangle\right)^* \tag{54}$$

is the hadronic part computed using HQET, and (taking $m_3 = 0$)

$$\begin{aligned} L^{\alpha\beta} &= \text{Tr}\left\{(\not{p}_2 + m_2)\gamma^\alpha(1-\gamma_5)(\not{p}_3 - m_3)(1+\gamma_5)\gamma^\beta\right\} \\ &= 8\left\{p_2^\alpha p_3^\beta - p_2\cdot p_3 g^{\alpha\beta} + p_3^\alpha p_2^\beta + i\epsilon^{\mu\nu\alpha\beta}p_{2\mu}p_{3\nu}\right\} \end{aligned} \tag{55}$$

is the leptonic part with $\epsilon_{0123} = 1$. This gives

$$\Gamma = \frac{1}{2m_B}\frac{V_{cb}^2 G_F^2}{2}\int\frac{d^3p_1}{2E_1(2\pi)^3}\frac{d^3p_2}{2E_2(2\pi)^3}\frac{d^3p_3}{2E_3(2\pi)^3}(2\pi)^4\delta^4(p_0-p_1-p_2-p_3)H_{\alpha\beta}L^{\alpha\beta}. \tag{56}$$

Now define

$$I^{\alpha\beta}(q) \equiv \int\frac{d^3p_2}{2E_2(2\pi)^3}\frac{d^3p_3}{2E_3(2\pi)^3}(2\pi)^4\delta^4(q-p_2-p_3)L^{\alpha\beta}. \tag{57}$$

Since $I^{\alpha\beta}$ depends only on q, we can use its Lorentz transformation properties to write

$$I^{\alpha\beta}(q) = A(q)g^{\alpha\beta} + B(q)q^{\alpha}q^{\beta}. \tag{58}$$

We compute A and B by using

$$\begin{aligned} g_{\alpha\beta}I^{\alpha\beta} &= 4A + q^2B, \\ q_{\alpha}q_{\beta}I^{\alpha\beta} &= q^2A + (q^2)^2B. \end{aligned} \tag{59}$$

Now compute the left hand sides of (59)

$$g_{\alpha\beta}I^{\alpha\beta} = \int \frac{d^3p_2}{2E_2(2\pi)^3}\frac{d^3p_3}{2E_3(2\pi)^3}(2\pi)^4\delta^4(q-p_2-p_3)8\{-2p_2\cdot p_3\}. \tag{60}$$

Take $m_2 = m_3 = 0$ giving $(p_2+p_3)^2 = 2p_2\cdot p_3 = q^2$ and work in the frame where $\vec{q}=0$ (which we can do since $g_{\alpha\beta}I^{\alpha\beta}$ is a Lorentz scalar):

$$\begin{aligned} g_{\alpha\beta}I^{\alpha\beta} &= \int \frac{d\Omega p^2dp}{2p(2\pi)^3}\frac{(2\pi)^4}{2p(2\pi)^3}\delta(q^0-2p)8\left\{-q^2\right\} \\ &= -\int \frac{2dp}{\pi}\delta(q^0-2p)q^2 \\ &= -\frac{1}{\pi}q^2. \end{aligned} \tag{61}$$

Now compute the left side of the second equation in (59)

$$q_{\alpha}q_{\beta}I^{\alpha\beta} = \int \frac{d^3p_2}{2E_2(2\pi)^3}\frac{d^3p_3}{2E_3(2\pi)^3}(2\pi)^4\delta^4(q-p_2-p_3)8\{2p_2\cdot qp_3\cdot q - p_2\cdot p_3q^2\}. \tag{62}$$

Again, we take $m_2 = m_3 = 0$ which gives us $p_2\cdot p_3 = q^2/2$, $p_2\cdot q = q^2/2$, and $p_3\cdot q = q^2/2$. From this we see that the quantity in braces above is zero, giving $q_{\alpha}q_{\beta}I^{\alpha\beta} = 0$. In retrospect it is obvious that we should get zero since both the vector and axial currents are conserved when $m_2 = m_3 = 0$. Plugging these results into (59) to determine A and B results in

$$A = -\frac{1}{3\pi}q^2, \quad B = \frac{1}{3\pi}, \tag{63}$$

giving

$$I^{\alpha\beta}(q) = \frac{1}{3\pi}\left[-q^2 g^{\alpha\beta} + q^\alpha q^\beta\right]. \tag{64}$$

Our expression for the decay rate is now

$$\Gamma = \frac{1}{2m_B}\frac{V_{cb}^2 G_F^2}{2}\int \frac{d^3p_1}{2E_1(2\pi)^3} H_{\alpha\beta} I^{\alpha\beta}. \tag{65}$$

Note that $I^{\alpha\beta}$ is symmetric under interchange of α and β (unlike $L^{\alpha\beta}$), so we can drop any antisymmetric part in $H_{\alpha\beta}$. We can write

$$d^3p_1 = d\Omega_1 p_1^2 dp_1 = 4\pi p_1 E_1 dE_1 = 4\pi m_D\sqrt{y^2-1}E_1 m_D dy \tag{66}$$

where $y \equiv v\cdot v' = p_0\cdot p_1/m_D m_B$ and we have replaced the integration over angles for p_1 by 4π because the integrand is invariant under rotation of the whole system so we are free to fix $\vec{p}_1$ to be along the z-axis. Finally, we have the expression

$$\frac{d\Gamma}{dy} = \frac{V_{cb}^2 G_F^2}{2^4\pi^2}\frac{m_D^2}{m_B}\sqrt{y^2-1}H_{\alpha\beta}I^{\alpha\beta}. \tag{67}$$

2.4.2 Specifics of $\bar{B}\to D\ell\bar{\nu}$

For this case we have (using (47) and (48))

$$H_{\alpha\beta} = m_B m_D \xi^2(y)(v_\alpha + v'_\alpha)(v_\beta + v'_\beta), \tag{68}$$

giving

$$I^{\alpha\beta}H_{\alpha\beta} = m_B m_D \xi^2(y)\frac{1}{3\pi}\left[-q^2(2+2v\cdot v') + (q\cdot v + q\cdot v')^2\right]. \tag{69}$$

If we define $r \equiv m_D/m_B$ and recall $y \equiv v\cdot v'$ we can write

$$\begin{aligned} q &= m_B(v - rv'), \\ q^2 &= m_B^2(1 + r^2 - 2ry), \\ q\cdot v &= m_B(1-ry), \end{aligned}$$

$$q \cdot v' \;=\; m_B(y-r), \tag{70}$$

giving

$$I^{\alpha\beta}H_{\alpha\beta} = \frac{m_B^3 m_D \xi^2(y)}{3\pi}\left[-(1+r^2-2ry)(2+2y)+(1-ry+y-r)^2\right]. \tag{71}$$

2.4.3 Specifics of $\bar{B} \to D^*\ell\bar{\nu}$

Here, we will sum over polarizations of the D^* when computing the rate. Starting with (50) and (51) (taking the polarization vectors to be real) we have

$$\langle D^*|V_\alpha - A_\alpha|B\rangle = \sqrt{m_{D^*}m_B}\xi(y)\left[i\epsilon_{\alpha\nu\lambda\kappa}\varepsilon^\nu v'^\lambda v^\kappa - (1+v\cdot v')\varepsilon_\alpha + (\varepsilon\cdot v)v'_\alpha\right], \tag{72}$$

giving

$$\begin{aligned} H_{\alpha\beta} \;=\; & \sum_{\text{pol}} m_{D^*}m_B\xi^2\left[i\epsilon_{\alpha\nu_1\lambda_1\kappa_1}\varepsilon^{\nu_1}v'^{\lambda_1}v^{\kappa_1} - (1+v\cdot v')\varepsilon_\alpha + (\varepsilon\cdot v)v'_\alpha\right] \\ & \cdot\left[-i\epsilon_{\beta\nu_2\lambda_2\kappa_2}\varepsilon^{\nu_1}v'^{\lambda_1}v^{\kappa_1} - (1+v\cdot v')\varepsilon_\beta + (\varepsilon\cdot v)v'_\beta\right]. \end{aligned} \tag{73}$$

Now we contract this with appropriate quantities

$$\begin{aligned} g^{\alpha\beta}H_{\alpha\beta} = \sum_{\text{pol}} m_{D^*}m_B\xi^2 \quad & \Big[\epsilon_{\alpha\nu_1\lambda_1\kappa_1}\varepsilon^{\nu_1}v'^{\lambda_1}v^{\kappa_1}\epsilon^\alpha{}_{\nu_2\lambda_2\kappa_2}\varepsilon^{\nu_2}v'^{\lambda_2}v^{\kappa_2} \\ & +(1+v\cdot v')^2\varepsilon\cdot\varepsilon + (\varepsilon\cdot v)^2\Big]. \end{aligned} \tag{74}$$

Make use of

$$\sum_{\text{pol}}\varepsilon^\mu\varepsilon^\nu = -g^{\mu\nu} + v'^\mu v'^\nu, \tag{75}$$

$$\sum_{\text{pol}}\varepsilon^\mu\varepsilon_\mu = -3, \tag{76}$$

giving

$$\begin{aligned} g^{\alpha\beta}H_{\alpha\beta} = m_{D^*}m_B\xi^2 \quad & \Big[\epsilon_{\alpha\nu_1\lambda_1\kappa_1}v'^{\lambda_1}v^{\kappa_1}(-g^{\nu_1\nu_2}+0)\epsilon^\alpha{}_{\nu_2\lambda_2\kappa_2}v'^{\lambda_2}v^{\kappa_2} \\ & -3(1+v\cdot v')^2 + v^\mu v^\nu(-g_{\mu\nu}+v'_\mu v'_\nu)\Big]. \end{aligned} \tag{77}$$

Now make use of

$$\epsilon_{\alpha\nu\lambda_1\kappa_1}\epsilon^{\alpha\nu}{}_{\lambda_2\kappa_2} = -2\left(g_{\lambda_1\lambda_2}g_{\kappa_1\kappa_2} - g_{\lambda_1\kappa_2}g_{\kappa_1\lambda_2}\right), \tag{78}$$

giving

$$g^{\alpha\beta}H_{\alpha\beta} = m_{D^*}m_B\xi^2\left[-2 - 6v\cdot v' - 4(v\cdot v')^2\right]. \tag{79}$$

The other expression we will need is

$$q^\alpha q^\beta H_{\alpha\beta} = \sum_{\text{pol}} m_{D^*}m_B\xi^2\left[-(1+v\cdot v')\varepsilon\cdot q + \varepsilon\cdot v(v'\cdot q)\right]^2. \tag{80}$$

Now make use of

$$\varepsilon\cdot q = \varepsilon\cdot(m_B v - m_{D^*}v') = m_B\varepsilon\cdot v, \tag{81}$$

and

$$v'\cdot q = m_B v\cdot v' - m_{D^*}, \tag{82}$$

giving

$$q^\alpha q^\beta H_{\alpha\beta} = \sum_{\text{pol}} m_{D^*}m_B\xi^2\left[-(1+v\cdot v')m_B + m_B v\cdot v' - m_{D^*}\right]^2(\varepsilon\cdot v)^2. \tag{83}$$

Performing the polarization sum gives

$$q^\alpha q^\beta H_{\alpha\beta} = m_{D^*}m_B\xi^2(m_B+m_{D^*})^2\left[-1+(v\cdot v')^2\right]. \tag{84}$$

Combining (64), (79), and (84), we have

$$\begin{aligned} H_{\alpha\beta}I^{\alpha\beta} = m_{D^*}m_B\xi^2\frac{1}{3\pi} \quad & \Big\{ -q^2\left[-2-6v\cdot v' - 4(v\cdot v')^2\right] \\ & +(m_B+m_{D^*})^2\left[-1+(v\cdot v')^2\right]\Big\}. \end{aligned} \tag{85}$$

Using $q^2 = m_B^2 + m_{D^*}^2 - 2m_B m_{D^*}v\cdot v'$ and $y \equiv v\cdot v'$ along with $r \equiv m_{D^*}/m_B$ gives

$$H_{\alpha\beta}I^{\alpha\beta} = \frac{m_B^3 m_{D^*}\xi^2(y)}{3\pi}\left[(1+r^2-2ry)(2+6y+4y^2) + (1+r^2+2r)(y^2-1)\right]. \tag{86}$$

This result agrees with [9].

This decay has been used in extracting the CKM matrix element $|V_{cb}|$ because model dependence only enters at $\mathcal{O}(\Lambda^2_{\rm QCD}/m_Q^2)$ since Luke's theorem [10] determines the normalization of the universal form factor, $\xi(1) = 1 + \mathcal{O}(1/m_Q^2)$ with no $1/m_Q$ correction. So, $|V_{cb}|$ is measured by measuring the decay at various values of $v \cdot v'$ and extrapolating to $v \cdot v' = 1$. For a recent analysis of the determination of $|V_{cb}|$ see [11].

3 Chiral Symmetry

When constructing an effective field theory that describes hadrons made of light quarks (u, d, and maybe s), we make use of a symmetry which arises for $m_q \ll \Lambda_{\rm QCD}$ to reduce the number of unknown coefficients in the effective Lagrangian. The Lagrangian will have an infinite number of terms involving more and more derivatives of the fields. As long as we restrict our attention to particles with small momenta we can keep only the first few terms in the Lagrangian since the others will be suppressed by powers of the momentum. Consider the Lagrangian for the light quarks:

$$\mathcal{L} = \bar{q}_i i \not{D} q_i - m_i \bar{q}_i q_i. \tag{87}$$

We rewrite this using $q = q^L + q^R$ where

$$q^L \equiv \frac{1}{2}(1-\gamma_5)q, \quad q^R \equiv \frac{1}{2}(1+\gamma_5)q, \quad \bar{q}^L = \bar{q}\frac{1}{2}(1+\gamma_5), \quad \bar{q}^R = \bar{q}\frac{1}{2}(1-\gamma_5), \tag{88}$$

we get

$$\mathcal{L} = \bar{q}_i^L i \not{D} q_i^L + \bar{q}_i^R i \not{D} q_i^R + m_i \bar{q}_i^R q_i^L + m_i \bar{q}_i^L q_i^R. \tag{89}$$

If we neglect the mass terms (we can account for them as a perturbation later since the mass is small) the Lagrangian is clearly unchanged by the transformation

$$q^L \to L q^L, \quad L \in SU(3)_L \tag{90}$$

and

$$q^R \to R q^R, \quad R \in SU(3)_R \tag{91}$$

so we have a $SU(3)_L \times SU(3)_R$ global symmetry. Since the full Lagrangian does not obey this symmetry due to the mass term, we expect the physical spectrum to show only approximate signs of the symmetry. To see the consequences of a symmetry for the mass (energy) of a state, consider two states $|A\rangle$ and $|B\rangle$

that are created by operators A and B respectively which are connected by the symmetry transformation $UAU^\dagger = B$. We look at the expectation value of the Hamiltonian:

$$E_A = \langle A|\mathcal{H}|A\rangle = \langle 0|A^\dagger \mathcal{H} A|0\rangle. \tag{92}$$

Now insert $U^\dagger U = 1$ around each operator and make use of $U\mathcal{H}U^\dagger = \mathcal{H}$ (since the transformation is a symmetry of the Hamiltonian) and $UAU^\dagger = B$. We get

$$E_A = \langle 0|U^\dagger B^\dagger \mathcal{H} B U|0\rangle. \tag{93}$$

From this, we see that if the vacuum obeys the symmetry of the Hamiltonian, i.e. $U|0\rangle = |0\rangle$, we have $E_A = E_B$, so there should be degeneracy in the spectrum between states connected by a symmetry transformation. This is familiar from rotational symmetry in quantum mechanics. The rotational symmetry of the Hamiltonian implies degenerate multiplets (states with the same $\vec{J}^2$ but different J_z). The possible sizes for a multiplet are determined by the possible representations of the symmetry group. Expectation values of the generator of the symmetry transformation, $\vec{J}$, distinguish the states in a multiplet.

However, if we look at the spectrum of observed hadronic states we find that the approximate (recall the explicit symmetry breaking due to quark masses) multiplets are not of the pattern we would expect for a $SU(3)_L \times SU(3)_R$ symmetry. This leads us to believe that the symmetry is spontaneously broken – the ground state does not obey the symmetry, i.e. $U|0\rangle \neq |0\rangle$. We must examine the consequences of spontaneous symmetry breaking before we can construct our effective Lagrangian.

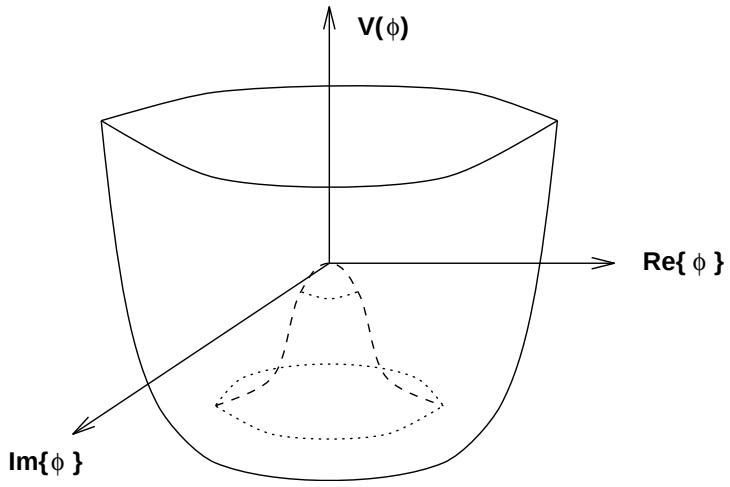

Figure 2: Potential for a simple example of spontaneous symmetry breaking ("Mexican Hat Potential").

3.1 Spontaneous Symmetry Breaking and Representations

First we examine the simplest theory that we can think of with a spontaneously broken continuous symmetry. We start with the Lagrangian:

$$\mathcal{L} = \frac{1}{2}\left|\partial_\mu \phi\right|^2 + \frac{1}{2}\mu^2\left|\phi\right|^2 - \frac{1}{4}\lambda\left|\phi\right|^4, \tag{94}$$

where ϕ is a complex scalar field and μ^2 and λ are positive. The Lagrangian is invariant under the transformation

$$\phi \to \phi' = e^{i\varepsilon}\phi. \tag{95}$$

The potential part of the Lagrangian is shown in Fig. 2. Note that the minimum of the potential is not at $\phi = 0$ but rather is at $|\phi|^2 = v^2$ where

$$v^2 \equiv \mu^2/\lambda. \tag{96}$$

Perturbation theory calculations require that we do an expansion about the minimum of the potential (so that field values are small around the minimum). Because of the symmetry of the Lagrangian under the transformation (95), if

the minimum of the potential does not occur at $\phi = 0$ there must be an infinite number of possible ground states which are related by the symmetry transformation – these states lie along the valley of the "Mexican Hat" shown in Fig. 2.

We choose our vacuum state to be $\phi = v$ and rewrite the Lagrangian in terms of new field variables which will have small values for small fluctuations about the vacuum. First we look at the "Cartesian" representation:

$$\phi \equiv v + R + iI \tag{97}$$

where R and I are real scalar fields. Our Lagrangian becomes (after dropping constant terms):

$$\mathcal{L}^C = \frac{1}{2}(\partial_\mu I)^2 + \frac{1}{2}(\partial_\mu R)^2 - \mu^2 R^2 - \lambda v R^3 - \lambda v R I^2 - \frac{1}{2}\lambda R^2 I^2 - \frac{1}{4}\lambda R^4 - \frac{1}{4}\lambda I^4. \tag{98}$$

Examination of the quadratic part of the Lagrangian shows that the I field describes a massless particle while the R field describes a particle with mass $\sqrt{2}\mu$. The I field is a Goldstone boson – it is massless because it represents movement from the vacuum toward an equivalent vacuum along the valley in the Mexican Hat. Since the equivalent vacuum has the same energy as the original one, a state with a zero-momentum I-particle must have zero energy, hence the I is massless. The transformation (95) is equivalent to the transformation:

$$R \to R' = (v + R)\cos\varepsilon - v - I\sin\varepsilon, \quad I \to I' = I\cos\varepsilon + (v + R)\sin\varepsilon, \tag{99}$$

which leaves $\mathcal{L}^C$ unchanged.

We could have chosen our fields differently. We now look at the "Polar" representation:

$$\phi \equiv (v + \eta)e^{i\theta/v}, \tag{100}$$

with real fields η and θ which gives a Lagrangian (after dropping constants):

$$\mathcal{L}^P = \frac{1}{2}(\partial_\mu\theta)^2 + \frac{1}{2}(\partial_\mu\eta)^2 - \mu^2\eta^2 - \lambda v\eta^3 + \frac{1}{v}\eta(\partial_\mu\theta)^2 + \frac{1}{2v^2}\eta^2(\partial_\mu\theta)^2 - \frac{1}{4}\lambda\eta^4. \quad (101)$$

The transformation equivalent to (95) is:

$$\eta \to \eta' = \eta, \quad \theta \to \theta' = \theta + v\varepsilon, \quad (102)$$

which leaves $\mathcal{L}^P$ unchanged. In this case, θ is the Goldstone boson.

The "Cartesian" and "Polar" theories are equivalent in the sense that on-shell scattering amplitudes at tree-level must be the same for corresponding fields. This result was shown in general in [12, 13, 14]. If a Lagrangian $\mathcal{L}(\phi)$ is rewritten as $\mathcal{L}(\chi F(\chi))$ where $F(0) = 1$, the tree and all orders on-shell amplitudes computed with ϕ and χ are the same. In our examples above $R = \eta(1+...)$ and $I = \theta(1 + ...)$. Note that although the original field ϕ transforms linearly under the symmetry (95), our new fields don't unless $v = 0$ (see (99) and (102)). From the reparameterization independence theorem above, we see that we could have chosen fields with very strange transformation properties without changing our results for the on-shell S-matrix.

Given the equivalence of various parameterizations, the question naturally arises: Which one is "best"? In the examples above, there is a very clear difference between the Lagrangians $\mathcal{L}^C$ and $\mathcal{L}^P$. In the "Polar" representation the Goldstone boson only appears with derivative couplings and it does not mix with the massive particle under the symmetry transformation. Both of these features are consequences of the fact that θ serves as the coordinate between equivalent vacua all along the valley of the Mexican Hat (the I-field only connects vacua around the infinitesimal neighborhood of $\phi = v$). The symmetry transformation is just an arbitrary (x-independent) shift of the coordinate (θ) along the valley of the Mexican Hat so adding a constant to θ does not change the energy, and

therefore θ must only appear in the Lagrangian differentiated so as to have no effect when a constant is added to it. The derivative interactions don't appear in $\mathcal{L}^C$, but they arise in calculations through assorted cancellations between pieces of diagrams.

The fact that the symmetry transformation does not mix the fields in the "Polar" representation has important consequences if we want to construct an effective theory that describes just the Goldstone boson. If we take μ to be large, we can integrate out the η field and be left with a useful theory involving only θ. The fields decouple, so the new coupling constants in our Lagrangian may have $1/\mu$ modifications, and we may get more vertices with various powers of $1/\mu$. What if we tried to apply the same procedure to the "Cartesian" representation? Clearly this cannot work because if we did somehow integrate the R field out, a symmetry transformation on the remaining I field would bring it back! This occurs because construction of a low energy effective theory requires fields which can describe all states connected by an infinitesimal energy excitation – the I field alone cannot do this because it cannot parameterize the whole valley of the Mexican Hat. For more information on integrating out fields, see [15].

We summarize the results of our simple example which will be relevant to the construction of effective field theories. First, the broken symmetry gives rise to massless Goldstone bosons. Second, the coupling constants in the broken Lagrangian are not all independent. Third, spontaneous symmetry breaking allows an operator with non-trivial transformation properties (such as ϕ) to have a non-zero vacuum expectation value because the vacuum does not obey the symmetry. Fourth, the representation we choose determines how the fields transform under the symmetry – it is generally not linear. In the representation where the Goldstone bosons are the coordinates of the symmetry transformation

the derivative interactions appear clearly in the Lagrangian, and the massive particles can be integrated out.

3.2 Constructing a Chiral Lagrangian

Now we return to the problem of constructing an effective Lagrangian which makes appropriate use of the symmetries of the QCD Lagrangian when the quark masses are small. We write the symmetry transformation in terms of the conserved charges Q^a which generate the transformation:

$$U = \exp\left\{i\alpha_a Q_a\right\}. \tag{103}$$

The Q's form a group (the group multiplication is the commutator) and they commute with the Hamiltonian. Only a subgroup $H \subset G$ annihilates the vacuum if the symmetry is spontaneously broken. For QCD the transformations (90) and (91) give rise to the Noether currents:

$$V_a^\mu = \bar{q}\gamma^\mu \frac{1}{2}\lambda_a q, \quad A_a^\mu = \bar{q}\gamma^\mu\gamma_5 \frac{1}{2}\lambda_a q, \tag{104}$$

where λ_a are Gell-Mann matrices in $SU(3)$ flavor space. The charges which generate the symmetry transformations are given in terms of the conserved currents by:

$$Q = \int d^3x J_0(x). \tag{105}$$

The transformations corresponding to the vector current, V_a^μ, mix quarks with different flavors. This symmetry does not seem to be spontaneously broken since we witness the near degeneracy of the octect of pseudoscalar mesons (π, K, η). The axial transformation, however, includes a γ_5 which changes the parity and we do not observe degenerate scalar partners for (π, K, η). We conclude that the axial subgroup is spontaneously broken, i.e. $Q_a^5 = \int d^3x q^\dagger \gamma_5 \frac{1}{2}\lambda_a q$ does not annihilate the vacuum. Note that Q_a^5 has the the same quantum numbers as the

zero momentum mesons in the octet (π, K, η). This explains why these mesons have such small masses – they would be massless Goldstone bosons if the u, d, s masses were actually zero instead of only being small.

Our goal in constructing an effective Lagrangian will be to choose a representation where the fields transform linearly under the unbroken $SU(3)_V$ symmetry while only giving derivative interactions to the Goldstone bosons – this will result in a non-linear transformation of the Goldstone bosons under $SU(3)_A$, but it allows us to construct a theory with an obvious momentum expansion that does not require extra massive particles. Note that we require a representation that is linear under $SU(3)_V$ so that we can classify particles in the normal way under the unbroken symmetry. If the representation is linear, the quadratic part of the Lagrangian (which is used to construct the Hilbert space of in and out states) is invariant under the transformation. In a non-linear representation this is not the case since a symmetry transformation mixes the quadratic and interaction parts of the Lagrangian. We seek a representation similar to the "Polar" representation in Sec. 3.1. A formalism for accomplishing this is given in [13, 14, 16]. We will proceed instead by following intuition gained in Sec. 3.1.

Any operator which is not a singlet under a transformation which leaves the vacuum unchanged must have vanishing vacuum expectation value since

$$\langle 0|\mathcal{O}|0\rangle = \langle 0|U^\dagger U\mathcal{O}U^\dagger U|0\rangle = \langle 0|U\mathcal{O}U^\dagger|0\rangle. \tag{106}$$

With a spontaneously broken symmetry there will be operators with non-zero vacuum expectation value which transform non-trivially under the broken symmetry (this is allowed because $U|0\rangle \neq |0\rangle$) – an example of this is the ϕ field in Sec. 3.1. The vacuum expectation values of such operators are called order parameters. Invariance of the vacuum under Lorentz transformations requires such operators to be scalars. The lowest dimension candidate for an order parameter

in QCD is the quark condensate $\langle 0|\bar{q}q|0\rangle$ (see [16] for other order parameters and discussion). We will follow [17] and focus on:

$$a\Sigma_{ij} \equiv \bar{q}_j^R q_i^L, \tag{107}$$

where a is the magnitude of the condensate and Σ is normalized so that $\Sigma\Sigma^\dagger = 1$. Note that $\bar{q}^R q^L = (\bar{q}q - \bar{q}\gamma_5 q)/2$ and the vacuum expectation value of $\bar{q}\gamma_5 q$ must be zero by parity. We know how q^R and q^L transform from (90) and (91), so

$$\Sigma \to \Sigma' = L\Sigma R^\dagger. \tag{108}$$

Since the vacuum is invariant under the $SU(3)_V$ transformation $L = R = V$:

$$\langle 0|\Sigma|0\rangle \to \langle 0|\Sigma'|0\rangle = \langle 0|V\Sigma V^\dagger|0\rangle = \langle 0|\Sigma|0\rangle, \tag{109}$$

so $\langle 0|\Sigma|0\rangle$ is simply the identity matrix. Under a $SU(3)_A$ transformation, $L = R^\dagger = A$ and $\langle 0|\Sigma|0\rangle$ is not invariant. Looking back at our example in Sec. 3.1, we see that our new field variable θ just acted like the parameter for a local (instead of global) transformation of the broken symmetry. By analogy, we introduce pions as the parameters for a local $SU(3)_A$ transformation acting on the vacuum expectation value of Σ. The dynamical field Σ is approximated at low energies by its VEV with a long wavelength chiral transformation (low energy pions) applied to it:

$$\Sigma(x) \approx \exp\left\{iM(x)/\sqrt{2}f_\pi\right\}\langle 0|\Sigma|0\rangle\exp\left\{iM(x)/\sqrt{2}f_\pi\right\} = \exp\left\{2iM(x)/\sqrt{2}f_\pi\right\}, \tag{110}$$

where $M(x) = \pi_a(x)\lambda_a/\sqrt{2}$, i.e.

$$M = \begin{bmatrix} \pi^0/\sqrt{2} + \eta/\sqrt{6} & \pi^+ & K^+ \\ \pi^- & -\pi^0/\sqrt{2} + \eta/\sqrt{6} & K^0 \\ K^- & \bar{K}^0 & -\eta\sqrt{2/3} \end{bmatrix}, \tag{111}$$

and $f_\pi = 93$MeV. From the transformation properties of Σ we deduce the transformation properties of the Goldstone bosons. Under $SU(3)_V$:

$$\Sigma' = V\Sigma V^\dagger \quad \Rightarrow \quad M' = VMV^\dagger, \tag{112}$$

so we see that the Goldstone bosons transform linearly under $SU(3)_V$ as desired. Under an infinitesimal $SU(3)_A$, $A = e^{i\varepsilon}$, with ε an infinitesimal matrix $\varepsilon = \varepsilon_a \lambda_a$:

$$\Sigma' = A\Sigma A = (1+2iM'/\sqrt{2}f_\pi+...) = (1+i\varepsilon+...)(1+2iM/\sqrt{2}f_\pi+...)(1+i\varepsilon+...) \tag{113}$$

so

$$M' = M + \sqrt{2}f_\pi\varepsilon + ... \tag{114}$$

Notice the similarity between the transformation in (114) and the transformation of the θ field in (102). The chiral transformation does not mix the Goldstone bosons with massive particles, it is non-linear, and to lowest order the field is simply shifted by a constant amount. The "+..." part of (114) represents higher powers of the Goldstone boson fields and it arises because the group is non-abelian.

Now we can construct a low energy theory for the Goldstone bosons by writing down the most general Lagrangian possible. If we only wish to describe the Goldstone bosons, the Σ field is a good field to work with since it has simple transformation properties (see (108)). Since the Lagrangian must be invariant under $SU(3)_L \times SU(3)_R$, we might try to put a term in the Lagrangian such as $\mathrm{Tr}\left\{\Sigma^\dagger\Sigma\right\}$ but this is just 1 – there is no non-trivial invariant term that we can construct that does not involve derivatives as we expect because of the representation we have chosen. So we have

$$\mathcal{L}_{eff} = \mathcal{L}^{(2)}_{eff} + \mathcal{L}^{(4)}_{eff} + \mathcal{L}^{(6)}_{eff} + ... \tag{115}$$

where the superscripts denote the number of derivatives. The lowest term in the energy expansion is

$$\mathcal{L}^{(2)}_{eff} = \frac{1}{4}f_\pi^2 \mathrm{Tr}\left\{\partial_\mu\Sigma^\dagger\partial^\mu\Sigma\right\}, \tag{116}$$

where we have chosen the coefficient to give a correctly normalized kinetic term for the pion:

$$\mathcal{L}^{(2)}_{eff} = \frac{1}{2}\partial_\mu \pi_a \partial^\mu \pi_a + ... \tag{117}$$

A procedure for efficiently determining currents from the Lagrangian is given in Sec. 5.6 of [18]. The result using $\mathcal{L}^{(2)}_{eff}$ is:

$$A^\mu_a = \frac{i}{4} f_\pi^2 \mathrm{Tr}\left\{\Sigma^\dagger \lambda_a \Sigma\right\} = -f_\pi \partial^\mu \pi_a + ... \tag{118}$$

which shows that the axial charge is related to zero momentum pions as expected. We can account for the non-zero quark masses by putting an explicit symmetry breaking term into the Lagrangian. To do this, we form the matrix $m = \mathrm{diag}\{m_u, m_d, m_s\}$ and we notice that if it transformed under $SU(3)_L \times SU(3)_R$ (although it does not because it involves constants, not fields) according to $m \to LmR^\dagger$ the quark-level Lagrangian (89) would be invariant even with the quark masses. So, we add terms to the effective Lagrangian which would be invariant if m really transformed according to $m \to LmR^\dagger$. An example of such a term is

$$\mathrm{Tr}\left\{\Sigma^\dagger m\right\} + \mathrm{h.c.} \tag{119}$$

which gives a term quadratic in the Goldstone boson field resulting in a pion mass *squared* which is linear in the quark masses. For a further discussion, see [16]. We have not discussed the effect of loop diagrams – the reader is referred to [15, 16].

4 Combining HQET and Chiral Symmetry

In order to compute decays such as $\bar{B} \to D\pi\ell\bar{\nu}$ we need to combine the results of HQET and chiral symmetry. This was done in [8]. Rather than working with Σ, it will be more convenient to work with the field

$$\xi(x) \equiv \sqrt{\Sigma(x)}, \tag{120}$$

as described in Ch. 6 of [18]. Writing the Lagrangian in terms of ξ will give derivative interactions only which makes the momentum dependence clear. From (108), we see that under a $SU(3)_L \times SU(3)_R$ transformation

$$\xi \to \xi' = L\xi U^\dagger = U\xi R^\dagger, \tag{121}$$

where in general U is a function of L, R, *and* ξ (i.e. it is a function of the Goldstone boson fields and thus depends on x also) for the last equality to hold. Note that under $SU(3)_V$, $L = R = V$ and $U = V$ is independent of ξ. We can construct two fields with simple transformation properties:

$$\mathcal{V}_\mu = \frac{1}{2}\left[\xi^\dagger\partial_\mu\xi + \xi\partial_\mu\xi^\dagger\right], \tag{122}$$

and

$$\mathcal{A}_\mu = \frac{i}{2}\left[\xi^\dagger\partial_\mu\xi - \xi\partial_\mu\xi^\dagger\right]. \tag{123}$$

The transformation properties are:

$$\mathcal{V}_\mu \to \mathcal{V}'_\mu = U\mathcal{V}_\mu U^\dagger + U\partial_\mu U^\dagger, \tag{124}$$

$$\mathcal{A}_\mu \to \mathcal{A}'_\mu = U\mathcal{A}_\mu U^\dagger. \tag{125}$$

To form a Lagrangian with heavy mesons we need to know their transformation properties. Since pseudoscalars P_Q each contain a light (one of u,d,s) antiquark (and a heavy quark Q), they transform under $SU(3)_V$ as an antitriplet:

$$P_Q \to P'_Q = P_Q V^\dagger. \tag{126}$$

We define their transformation properties under $SU(3)_L \times SU(3)_R$ as

$$P_Q \to P'_Q = P_Q U^\dagger. \tag{127}$$

It is convenient to define

$$D_\mu P_Q^\dagger \equiv (\partial_\mu + \mathcal{V}_\mu) P_Q^\dagger, \tag{128}$$

which transforms simply:

$$D_\mu P_Q^\dagger \to U D_\mu P_Q^\dagger. \tag{129}$$

Dropping the subscripted Q's we construct the most general $SU(3)_L \times SU(3)_R$ symmetric Lagrangian up to one derivative:

$$\begin{aligned} \mathcal{L}_{PP^*} &= D_\mu P D^\mu P^\dagger - M_P^2 P P^\dagger + f_Q (P \mathcal{A}^\mu P_\mu^{*\dagger} + P_\mu^* \mathcal{A}^\mu P^\dagger) \\ &- \frac{1}{2} P^{*\mu\nu} P_{\mu\nu}^{*\dagger} + M_{P^*}^2 P^{*\mu} P_\mu^{*\dagger} \\ &+ \frac{1}{2} g_Q \epsilon_{\mu\nu\lambda\kappa} (P^{*\mu\nu} \mathcal{A}^\lambda P^{*\kappa\dagger} + P^{*\kappa} \mathcal{A}^\lambda P^{*\mu\nu\dagger}), \end{aligned} \tag{130}$$

with

$$P_{\mu\nu}^{*\dagger} \equiv D_\mu P_\nu^{*\dagger} - D_\nu P_\mu^{*\dagger}. \tag{131}$$

Note that in these equations the asterisks indicate spin-1 mesons, not complex conjugation. It is shown in [8] that heavy quark symmetry requires:

$$f_Q = \sqrt{M_{P_Q} M_{P_Q^*}} f, \quad g_Q = \frac{1}{2} f, \tag{132}$$

where f is independent of the heavy quark Q. This leaves us with a single unknown coupling f. We can use $\mathcal{L}_{PP^*}$ to compute interactions between the heavy mesons and pions as long as the pion momentum is small since we neglect higher derivative terms. By combining this result with the $V-A$ matrix elements for weak decays, one can find amplitudes for decays such as $\bar{B} \to D^* \pi \ell \bar{\nu}$ and $\bar{B} \to D \pi \ell \bar{\nu}$. This is done in [8]. Similar calculations for baryons are also performed there.

5 $\bar{B} \to (D, D^*)\pi\ell\bar{\nu}$

We study in detail the predictions for the semileptonic decays $\bar{B} \to D(D^*)\pi\ell\bar{\nu}$ by heavy quark and chiral symmetry. The branching ratio for $\bar{B} \to D\pi\ell\bar{\nu}$ is quite significant, as big as $(0.5 - 1)\%$. The branching ratio for $\bar{B} \to D^*\pi\ell\bar{\nu}$ is only of order $10^{-4} - 10^{-5}$ although this calculation does not include possible contributions from diagrams containing an intermediate D^{**}. Numerical results for various single particle spectra and their dependence on the pion momentum cutoff schemes are presented in a series of figures. We also study the parity-violation effects on the decay rates for different polarizations of the D^*.

5.1 Introduction

The semileptonic decays with a soft pion are completely determined by the Isgur-Wise function measured in $\bar{B} \to D^*\ell\bar{\nu}$ and the coupling constant that describes the strong decay $D^* \to D\pi$. The Feynman diagrams we use to compute $\bar{B} \to (D, D^*)\pi\ell\bar{\nu}$ are shown in Figs. 3 and 4. The matrix elements for these decays are explicitly given in [8]. Here, we explore the implications in detail. Furthermore, since the unknowns appear as an overall factor of the decay matrix elements, many of the ratios of the differential spectra are free of any adjustable parameter. Some of these ratios are presented in [19].

There is an experimental motivation to study the semileptonic decays of the $\bar{B}$ meson with emission of additional pions. The 1992 Particle Data Group (PDG) [20] gives

$$B(B^0 \to D^-\ell^+\nu) = (1.8 \pm 0.5)\% \,, \tag{133}$$

$$B(B^0 \to D^{*-}\ell^+\nu) = (4.9 \pm 0.8)\% \,, \tag{134}$$

$$B(B^+ \to \bar{D}^0\ell^+\nu) = (1.6 \pm 0.7)\% \,, \tag{135}$$

$$B(B^+ \to \bar{D}^{*0}\ell^+\nu) = (4.6 \pm 1.0)\% \,, \tag{136}$$

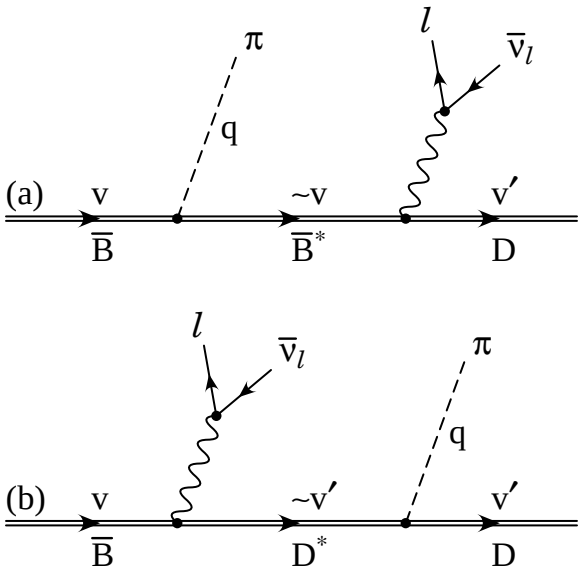

Figure 3: Feynman diagrams for $\bar{B} \to D\pi\ell\bar{\nu}$.

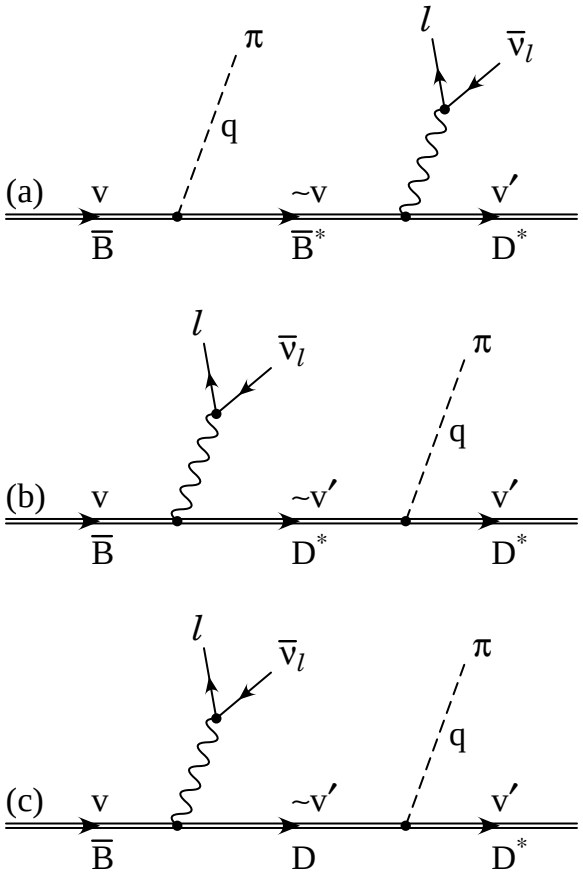

Figure 4: Feynman diagrams for $\bar{B} \to D^*\pi\ell\bar{\nu}$.

$$B(B \to e^{\pm}\nu_e \text{ hadrons}) \ = (10.7 \pm 0.5)\% \ , \tag{137}$$

where ℓ indicates e or μ mode (not sum over modes), and the charge of B is not determined in the last branching ratio (137). Clearly, beside the $D\ell\bar{\nu}$ and $D^*\ell\bar{\nu}$ modes, there exist other important semileptonic decays of the $\bar{B}$ meson. There are indications from ARGUS [21] and CLEO [22] that $\bar{B} \to D^{**}\ell\bar{\nu}$ gives a significant contribution. It is still interesting to ask how large the branching ratios for $\bar{B} \to D\pi\ell\bar{\nu}$ and $\bar{B} \to D^*\pi\ell\bar{\nu}$ are. It turns out that the branching ratio for $\bar{B} \to D\pi\ell\bar{\nu}$ can be quite significant, perhaps as large as 1%, while the branching ratio for $\bar{B} \to D^*\pi\ell\bar{\nu}$ is much smaller, of order 10^{-4} to 10^{-5}.

For a comparison of our work to other recent studies the reader is referred to [19]. In our work, starting with the amplitudes given in [8], we derive explicit formulae for the differential decay rates of both $\bar{B} \to D\pi\ell\bar{\nu}$ and $\bar{B} \to D^*\pi\ell\bar{\nu}$. Single particle energy spectra for D or D^*, the electron and the pion are evaluated numerically using Monte Carlo integration; their dependence on the pion momentum cutoff schemes is studied. In the case of $\bar{B} \to D\pi\ell\bar{\nu}$, the D^* pole dominates the amplitude, and the rates for the $D\pi$ system in the resonant and nonresonant regions (to be defined in Sec. 5.5) are sensitive to the total decay width of D^*. Although the charged $D^{*\pm}$ decay almost exclusively to $D\pi$, the neutral D^{*0} has a substantial radiative decay contribution [23, 24]. Consequently, the widths of D^* are not simply related to the $D^*D\pi$ coupling constant. With theoretical results for the $D^*D\pi$ coupling constant and the total widths of $D^{*\pm}$ and D^{*0} [23], we are able to predict the decay rates for $\bar{B} \to D^*\ell\bar{\nu}$ and $\bar{B} \to (D\pi)_{\text{nonres}}\ell\bar{\nu}$. The definitions of resonating $D\pi$ (to be identified with D^*) and nonresonating $D\pi$ are given in Sec. 5.5. Our results for $\bar{B} \to D^*\ell\bar{\nu}$ for both charged and neutral $\bar{B}$ mesons agree with the available data (134) and (136).

In the case of $\bar{B} \to D^*\pi\ell\bar{\nu}$, the single particle spectra are calculated for

polarized D^*. The underlying $V-A$ interaction of the quarks makes the spectra polarization dependent. Instead of describing all these results in words, we present them in a series of figures.

5.2 Kinematics

In this section we will review the kinematics of the decays

$$\bar{B} \to D + \pi + \ell\bar{\nu} \ , \tag{138}$$

$$\bar{B} \to D^* + \pi + \ell\bar{\nu} \ . \tag{139}$$

General kinematics for such processes has been studied by several authors before [25, 26, 27, 28, 29]. We will pay special attention to the new features for the latter where the polarization of D^* is involved. It is well known that there are five independent kinematic variables for these processes if the spin of the initial state is zero or is not observed. Let the momentum of the $\bar{B}$ meson, D (or D^*), the pion, the charged lepton, and the neutrino be P_B, p, q, p_ℓ and p_ν, respectively. For the five variables we follow earlier authors' convention and pick

$s_M = (p+q)^2$,

$s_L = (p_\ell + p_\nu)^2$,

$\theta =$ the angle between $\vec{p}$ in the $D(D^*)\pi$ rest frame and the line of the flight of the $D(D^*)\pi$ system in the $\bar{B}$ meson's rest frame,

$\theta_\ell =$ the angle between $\vec{p_\ell}$ in the $\ell\bar{\nu}$ rest frame and the line of flight of the $\ell\bar{\nu}$ system in the $\bar{B}$ meson's rest frame,

$\phi =$ the angle between the normals to the planes defined in the $\bar{B}$ meson's rest frame by the momenta of the $D(D^*)\pi$ pair and the $\ell\bar{\nu}$ pair, respectively. The sense of ϕ is from the $D(D^*)\pi$ plane to the $\ell\bar{\nu}$ plane.

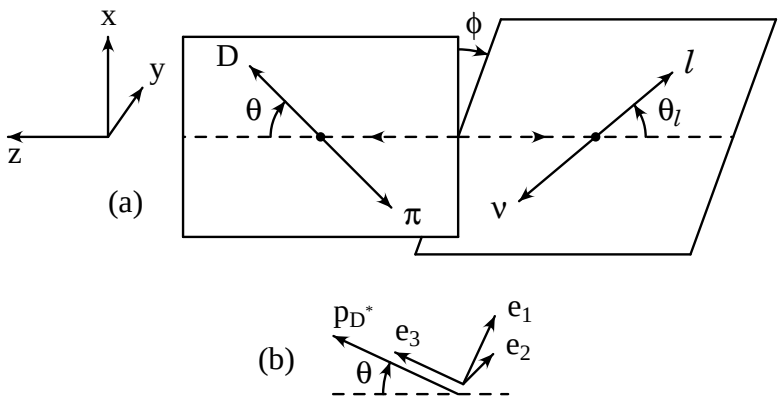

Figure 5: **(a)** General kinematics of $\bar{B} \to D(D^*)\pi\ell\bar{\nu}$. The dashed lines are the lines of flight of the $D(D^*)\pi$ pair and lepton pair in the rest frame of the $\bar{B}$ meson. Solid lines denote the line of flight of D (D^*) and π in the M-frame and that of the lepton and neutrino in the L-frame. The coordinates x, y, and z are indicated, and the angles θ, θ_ℓ and ϕ are labeled. **(b)** The three linear polarization vectors of D^* in the M-frame. The vector $\vec{e}_1$ is in x-z plane, $\vec{e}_2$ is along the $\hat{y}$ axis and $\vec{e}_3$ is along $\vec{p}$.

These variables are depicted in Fig. 5. In the same figure, we also display the three orthonormal vectors associated with the 3-momentum of D^* in the $D^*\pi$ rest-frame. They will be useful for describing the polarization states of D^*. The positive z-axis is along the line of flight of the $D(D^*)\pi$ system in the $\bar{B}$ meson's rest frame; the x-axis is in the $D(D^*)\pi$ plane. The lepton mass will be neglected. Now we form the combinations,

$$P = p + q \ , \quad Q = p - q \ , \tag{140}$$

$$L = p_\ell + p_\nu \ , \quad N = p_\ell - p_\nu \ \ , \tag{141}$$

and find

$$P \cdot L = \frac{1}{2}(m_B^2 - s_M - s_L) \ , \tag{142}$$

$$L \cdot N = 0 \ , \tag{143}$$

$$P \cdot Q = m^2 - m_\pi^2 \ , \tag{144}$$

$$Q^2 = 2(m^2 + m_\pi^2) - s_M \ , \tag{145}$$

$$N^2 = -s_L \ , \tag{146}$$

where $m^2 = m_D^2$ or $m_{D^*}^2$ as the case may be.

Three frames of reference are of particular interest: the B-frame in which the $\bar{B}$ meson is at rest, the M-frame which is the center-of-mass frame of the $D(D^*)\pi$ system, and the L-frame which is the center-of-mass frame of the lepton pair. To construct some of the Lorentz invariants, it is often necessary to specify the individual components of various four-vectors in one of these coordinate systems. This information is provided in Appendix A. In particular, we find

$$\begin{aligned} Q \cdot N &= \left(\frac{m^2 - m_\pi^2}{s_M}\right) X \cos\theta_\ell + \beta (P \cdot L) \cos\theta \cos\theta_\ell \\ &\quad -\sqrt{s_M s_L}\beta \sin\theta \sin\theta_\ell \cos\phi \ , \end{aligned} \tag{147}$$

$$\sigma \equiv \epsilon_{\mu\nu\lambda\kappa} Q^\mu P^\nu N^\lambda L^\kappa = -\sqrt{s_M s_L}\beta X \sin\theta \sin\theta_\ell \sin\phi \tag{148}$$

$$P_B \cdot p = \frac{1}{2}\left[\frac{s_M + m^2 - m_\pi^2}{2s_M}\left(m_B^2 + s_M - s_L\right) + X\beta\cos\theta\right] \ , \tag{149}$$

$$P_B \cdot q = \frac{1}{2}\left[\frac{s_M + m_\pi^2 - m^2}{2s_M}\left(m_B^2 + s_M - s_L\right) - X\beta\cos\theta\right] \ , \tag{150}$$

$$P_B \cdot p_\ell = \frac{1}{2}\left[\frac{1}{2}\left(m_B^2 + s_L - s_M\right) + X\cos\theta_\ell\right] \ , \tag{151}$$

where X and β are defined in Appendix A, and our convention is $\epsilon_{0123} = 1$.

In the laboratory frame (the B-frame), the above relations become

$$P_B \cdot p = m_B E_p \ , \tag{152}$$

$$P_B \cdot q = m_B E_q \ , \tag{153}$$

$$P_B \cdot p_\ell = m_B E_\ell \ . \tag{154}$$

The four-body phase space element is given by

$$\begin{aligned} d(PS) &= \frac{d^3p}{(2\pi)^3 2E_p}\frac{d^3q}{(2\pi)^3 2E_q}\frac{d^3p_\ell}{(2\pi)^3 2E_\ell}\frac{d^3p_\nu}{(2\pi)^3 2E_\nu} \\ &\quad \times (2\pi)^4 \delta^4(P_B - p - q - p_\ell - p_\nu) \ . \end{aligned} \tag{155}$$

To reduce the above expression to a five-dimensional integral, we insert the factors

$$1 = \int \frac{d^3P}{2E_P} ds_M \delta^4(P - p - q) \quad , \quad E_P = \sqrt{\vec{P}^2 + s_M}, \tag{156}$$

$$1 = \int \frac{d^3L}{2E_L} ds_L \delta^4(L - p_\ell - p_\nu) \quad , \quad E_L = \sqrt{\vec{L}^2 + s_L}, \tag{157}$$

then

$$d(PS) = ds_M ds_L \frac{1}{(2\pi)^8} I_M I_L I_B \quad , \tag{158}$$

where

$$\begin{aligned} I_M &= \int \frac{d^3p}{2E_p} \frac{d^3q}{2E_q} \delta^4(P - p - q) \\ &= \frac{\pi}{4} \beta d\cos\theta \quad , \end{aligned} \tag{159}$$

$$\begin{aligned} I_L &= \int \frac{d^3p_\ell}{2E_\ell} \frac{d^3p_\nu}{2E_\nu} \delta^4(L - p_\ell - p_\nu) \\ &= \frac{1}{8} d\cos\theta_\ell d\phi \quad , \end{aligned} \tag{160}$$

$$\begin{aligned} I_B &= \int \frac{d^3P}{2E_P} \frac{d^3L}{2E_L} \delta^4(P_B - P - L) \\ &= \pi \frac{X}{m_B^2} \quad . \end{aligned} \tag{161}$$

Finally, we obtain the desired result

$$d(PS) = \frac{1}{2(4\pi)^6 m_B^2} X \beta ds_M ds_L d\cos\theta d\cos\theta_\ell d\phi \quad . \tag{162}$$

The region of integration is specified by

$$0 < s_L < (m_B - \sqrt{s_M})^2 \quad , \tag{163}$$

$$(m + m_\pi)^2 < s_M < m_B^2 \quad , \tag{164}$$

$$0 < \theta \, , \theta_\ell < \pi \quad , \tag{165}$$

$$0 < \phi < 2\pi \quad . \tag{166}$$

In the next two sections we will consider the single particle energy spectra in the laboratory frame (the B-frame). For this purpose we can make use of the relations (147)-(151) and (152)-(154) to change variables from s_M and s_L to E_p and E_ℓ or E_q and E_ℓ. For example,

$$ds_M ds_L = \left[\frac{\partial(E_p \, , E_\ell)}{\partial(s_M \, , s_L)}\right]^{-1} dE_p dE_\ell \quad . \tag{167}$$

The Jacobian in (167) can be computed from (147)-(151) and (152)-(154). Other expressions for the four-body phase space element which were useful in doing numerical calculations and verifying results are found in [30].

When performing Monte Carlo integration to compute a decay rate, convergence is improved significantly by performing a change of variables which "smooths-out" the integrand (variance reduction). When computing $\bar{B} \to D\pi\ell\bar{\nu}$ it is important to use this method since the resonance causes the propagator of the intermediate D^* to be very sharply peaked. A useful change of variables is:

$$\int_c^d dx f(x) = \int_0^1 d\eta N \left[(x-a)^2 + b^2\right] f(x) \tag{168}$$

where

$$x(\eta) \equiv a + b \tan\left[\tan^{-1}\left(\frac{c-a}{b}\right) + Nb\eta\right] \tag{169}$$

and

$$N \equiv \frac{1}{b}\left[\tan^{-1}\left(\frac{d-a}{b}\right) - \tan^{-1}\left(\frac{c-a}{b}\right)\right]. \tag{170}$$

The quantity in square brackets in (168) is used to cancel the nearly divergent denominator of the D^* propagator, thus reducing the variance of the integral.

5.3 The Semileptonic Decay $\bar{B} \to D + \pi + \ell\bar{\nu}$

The general formalism for this type of decay has been worked out by several authors [8, 25, 26, 27]. The hadronic matrix element for this process contains four form factors. We will not repeat the analysis here. As described in Sec. 4, the combined heavy quark symmetry and chiral symmetry requires only a single form factor to describe the decay, provided the emitted pion is soft.

The essential results are summarized below. The effective Lagrangian for semileptonic weak decays is given by

$$\mathcal{L}_{\text{eff}} = \frac{G_F}{\sqrt{2}} J^\mu j_\mu \quad , \tag{171}$$

where G_F is the Fermi coupling constant, J_μ the charged hadronic weak current and j_μ the lepton's charged weak current. To be specific, let us consider $\bar{B}^0 \to D^+ + \pi^0 + e^- \bar{\nu}_e$. We have followed the convention that a $\bar{B}$ meson contains a b quark, while a D meson contains a c quark. The matrix element is given by

$$M_{fi} = \frac{G_F}{\sqrt{2}} V_{cb} \langle \pi^0(q) D^+(p) \mid J_\mu^{cb} \mid \bar{B}^0(P_B) \rangle \bar{u}(p_\ell) \gamma^\mu (1 - \gamma_5) v(p_\nu) \quad , \tag{172}$$

where V_{cb} is the CKM matrix element [31] for $b \to c$ transitions. We will write

$$\langle \pi^0(q) D^+(p) \mid J_\mu^{cb} \mid \bar{B}^0(P_B) \rangle = \frac{if}{2f_\pi} \sqrt{m_B m_D} C_{cb} \xi H_\mu \quad , \tag{173}$$

where the pion decay constant $f_\pi = 93$ MeV, f is the $D^* D\pi$ coupling constant, ξ is the universal Isgur-Wise function normalized to

$$\xi(v \cdot v') = 1 \quad \text{at} \quad v = v' \quad , \tag{174}$$

and C_{cb} is the QCD correction factor

$$C_{cb}(v\cdot v') = \left[\frac{\alpha_s(m_b)}{\alpha_s(m_c)}\right]^{-\frac{6}{25}} \left[\frac{\alpha_s(m_c)}{\alpha_s(\mu)}\right]^{a_L(v\cdot v')} \quad , \tag{175}$$

$$a_L(w) = \frac{8}{27}\left[\frac{w}{\sqrt{w^2-1}}\ln\left(w+\sqrt{w^2-1}\right)-1\right] \quad . \tag{176}$$

The quantity H_μ can be extracted from the result in [8]; it is given by

$$H_\mu = w_1 v_\mu + w_2 v'_\mu + r q_\mu + ih\epsilon_{\mu\nu\lambda\kappa} q^\nu v'^\lambda v^\kappa \quad , \tag{177}$$

where the four-velocities v and v' are defined by

$$P_B = m_B v \quad , \qquad p = m_D v' \quad . \tag{178}$$

The form factors $w_{1,2}$, r and h are explicitly known in the soft pion limit:

$$w_1 = \frac{q\cdot(v+v')}{2v\cdot q + 2\Delta_B} \quad , \tag{179}$$

$$w_2 = -\frac{q\cdot(v+v')}{2v'\cdot q - 2\Delta_D} \quad , \tag{180}$$

$$r = -(1+v\cdot v')\left[\frac{1}{2v\cdot q+2\Delta_B} - \frac{1}{2v'\cdot q - 2\Delta_D}\right] \quad , \tag{181}$$

$$h = \frac{1}{2v\cdot q+2\Delta_B} - \frac{1}{2v'\cdot q-2\Delta_D} \quad , \tag{182}$$

$$\Delta_B \equiv m_{B^*} - m_B \quad , \qquad \Delta_D \equiv m_{D^*} - m_D \quad . \tag{183}$$

In the numerical calculations, we have incorporated the finite width of D^*, Γ_{D^*}, to properly handle the D^* resonance by making the replacement:

$$\frac{1}{2v'\cdot q - 2\Delta_D} \rightarrow \frac{m_{D^*}}{(p+q)^2 - m_{D^*}^2 + i m_{D^*}\Gamma_{D^*}} \quad . \tag{184}$$

The differential decay rate is then

$$\begin{aligned} d\Gamma\left(\bar{B}^0 \rightarrow D^+ + \pi^0 + e^-\bar{\nu}_\ell\right) &= \frac{1}{2m_B} \mid M_{fi} \mid^2 d(PS) \\ &= \frac{G_F^2 m_D}{8m_B^2(4\pi)^6}\left(\frac{f}{f_\pi}C_{cb}\xi\right)^2 \mid V_{cb} \mid^2 \left(\frac{1}{4}H_\mu H_\nu^* L^{\mu\nu}\right) \\ &\times \beta X ds_M ds_L d\cos\theta d\cos\theta_\ell d\phi \quad , \end{aligned} \tag{185}$$

where the lepton tensor $L_{\mu\nu}$ is given by

$$L_{\mu\nu} = 4(L_\mu L_\nu - N_\mu N_\nu - s_L g_{\mu\nu} - i\epsilon_{\mu\nu\lambda\kappa}L^\lambda N^\kappa) \quad . \tag{186}$$

For a charged pion in the final state, the above expression (185) for $d\Gamma$ has to be multiplied by 2 due to isospin. A straightforward but tedious calculation gives

$$\begin{aligned} \frac{1}{4}H_\mu H_\nu^* L^{\mu\nu} &= \mid w_1 v\cdot L + w_2 v'\cdot L + r q\cdot L \mid^2 \\ &\quad - \mid w_1 v\cdot N + w_2 v'\cdot N + r q\cdot N - i\frac{h}{2m_B m_D}\sigma \mid^2 \\ &\quad - s_L\Big\{\mid w_1 \mid^2 + (w_1 w_2^* + w_1^* w_2) v\cdot v' + (w_1 r^* + w_1^* r) v\cdot q \\ &\quad + \mid w_2 \mid^2 + (w_2 r^* + w_2^* r) v'\cdot q + \mid r \mid^2 m_\pi^2 + \\ &\quad + \mid h \mid^2 \Big[m_\pi^2\Big((v\cdot v')^2 - 1\Big) - 2(v\cdot q)(v'\cdot q)(v\cdot v') + (q\cdot v)^2 \\ &\qquad + (q\cdot v')^2\Big]\Big\} \\ &\quad - i\left\{\frac{1}{2m_B m_D}(w_1 w_2^* - w_1^* w_2) - \frac{1}{2m_B}(w_1 r^* - w_1^* r)\right. \\ &\qquad \left. - \frac{1}{2m_D}(w_2 r^* - w_2^* r)\right\}\sigma \\ &\quad + (h w_1^* + h^* w_1)\left[-(v\cdot q)(L\cdot v')(N\cdot v) - (v\cdot v')(L\cdot v)(N\cdot q)\right. \\ &\qquad - (L\cdot q)(N\cdot v') + (v\cdot v')(L\cdot q)(N\cdot v) + (L\cdot v')(N\cdot q) \\ &\qquad \left. + (v\cdot q)(L\cdot v)(N\cdot v')\right] \end{aligned}$$

$$
\begin{aligned}
&+(hw_2^* + h^* w_2)\,[-(v'\cdot q)(L\cdot v')(N\cdot v) - (L\cdot v)(N\cdot q) \\
&\quad -(v\cdot v')(L\cdot q)(N\cdot v') \\
&+(L\cdot q)(N\cdot v) + (v\cdot v')(L\cdot v')(N\cdot q) + (v'\cdot q)(L\cdot v)(N\cdot v')] \\
&+(hr^* + h^* r)\,\Big[-m_\pi^2(L\cdot v')(N\cdot v) - (q\cdot v')(L\cdot v)(N\cdot q) \\
&\quad -(q\cdot v)(L\cdot q)(N\cdot v') + (q\cdot v')(L\cdot q)(N\cdot v) \\
&\quad +(q\cdot v)(L\cdot v')(N\cdot q) + m_\pi^2(L\cdot v)(N\cdot v')\Big] \quad . \qquad (187)
\end{aligned}
$$

where σ is the pseudoscalar defined by (148). In deriving (187) we have also made use of the relations

$$\epsilon_{\mu\nu\lambda\kappa} N^\mu q^\nu v'^\lambda v^\kappa = -\frac{1}{2m_B m_D}\sigma \quad , \qquad (188)$$

$$\epsilon_{\mu\nu\lambda\kappa} L^\mu N^\nu v^\lambda v'^\kappa = \frac{1}{2m_B m_D}\sigma \quad , \qquad (189)$$

$$\epsilon_{\mu\nu\lambda\kappa} v'^\mu q^\nu L^\lambda N^\kappa = -\frac{1}{2m_D}\sigma \quad , \qquad (190)$$

$$\epsilon_{\mu\nu\lambda\kappa} v^\mu q^\nu L^\lambda N^\kappa = -\frac{1}{2m_B}\sigma \quad . \qquad (191)$$

With the help of (147)-(151), (152)-(154) and (167), we can work out the single-particle spectra $d\Gamma/dE_D$, $d\Gamma/dE_\pi$ and $d\Gamma/dE_\ell$. They will be discussed in Sec. 5.5.

5.4 The Semileptonic Decay $\bar{B} \to D^* + \pi + \ell\bar{\nu}$

The kinematics for this decay is very similar to the one discussed in previous sections. The new feature here is the polarization of the vector meson D^* which we will exploit in our study.

In analogy with (173) for $\bar{B} \to D\pi\ell\bar{\nu}$ we define

$$\langle D^{*+}(p)\pi^0(q) \mid J_\mu^{cb} \mid \bar{B}^0(P_B)\rangle = -\frac{i}{2}\sqrt{m_B m_{D^*}}\frac{f}{f_\pi}C_{cb}\xi H'_\mu \quad , \tag{192}$$

where an extra minus sign is introduced here compared with (173) due to the scalar products involving the polarization vector ε_μ of D^*. Heavy quark symmetry and chiral dynamics have a definite prediction for H'_μ when the emitted pion is soft. In this limit we find from [8]

$$\begin{aligned} H'_\mu &= a_1 v_\mu + a_2 v'_\mu + a_3 q_\mu + a_4 \varepsilon^*_\mu \\ &+ i\epsilon_{\mu\nu\lambda\kappa}\varepsilon^{*\nu}\left(b_1 q^\lambda v'^\kappa + b_2 q^\lambda v^\kappa + b_3 v^\lambda v'^\kappa\right) \quad , \end{aligned} \tag{193}$$

where

$$P_B = m_B v \quad , \qquad p = m_{D^*} v' \quad , \tag{194}$$

and

$$a_1 = -\left[\frac{1}{-2v\cdot q - 2\Delta_B} + \frac{1}{2v'\cdot q + 2\Delta_D}\right](\varepsilon^*\cdot q) \quad , \tag{195}$$

$$\begin{aligned} a_2 &= \frac{1}{-2v\cdot q - 2\Delta_B}\left[(\varepsilon^*\cdot v)(v\cdot q) - \varepsilon^*\cdot q\right] \\ &\quad -\frac{1}{2v'\cdot q}\left[i\epsilon_{\rho\sigma\lambda\kappa}q^\rho\varepsilon^{*\sigma}v'^\lambda v^\kappa + (q\cdot v')(\varepsilon^*\cdot v)\right] \\ &\quad -\frac{1}{2v'\cdot q + 2\Delta_D}(\varepsilon^*\cdot q) \quad , \end{aligned} \tag{196}$$

$$a_3 = \left[\frac{1}{-2v\cdot q - 2\Delta_B} + \frac{1}{2v'\cdot q}\right](\varepsilon^*\cdot v) \quad , \tag{197}$$

$$a_4 = \frac{1}{-2v\cdot q - 2\Delta_B}\left[(q\cdot v') - (v\cdot v')(v\cdot q)\right]$$

$$-\frac{1}{2v'\cdot q}\left[(q\cdot v)-(v\cdot v')(v'\cdot q)\right] \quad , \tag{198}$$

$$b_1=\frac{1}{-2v\cdot q-2\Delta_B}+\frac{1}{2v'\cdot q}(1+v\cdot v') \quad , \tag{199}$$

$$b_2=\frac{1}{-2v\cdot q-2\Delta_B} \quad , \tag{200}$$

$$b_3=\frac{-(q\cdot v)}{-2v\cdot q-2\Delta_B} \quad . \tag{201}$$

In our numerical calculations for this process we will not employ the full propagator (184) as we do for the decay $\bar{B}\to D\pi\ell\bar{\nu}$, since none of the intermediate states can become real here.

The absolute value squared of the matrix element involves

$$\begin{aligned}\frac{1}{4}H'_\mu H'^*_\nu L^{\mu\nu} &= \mid H'\cdot L\mid^2-\mid H'\cdot N\mid^2-s_L H'\cdot H'^* \\ &\quad -i\epsilon^{\mu\nu\lambda\kappa}H'_\mu H'^*_\nu L_\lambda N_\kappa \quad ,\end{aligned} \tag{202}$$

where the lepton tensor $L_{\mu\nu}$ is the same as the one given by (186). Each term in (202) is straightforward to compute, though it is tedious sometimes.

To begin with, we introduce the quantities

$$\sigma_1=\epsilon_{\mu\nu\lambda\kappa}N^\mu\varepsilon^{*\nu}q^\lambda v'^\kappa \quad , \tag{203}$$

$$\sigma_2=\epsilon_{\mu\nu\lambda\kappa}N^\mu\varepsilon^{*\nu}q^\lambda v^\kappa \quad , \tag{204}$$

$$\sigma_3=\epsilon_{\mu\nu\lambda\kappa}N^\mu\varepsilon^{*\nu}v^\lambda v'^\kappa \quad , \tag{205}$$

$$\sigma_4=\epsilon_{\mu\nu\lambda\kappa}v^\mu\varepsilon^{*\nu}q^\lambda v'^\kappa \quad . \tag{206}$$

and

$$\sigma'_1=\epsilon_{\mu\nu\lambda\kappa}\varepsilon^{*\mu}\varepsilon^\nu q^\lambda v'^\kappa \quad , \tag{207}$$

$$\sigma_2' = \epsilon_{\mu\nu\lambda\kappa}\varepsilon^{*\mu}\varepsilon^{\nu}q^{\lambda}v^{\kappa} \quad , \tag{208}$$

$$\sigma_3' = \epsilon_{\mu\nu\lambda\kappa}\varepsilon^{*\mu}\varepsilon^{\nu}v^{\lambda}v'^{\kappa} \quad , \tag{209}$$

$$\sigma_4' = \epsilon_{\mu\nu\lambda\kappa}\varepsilon^{*\mu}\varepsilon^{\nu}L^{\lambda}N^{\kappa} \quad . \tag{210}$$

Then, we find

$$\begin{aligned} H' \cdot L &= a_1 v \cdot L + a_2 v' \cdot L + a_3 q \cdot L + a_4 \varepsilon^* \cdot L \\ &\quad + i\sigma_4(m_B b_1 + m_{D^*} b_2 + b_3) \quad , \end{aligned} \tag{211}$$

$$\begin{aligned} H' \cdot N &= a_1 v \cdot N + a_2 v' \cdot N + a_3 q \cdot N + a_4 \varepsilon^* \cdot N \\ &\quad + i(\sigma_1 b_1 + \sigma_2 b_2 + \sigma_3 b_3) \quad , \end{aligned} \tag{212}$$

$$H' \cdot H'^* = T_a + T_{ab} + T_b \quad , \tag{213}$$

$$\begin{aligned} T_a &= \mid a_1 \mid^2 + \mid a_2 \mid^2 + \mid a_3 \mid^2 m_\pi^2 - \mid a_4 \mid^2 + (a_1 a_2^* + a_1^* a_2) v \cdot v' \\ &\quad + (a_1 a_3^* + a_1^* a_3) v \cdot q + (a_2 a_3^* + a_2^* a_3) v' \cdot q \\ &\quad + a_1 a_4^* \varepsilon \cdot v + a_1^* a_4 \varepsilon^* \cdot v + a_3 a_4^* \varepsilon \cdot q + a_3^* a_4 \varepsilon^* \cdot q \quad , \end{aligned} \tag{214}$$

$$\begin{aligned} T_{ab} &= -i a_1 b_1^* \sigma_4^* + i a_1^* b_1 \sigma_4 + i a_2 b_2^* \sigma_4^* - i a_2^* b_2 \sigma_4 \\ &\quad + i a_3 b_3^* \sigma_4^* - i a_3^* b_3 \sigma_4 \\ &\quad - i(a_4 b_1^* + a_4^* b_1)\sigma_1' - i(a_4 b_2^* + a_4^* b_2)\sigma_2' \\ &\quad - i(a_4 b_3^* + a_4^* b_3)\sigma_3' \quad , \end{aligned} \tag{215}$$

$$T_b = \mid b_1 \mid^2 \left[m_\pi^2 + \mid \varepsilon \cdot q \mid^2 - (q \cdot v')^2 \right]$$

$$
\begin{aligned}
&+\mid b_2 \mid^2 \Big[m_\pi^2-(\varepsilon^*\cdot q)(\varepsilon\cdot v)(q\cdot v)-(\varepsilon^*\cdot v)(\varepsilon\cdot q)(q\cdot v)+\mid \varepsilon\cdot q\mid^2\\
&\qquad +|\varepsilon\cdot v|^2 m_\pi^2-(q\cdot v)^2\Big]\\
&+\mid b_3\mid^2\Big[1+\mid \varepsilon\cdot v\mid^2-(v\cdot v')^2\Big]\\
&+b_1b_2^*\Big[m_\pi^2(v\cdot v')-(\varepsilon^*\cdot v)(\varepsilon\cdot q)(v'\cdot q)+\mid\varepsilon^*\cdot q\mid^2(v\cdot v')-(q\cdot v)(q\cdot v')\Big]\\
&+b_1^*b_2\Big[m_\pi^2(v\cdot v')-(\varepsilon\cdot v)(\varepsilon^*\cdot q)(v'\cdot q)+\mid\varepsilon^*\cdot q\mid^2(v\cdot v')-(q\cdot v)(q\cdot v')\Big]\\
&+b_2b_3^*\Big[(q\cdot v)(v\cdot v')-\mid\varepsilon\cdot v\mid^2(q\cdot v')+(\varepsilon^*\cdot v)(\varepsilon\cdot q)(v\cdot v')\\
&\quad -(q\cdot v')]\\
&+b_2^*b_3\Big[(q\cdot v)(v\cdot v')-\mid\varepsilon\cdot v\mid^2(q\cdot v')+(\varepsilon\cdot v)(\varepsilon^*\cdot q)(v\cdot v')\\
&\quad -(q\cdot v')]\\
&+b_3b_1^*\left[(q\cdot v)+(\varepsilon^*\cdot q)(\varepsilon\cdot v)-(q\cdot v')(v\cdot v')\right]\\
&+b_3^*b_1\left[(q\cdot v)+(\varepsilon\cdot q)(\varepsilon^*\cdot v)-(q\cdot v')(v\cdot v')\right] \quad . \qquad (216)
\end{aligned}
$$

Similarly, we write

$$
i\epsilon^{\mu\nu\lambda\kappa}H'_\mu H'^*_\nu L_\lambda N_\kappa = R_a + R_{ab} + R_b \quad , \qquad (217)
$$

where

$$
\begin{aligned}
R_a \;=\;& i\mid a_4\mid^2\sigma'_4+\mathrm{Im}\Big\{\sigma\left(-\frac{1}{m_Bm_{D^*}}a_1a_2^*+\frac{1}{m_B}a_1a_3^*+\frac{1}{m_{D^*}}a_2a_3^*\right)\\
&-2\sigma_1^*(a_2a_4^*-m_{D^*}a_3a_4^*)-2\sigma_2^*(m_Ba_3a_4^*+a_1a_4^*)\\
&+2\sigma_3^*(m_{D^*}a_1a_4^*+m_Ba_2a_4^*)\Big\} \qquad (218)
\end{aligned}
$$

$$
\begin{aligned}
R_{ab} \;=\;& 2\mathrm{Re}\left\{a_1^*b_1\left[(v\cdot\varepsilon^*)(L\cdot q)(N\cdot v')+(N\cdot\varepsilon^*)(v\cdot q)(L\cdot v')\right.\right.\\
&+(L\cdot\varepsilon^*)(N\cdot q)(v\cdot v')\\
&\left.-(L\cdot\varepsilon^*)(v\cdot q)(N\cdot v')-(N\cdot\varepsilon^*)(L\cdot q)(v\cdot v')-(v\cdot\varepsilon^*)(N\cdot q)(L\cdot v')\right]\\
&+a_1^*b_2\left[(v\cdot\varepsilon^*)(L\cdot q)(N\cdot v)+(N\cdot\varepsilon^*)(v\cdot q)(L\cdot v)+(L\cdot\varepsilon^*)(N\cdot q)\right.\\
&\left.-(L\cdot\varepsilon^*)(v\cdot q)(N\cdot v)-(N\cdot\varepsilon^*)(L\cdot q)-(v\cdot\varepsilon^*)(N\cdot q)(L\cdot v)\right]
\end{aligned}
$$

$$
\begin{aligned}
&+a_1^* b_3\,[(v\cdot\varepsilon^*)(L\cdot v)(N\cdot v')+(N\cdot\varepsilon^*)(L\cdot v')+(L\cdot\varepsilon^*)(N\cdot v)(v\cdot v')\\
&-(L\cdot\varepsilon^*)(N\cdot v')-(N\cdot\varepsilon^*)(L\cdot v)(v\cdot v')-(v\cdot\varepsilon^*)(N\cdot v)(L\cdot v')]\\
&+a_2^* b_1\,[(N\cdot\varepsilon^*)(v'\cdot q)(L\cdot v')+(L\cdot\varepsilon^*)(N\cdot q)\\
&-(L\cdot\varepsilon^*)(v'\cdot q)(N\cdot v')-(N\cdot\varepsilon^*)(L\cdot q)]\\
&+a_2^* b_2\,[(N\cdot\varepsilon^*)(v'\cdot q)(L\cdot v)+(L\cdot\varepsilon^*)(N\cdot q)(v\cdot v')\\
&\quad-(L\cdot\varepsilon^*)(v'\cdot q)(N\cdot v)-(N\cdot\varepsilon^*)(L\cdot q)(v\cdot v')]\\
&+a_2^* b_3\,[(N\cdot\varepsilon^*)(v\cdot v')(L\cdot v')+(L\cdot\varepsilon^*)(N\cdot v)-(L\cdot\varepsilon^*)(v\cdot v')(N\cdot v')\\
&-(N\cdot\varepsilon^*)(L\cdot v)]\\
&+a_3^* b_1\,\Big[(q\cdot\varepsilon^*)(L\cdot q)(N\cdot v')+(N\cdot\varepsilon^*)m_\pi^2(L\cdot v')\\
&+(L\cdot\varepsilon^*)(N\cdot q)(q\cdot v')\\
&-(L\cdot\varepsilon^*)m_\pi^2(N\cdot v')-(N\cdot\varepsilon^*)(L\cdot q)(q\cdot v')-(q\cdot\varepsilon^*)(N\cdot q)(L\cdot v')\Big]\\
&+a_3^* b_2\,\Big[(q\cdot\varepsilon^*)(L\cdot q)(N\cdot v)+(N\cdot\varepsilon^*)m_\pi^2(L\cdot v)+(L\cdot\varepsilon^*)(N\cdot q)(q\cdot v)\\
&-(L\cdot\varepsilon^*)m_\pi^2(N\cdot v)-(N\cdot\varepsilon^*)(L\cdot q)(q\cdot v)-(q\cdot\varepsilon^*)(N\cdot q)(L\cdot v)\Big]\\
&+a_3^* b_3\,[(q\cdot\varepsilon^*)(L\cdot v)(N\cdot v')+(N\cdot\varepsilon^*)(q\cdot v)(L\cdot v')\\
&+(L\cdot\varepsilon^*)(N\cdot v)(q\cdot v')\\
&-(L\cdot\varepsilon^*)(q\cdot v)(N\cdot v')-(N\cdot\varepsilon^*)(L\cdot v)(q\cdot v')-(q\cdot\varepsilon^*)(N\cdot v)(L\cdot v')]\\
&+a_4^* b_1\,[-(L\cdot q)(N\cdot v')+(N\cdot\varepsilon^*)(\varepsilon\cdot q)(L\cdot v')-(L\cdot\varepsilon^*)(\varepsilon\cdot q)(N\cdot v')\\
&+(N\cdot q)(L\cdot v')]\\
&+a_4^* b_2\,[-(L\cdot q)(N\cdot v)+(N\cdot\varepsilon^*)(\varepsilon\cdot q)(L\cdot v)+(L\cdot\varepsilon^*)(N\cdot q)(\varepsilon\cdot v)\\
&-(L\cdot\varepsilon^*)(\varepsilon\cdot q)(N\cdot v)-(N\cdot\varepsilon^*)(L\cdot q)(\varepsilon\cdot v)+(N\cdot q)(L\cdot v)]\\
&+a_4^* b_3\,[-(L\cdot v)(N\cdot v')+(N\cdot\varepsilon^*)(\varepsilon\cdot v)(L\cdot v')-(L\cdot\varepsilon^*)(\varepsilon\cdot v)(N\cdot v')\\
&+(N\cdot v)(L\cdot v')]\}\quad , \qquad (219)
\end{aligned}
$$

and

$$
\begin{aligned}
R_b \;=\; &-\mathrm{Im}\Big\{\,[(L\cdot v')(N\cdot q)-(L\cdot q)(N\cdot v')]\left(\mid b_1\mid^2\sigma_1'+b_2^*b_1\sigma_2'+b_3^*b_1\sigma_3'\right)\\
&+[(L\cdot v)(N\cdot q)-(L\cdot q)(N\cdot v)]\left(\mid b_2\mid^2\sigma_2'+b_1^*b_2\sigma_1'+b_3^*b_2\sigma_3'\right)\\
&+[(L\cdot v')(N\cdot v)-(L\cdot v)(N\cdot v')]\left(\mid b_3\mid^2\sigma_3'+b_2^*b_3\sigma_2'+b_1^*b_3\sigma_1'\right)
\end{aligned}
$$

$$+\left[(L\cdot q)(N\cdot\varepsilon^*)-(L\cdot\varepsilon^*)(N\cdot q)\right](b_1^*b_2-b_2^*b_1)\,\sigma_4^*$$
$$+\left[(L\cdot\varepsilon^*)(N\cdot v)-(L\cdot v)(N\cdot\varepsilon^*)\right](b_2^*b_3-b_3^*b_2)\,\sigma_4^*$$
$$+\left[(L\cdot v')(N\cdot\varepsilon^*)-(L\cdot\varepsilon^*)(N\cdot v')\right](b_3^*b_1-b_1^*b_3)\,\sigma_4^*\Big\}\quad . \tag{220}$$

The polarization state of a massive vector meson is not a Lorentz invariant concept. A state with a definite polarization in one frame of reference will become a linear combination of states with different polarizations in another frame of reference. When the polarization of a vector meson is specified, we have to give the frame of reference in which it is defined. In our numerical calculations and results to be presented in the next section, we will employ states of D^* with definite polarizations in the rest frame of the $\bar{B}$ meson (the B-frame). The polarization vectors in the M-frame and their Lorentz transforms in the L-frame are provided in Appendix A. Polarization vectors in the B-frame are not explicitly given, but they are not difficult to construct.

5.5 Results and Discussion

In this section we make use of the results obtained in the last two sections to compute the single particle spectra for the charmed meson (D or D^*), the pion and the electron, and the total rates for $\bar{B}\to D+\pi+\ell\bar{\nu}$ and $\bar{B}\to D^*+\pi+\ell\bar{\nu}$. These results are presented in a series of figures. The energies in the single particle spectra of these figures are those measured in the rest frame of the $\bar{B}$ meson; the polarizations of D^* are also specified in the B-frame. Since the validity of chiral symmetry demands the emitted pions be soft, we must impose cutoffs on the pion momenta in our calculation. It is not clear how soft a pion must be for chiral symmetry to work, nor is it obvious in which reference frame the pion has to be soft. For the problem at hand, there are two obvious frames: the rest frame of the $\bar{B}$ meson and the rest frame of $D(D^*)$ system. As the

pion is soft, the center of mass frame of the $D(D^*)\pi$ system is approximately the same as the rest frame of the $D(D^*)$ meson. We refer to the latter as the D-frame or the D^*-frame as the case may be. Results are presented with the pion momentum cutoff in the B-frame, the D-frame, or both. We simply cut off the pion's 3-momentum at 100 MeV/c or 200 MeV/c in the appropriate frame of reference. Comparison among the plots for different cutoffs should give some idea of the sensitivity of our results to the different cutoff procedures. Generally speaking, the shapes of various spectra do not differ very much. The rate for $\bar{B} \to D\pi\ell\bar{\nu}$ does not change by much, but that for $\bar{B} \to D^*\pi\ell\bar{\nu}$ varies by almost an order of magnitude.

Throughout our calculations, we use the following values of the well-measured parameters [20, 32]:

$$\begin{aligned} m_{B^\pm} &= 5278.6 \text{ MeV}, \qquad m_{B^0} = 5278.7 \text{ MeV}, \quad m_{B^*} = 5331.3 \text{ MeV}, \\ m_{D^0} &= 1864.5 \text{ MeV}, \qquad m_{D^\pm} = 1869.3 \text{ MeV}, \quad m_{D^{*\pm}} = 2010.1 \text{ MeV}, \\ m_{D^{*0}} &= 2007.1 \text{ MeV}, \quad f_\pi = 93.0 \text{ MeV}, \quad G_F = 1.16637 \times 10^{-11} \text{ MeV}^{-2}. \end{aligned} \tag{221}$$

We also use

$$f = -1.5 \ , \qquad \Gamma_{D^{*+}} = 141 \text{ keV} \ , \qquad \Gamma_{D^{*0}} = 102 \text{ keV} \ . \tag{222}$$

In (222), the value for the fundamental coupling constant f is the one from the quark model given in [8], and the D^* widths are the prediction from [23]. We also used other values for Γ_{D^*} as shown in Figs. 9-12. As for the Isgur-Wise form factor, we use the one given by Burdman [33]

$$\xi(y) = 1 - \rho^2(y-1) + c(y-1)^2 \ . \tag{223}$$

with

$$\rho = 1.08 \pm 0.10 \ , \qquad c = 0.62 \pm 0.15 \ . \tag{224}$$

In his fit Burdman found

$$|V_{cb}| = 0.041 \pm 0.005 \pm 0.002 \ , \tag{225}$$

which is somewhat smaller than the values obtained by several experimental analyses [34]. But it is not easy to compare (225) with other analyses since Burdman's fit includes QCD corrections. As a result, $\xi(y)$ given by (223) is only applicable to $\bar{B} \to D(D^*)$ decays.

We now consider some details of the decays $\bar{B}^0 \to D + \pi + \ell\bar{\nu}$. Since the intermediate D^* can be on its mass shell, results for this decay rate are separated into two categories: resonant and nonresonant. The resonant part is defined as those events with the invariant mass of $D\pi$ satisfying [35]:

$$\mid m(D\pi) - m_{D^*} \mid < 3\Gamma_{D^*} \ . \tag{226}$$

All others are nonresonant. For comparison with experiment, the resonant part is identified as $\bar{B}^0 \to D^*\ell\bar{\nu}$ followed by the decay of the D^* to the specific $D\pi$ state, while the nonresonant part is identified as $\bar{B}^0 \to D\pi\ell\bar{\nu}$. We have found that the contribution from the D^* pole dominates both the resonant and nonresonant decays. Since the most important Feynman diagram is Fig. 3b, where the pion is emitted in a transition from D^* to D, it is most reasonable to cut the pion's three momentum off in the D-frame. We see from Figs. 6-8 that the shapes do not change much between the single-particle spectra in the resonant region and their counterparts in the nonresonant region. However, the rates in the resonant region are larger than those in the nonresonant region by a factor of 7. When the cutoff increases from 100 MeV to 200 MeV, the

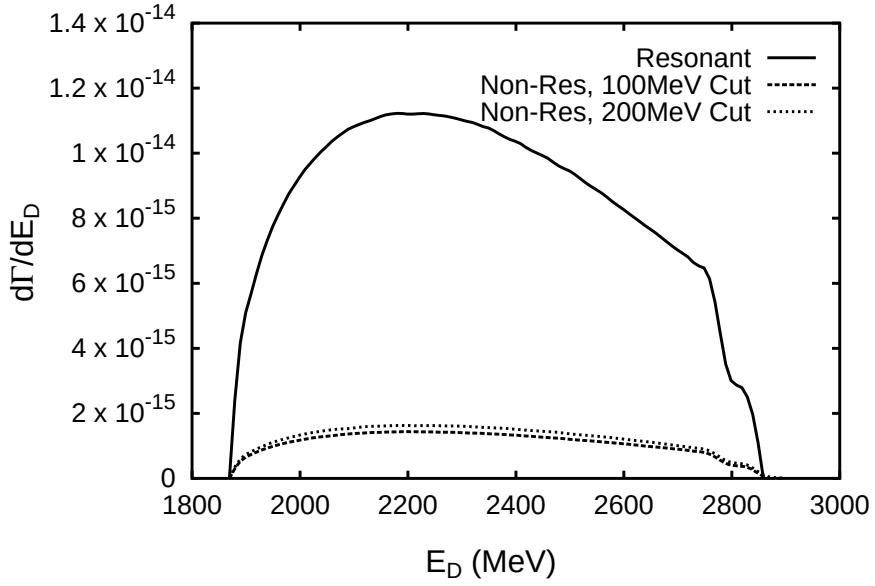

Figure 6: The energy spectra of the D meson from $\bar{B}^0 \to D^+\pi^0 e^-\bar{\nu}_e$ in the resonant region (solid line) and in the nonresonant region (broken lines). Shown are effects of two pion momentum cutoffs (100 MeV and 200 MeV) in the D-frame on the nonresonant contributions. The bump at the high energy end is an artifact of the simple cutoff imposed on the pion. The resonant contribution is not affected by these pion momentum cutoffs. The spectrum is in units of MeV / MeV.

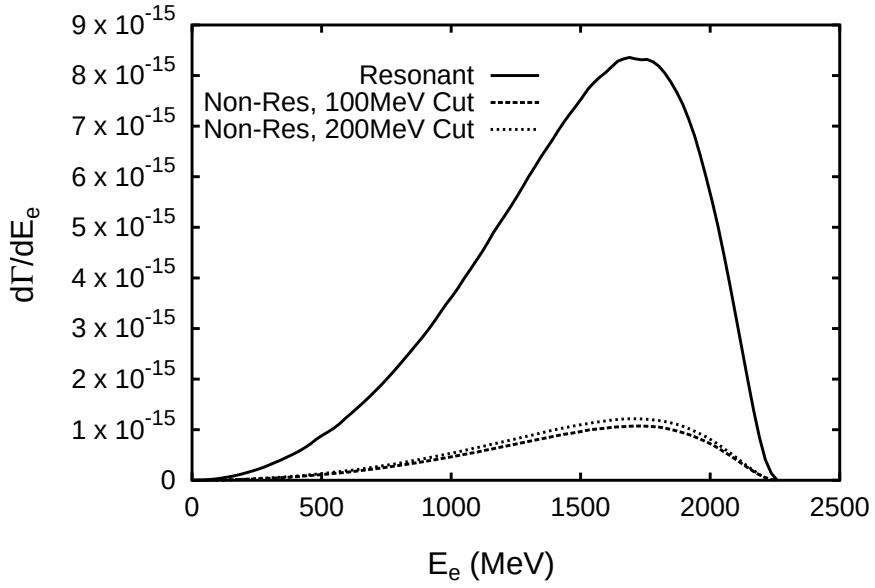

Figure 7: The energy spectra of the electron from $\bar{B}^0 \to D^+\pi^0 e^-\bar{\nu}_e$ in the resonant region (solid line) and in the nonresonant region (broken lines). Shown are effects of two pion momentum cutoffs (100 MeV and 200 MeV) in the D-frame on the nonresonant contributions. The resonant contribution is not affected by these pion momentum cutoffs. The spectrum is in units of MeV / MeV.

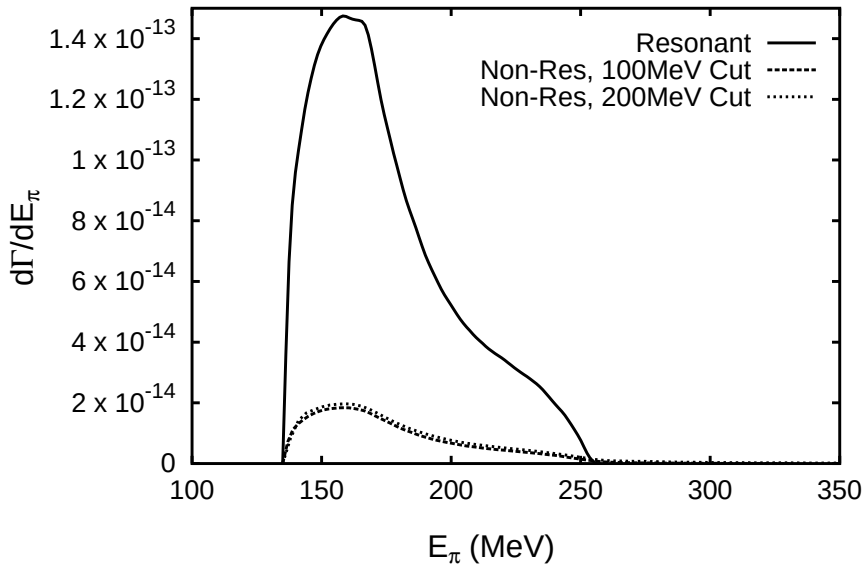

Figure 8: The energy spectra of the pion from $\bar{B}^0 \to D^+\pi^0 e^-\bar{\nu}_e$ in the resonant region (solid line) and in the nonresonant region (broken lines). Shown are effects of two pion momentum cutoffs (100 MeV and 200 MeV) in the D-frame on the nonresonant contributions. The resonant contribution is not affected by these pion momentum cutoffs. The spectrum is in units of MeV / MeV.

nonresonant rate increases by about 15%. The pion momentum cutoff of 100 MeV or 200 MeV in the D-frame has no effect on the resonant contribution, since the pion momentum in this frame is only about 40 MeV. We have investigated the sensitivity to Γ_{D^*} of the shapes of the single particle spectra. They hardly change as Γ_{D^*} varies from 0.1 MeV to 1 MeV.

To estimate the branching ratios of decays $\bar{B}^0 \to (D\pi)_{\rm res} + e^-\bar{\nu}_e$ and $\bar{B}^0 \to (D\pi)_{\rm nonres} + e^-\bar{\nu}_e$, we first convert the mean lifetime of $\bar{B}$ mesons [20]

$$\tau_B = (12.9 \pm 0.5) \times 10^{-13} s \ , \tag{227}$$

to a total decay width of

$$\Gamma_B = \frac{\hbar}{\tau} = (0.51 \pm 0.02) \times 10^{-9} \text{ MeV} \ . \tag{228}$$

The width Γ_{D^*} also affects the total decay rates for $\bar{B}^0 \to (D\pi)_{\rm res} + e^-\bar{\nu}_e$ and $\bar{B}^0 \to (D\pi)_{\rm nonres} + e^-\bar{\nu}_e$. The dependence of the integrated rates on Γ_{D^*} is displayed in Figs. 9-12. We have fixed the value of f in the amplitudes by (222), but have treated Γ_{D^*} as a free parameter in the D^* propagator (184). In this way, a linear relationship between the integrated rates and $1/\Gamma_{D^*}$ is expected theoretically. The details are presented in Appendix B. We notice that as Γ_{D^*} varies from 0.1 MeV to 1 MeV, $\Gamma[\bar{B}^0 \to (D^+\pi^0)_{\rm res} + e^-\bar{\nu}_e]$ decreases from about 1.2×10^{-11} MeV to 1.2×10^{-12} MeV for $q_{\rm max} = 100$ MeV or $q_{\rm max} = 200$ MeV. For $q_{\rm max} = 100$ MeV, the corresponding change for the rate $\Gamma[\bar{B}^0 \to (D^+\pi^0)_{\rm nonres} + e^-\bar{\nu}_e]$ is from 1.5×10^{-12} MeV to 2.2×10^{-13} MeV. For $q_{\rm max} = 200$ MeV, the corresponding change in the nonresonant rate is from 1.6×10^{-12} MeV to 3.7×10^{-13} MeV. Similar variations are also found in the rates for $B^- \to D^0\pi^0 e^-\bar{\nu}_e$ with respect to changes of Γ_{D^*} and the pion momentum cutoffs. Because $m_{D^{*0}} < m_{D^+} + m_{\pi^-}$, the rates for $B^- \to (D^+\pi^-)_{\rm res} e^-\bar{\nu}_e$ are completely

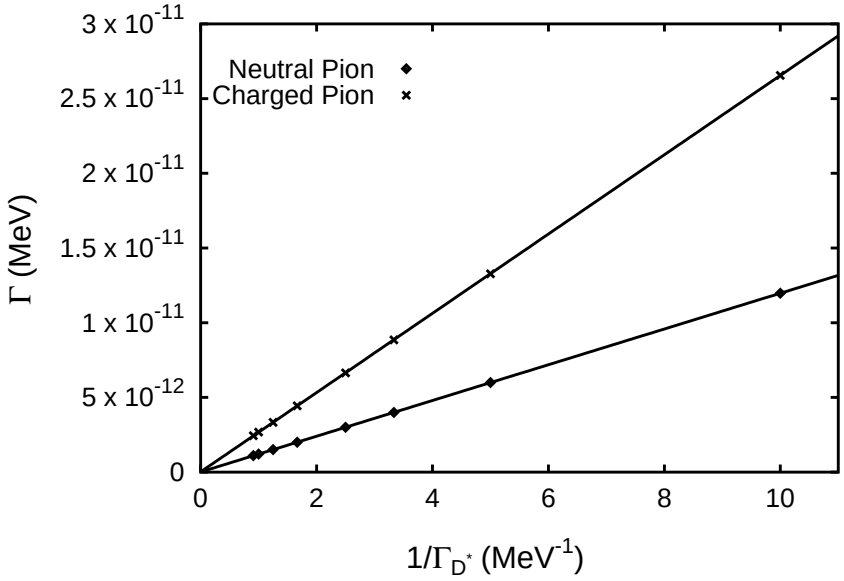

Figure 9: The decay rates $\Gamma(\bar{B}^0 \to D^+\pi^0 e^-\bar{\nu}_e)$ (labeled as neutral pion) and $\Gamma(\bar{B}^0 \to D^0\pi^+ e^-\bar{\nu}_e)$ (labeled as charged pion) in the resonant region as a function of $1/\Gamma_{D^*}$. The pion momentum cutoff of 100 MeV or 200 MeV in the D-frame has no effect on these rates.

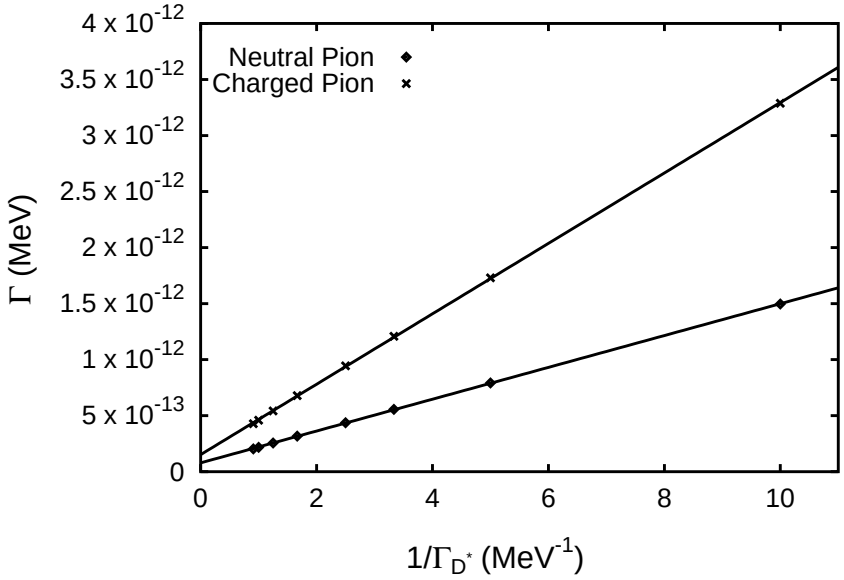

Figure 10: The decay rates $\Gamma(\bar{B}^0 \to D^+\pi^0 e^-\bar{\nu}_e)$ (labeled as neutral pion) and $\Gamma(\bar{B}^0 \to D^0\pi^+ e^-\bar{\nu}_e)$ (labeled as charged pion) in the nonresonant region as a function of $1/\Gamma_{D^*}$. The pion momentum cutoff is 100 MeV in the D-frame.

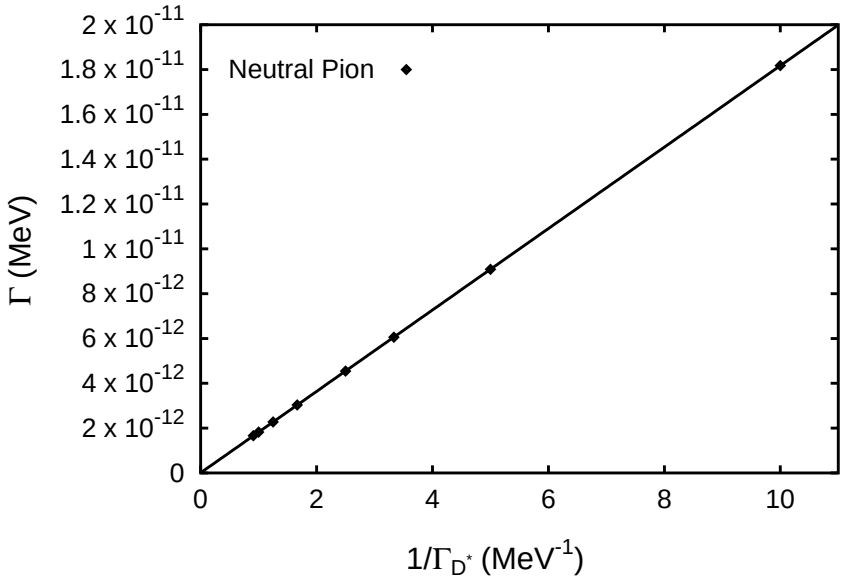

Figure 11: The decay rates $\Gamma(B^- \to D^0\pi^0 e^-\bar{\nu}_e)$ (labeled as neutral pion) in the resonant region as a function of $1/\Gamma_{D^*}$. The other mode $B^- \to D^+\pi^- e^-\bar{\nu}_e$ is kinematically forbidden in the resonant region. The pion momentum cutoff of 100 MeV or 200 MeV in the D-frame has no effect on these rates.

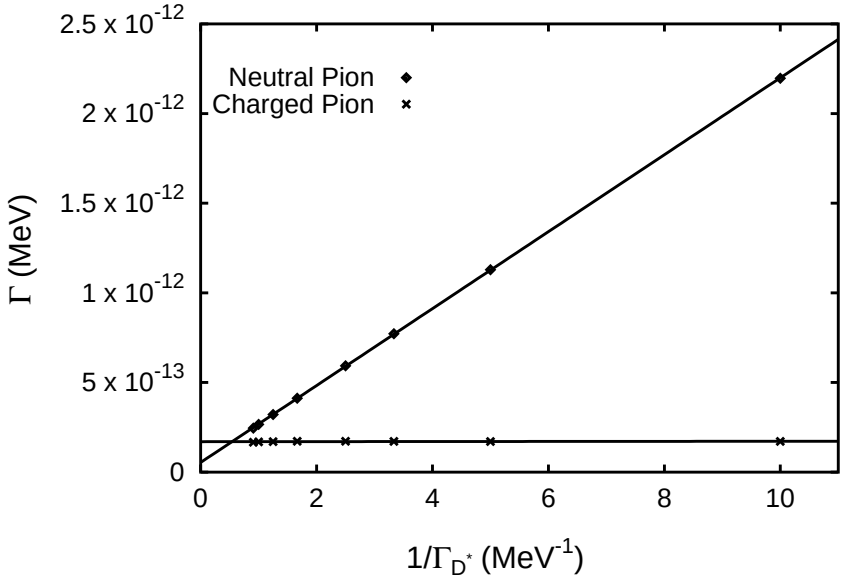

Figure 12: The decay rates $\Gamma(B^- \to D^0\pi^0 e^-\bar{\nu}_e)$ (labeled as neutral pion) and $\Gamma(B^- \to D^+\pi^- e^-\bar{\nu}_e)$ (labeled as charged pion) in the nonresonant region as a function of $1/\Gamma_{D^*}$. The pion momentum cutoff is 100 MeV in the D-frame. See Appendix B for an explanation of the different behavior of the two decay rates.

negligible. The rates for $B^- \to (D^+\pi^-)_{\rm nonres} e^-\bar{\nu}_e$ are nearly independent of Γ_{D^*}. See Appendix B for more discussion on $B^- \to D^+\pi^- e^-\bar{\nu}_e$.

From Figs. 9-12, we find the decay rates with a neutral pion

$$\Gamma[\bar{B}^0 \to (D^+\pi^0)_{\rm res} + e^-\bar{\nu}_e] = 8.50 \times 10^{-12}\,{\rm MeV}, \tag{229}$$

$$\Gamma[\bar{B}^0 \to (D^+\pi^0)_{\rm nonres} + e^-\bar{\nu}_e] = 1.09 \times 10^{-12}\,{\rm MeV}, \tag{230}$$

$$\Gamma[B^- \to (D^0\pi^0)_{\rm res} + e^-\bar{\nu}_e] = 1.78 \times 10^{-11}\,{\rm MeV}, \tag{231}$$

$$\Gamma[B^- \to (D^0\pi^0)_{\rm nonres} + e^-\bar{\nu}_e] = 2.16 \times 10^{-12}\,{\rm MeV}. \tag{232}$$

The corresponding branching ratios are

$$B[\bar{B}^0 \to (D^+\pi^0)_{\rm res} + e^-\bar{\nu}_e] = 1.67\%, \tag{233}$$

$$B[\bar{B}^0 \to (D^+\pi^0)_{\rm nonres} + e^-\bar{\nu}_e] = 0.21\%, \tag{234}$$

$$B[B^- \to (D^0\pi^0)_{\rm res} + e^-\bar{\nu}_e] = 3.49\%, \tag{235}$$

$$B[B^- \to (D^0\pi^0)_{\rm nonres} + e^-\bar{\nu}_e] = 0.42\%. \tag{236}$$

If we identify the $D\pi$'s in the resonant region with the D^*, (233) is the combined branching ratio for $\bar{B}^0 \to D^{*+} e^-\bar{\nu}_e$ and $D^{*+} \to D^+\pi^0$. The decay $D^{*+} \to D^+\pi^0$ is predicted to have a branching ratio of 31.2% [23], thus

$$\begin{aligned} B[\bar{B}^0 \to D^{*+} + e^-\bar{\nu}_e] &= \frac{B[\bar{B}^0 \to (D^+\pi^0)_{\rm res} + e^-\bar{\nu}_e]}{B[D^{*+} \to D^+\pi^0]} \\ &= 5.35\%. \end{aligned} \tag{237}$$

The agreement between (237) and the data (134) is very good. Encouraged by this success, we would like to relate (235) to the branching ratio of $B^- \to D^{*0} e^-\bar{\nu}_e$. To do this we notice that $D^{*0} \to D^+\pi^-$ is kinematically forbidden, and D^{*0} has a substantial radiative decay. Using the branching ratio of 66.7% for $D^{*0} \to D^0\pi^0$ [23], we find

$$B[B^- \to D^{*0} + e^-\bar{\nu}_e] = 5.23\%, \tag{238}$$

which agrees with the data (136). The success of the predictions (237) and (238) represents a triumph for heavy quark symmetry; it is independent of the chiral symmetry of light quarks. For the nonresonant $D\pi$ final states, we can read off from Figs. 10 and 12 the contribution from processes with a charged pion. Combining this with (229)-(232) and (233)-(236), we find

$$B[\bar{B}^0 \to (D\pi)^+_{\rm nonres} + e^-\bar{\nu}_e] = 0.68\%, \tag{239}$$

$$B[B^- \to (D\pi)^0_{\rm nonres} + e^-\bar{\nu}_e] = 0.45\%. \tag{240}$$

We notice in passing that isospin symmetry is reasonably good for $\bar{B}^0$ decays but not so for B^- decays, as a consequence of the fact that $m_{D^{*0}} < m_{D^+} + m_{\pi^-}$. So far, the results quoted above are for $q_{\rm max} = 100$ MeV in the D^* frame. For $q_{\rm max} = 200$ MeV, we obtain

$$B[\bar{B}^0 \to (D\pi)^+_{\rm nonres} + e^-\bar{\nu}_e] = 0.77\%, \tag{241}$$

$$B[B^- \to (D\pi)^0_{\rm nonres} + e^-\bar{\nu}_e] = 0.53\%. \tag{242}$$

As mentioned in Sec. 5.1, there appears to be a deficit between the branching ratio for the inclusive semileptonic decays $B \to e^\pm\nu_e$+hadrons and the sum of the two exclusive channels $B^0 \to D^-\ell^+\nu$ and $B^0 \to D^{*-}\ell^+\nu$. Our study shows that the nonresonant decay $\bar{B}^0 \to D\pi\ell\bar{\nu}$ can have a substantial branching ratio, although not enough to account for the difference. Nevertheless, it is measurable and is interesting in its own right.

Before we leave the subject of $\bar{B} \to (D\pi)_{\rm nonres}\ell\bar{\nu}$, we would like to repeat a comment made in Appendix B. The results for nonresonant contributions (230), (232), (239)-(240) and (241)-(242) are very sensitive to the definition (226) for resonant contributions. To compare our predictions with future experiments, we must bear this point in mind. Of course, the sum of the resonant and

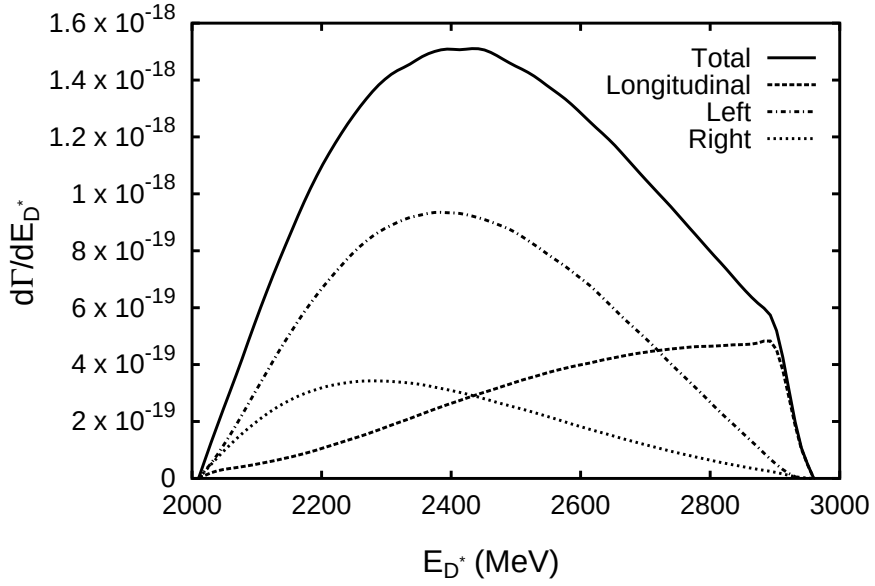

Figure 13: The energy spectra of the D^* meson with different polarizations in the B-frame from $\bar{B}^0 \to D^{*+}\pi^0 e^- \bar{\nu}_e$ with a pion momentum cutoff of 100 MeV in both the B- and D^*-frames.

nonresonant contributions is independent of this arbitrary division into resonant and nonresonant parts.

We now turn to the decay $\bar{B}^0 \to D^{*+}\pi^0 e^- \bar{\nu}_e$. The results for the pion momentum cutoff in both the B and D^* frames are shown in Figs. 13-15. For similar graphs where the pion momentum is cut off only in the B frame see Figs. 11-13 of [19]. The overall rates are smaller than $\bar{B}^0 \to D\pi\ell\bar{\nu}$ by two or three orders of magnitude. For this process, we have imposed the pion momentum cutoff in the B-frame or in both the B-frame and the D^*-frame. We see that different cutoffs give significantly different rates. In addition to the figures, integrated rates for $\bar{B}^0 \to D^{*+}\pi^0 e^- \bar{\nu}_e$ are given in Table 1.

The polarization of the vector meson D^* is a new feature of this decay. It can be exploited to study the nature of weak interaction dynamics. In Figs. 13-15, we show the single particle spectra for each polarization of D^* in the B-frame. In all cases, contributions from the left-handed and longitudinal polarizations

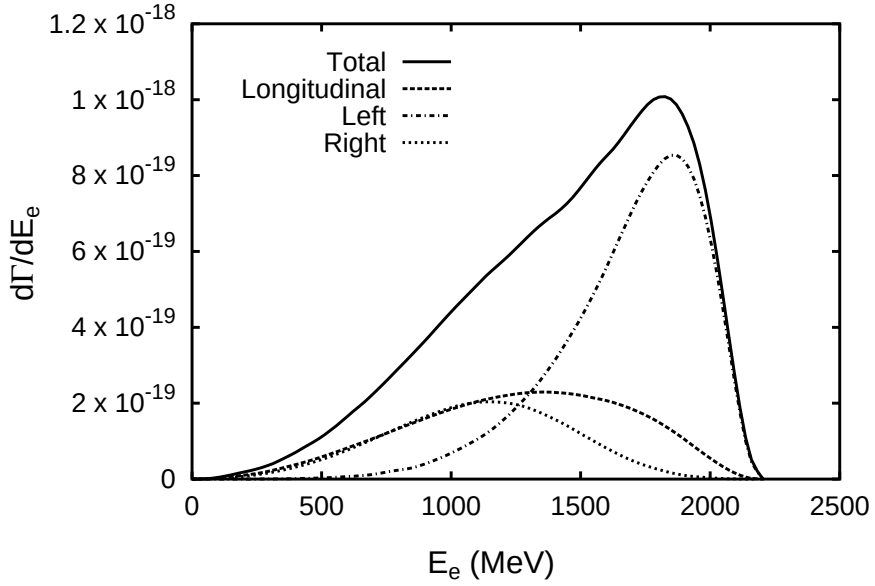

Figure 14: The energy spectra of the electron from $\bar{B}^0 \to D^{*+}\pi^0 e^- \bar{\nu}_e$ for different D^* polarizations in the B-frame with a pion momentum cutoff of 100 MeV in both the B- and D^*-frames.

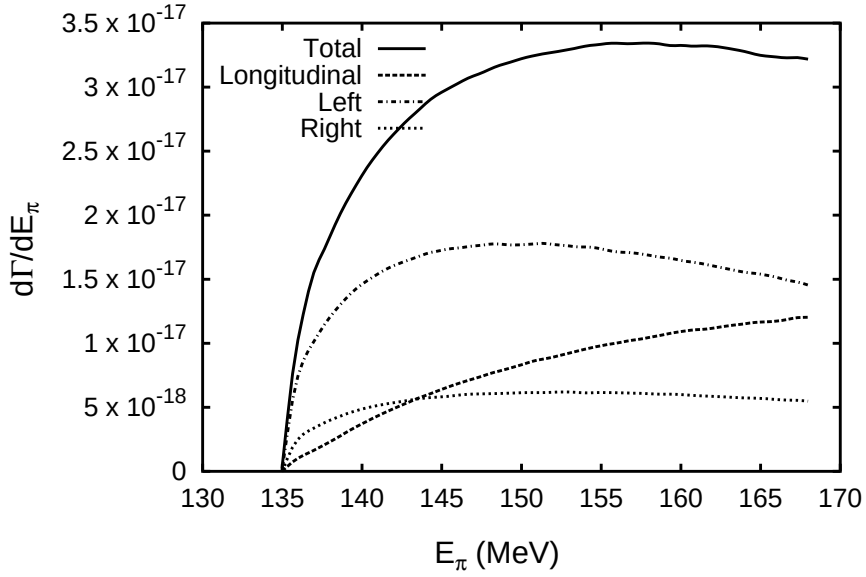

Figure 15: The energy spectra of the pion from $\bar{B}^0 \to D^{*+}\pi^0 e^- \bar{\nu}_e$ for different D^* polarizations in the B-frame with a pion momentum cutoff of 100 MeV in both the B- and D^*-frames.

Table 1: Integrated rates of $\bar{B}^0 \to D^{*+}\pi^0 e^- \bar{\nu}_e$ with different pion momentum cutoff. We also list the branching ratios and the percentage contributions from each polarization of D^* in the B-frame. The longitudinal, left-handed and right-handed polarizations are labeled L_0, L and R, respectively.

cutoff frame	pion mom. cut (MeV)	rate (MeV)	branching ratio	$L_0(\%)$	$L(\%)$	$R(\%)$
B	100	3.20×10^{-15}	0.63×10^{-5}	26	57	17
B	200	1.84×10^{-14}	0.36×10^{-4}	30	52	18
B and D^*	100	9.62×10^{-16}	0.19×10^{-5}	27	54	19
B and D^*	200	1.04×10^{-14}	0.20×10^{-4}	33	48	19

dominate that from the right-handed polarization. This can be simply understood as a result of the $V - A$ coupling of the quarks to the $W^{\pm}$ bosons. The charmed quark produced by the $\bar{B}$ decay is predominantly left-handed. The helicity of this charmed quark will not be affected by the creation of the soft pion by the light quark interactions. A simple reflection will show that a left-handed charmed quark can only lead to a vector meson D^* with a left-handed polarization or a longitudinal polarization. Since the charmed quark has a finite mass, there is some contamination from the right-handed component. This contamination should be small when the charmed quark (hence D^*) is energetic. This reasoning is indeed borne out by our calculations.

Our results so far rely on a specific fit to the Isgur-Wise form factor and a choice of the values of f, V_{cb}, etc. All these uncertainties will disappear if we take the ratio of the corresponding quantities at the same value of $v \cdot v'$ in the decays $\bar{B} \to D\pi\ell\bar{\nu}$ and $\bar{B} \to D^*\pi\ell\bar{\nu}$. These ratios are the model independent predictions from the heavy quark symmetry and chiral symmetry. They are displayed in Figs. 17-20 of [19]. We await the day when we will be able to compare these curves with experimental data.

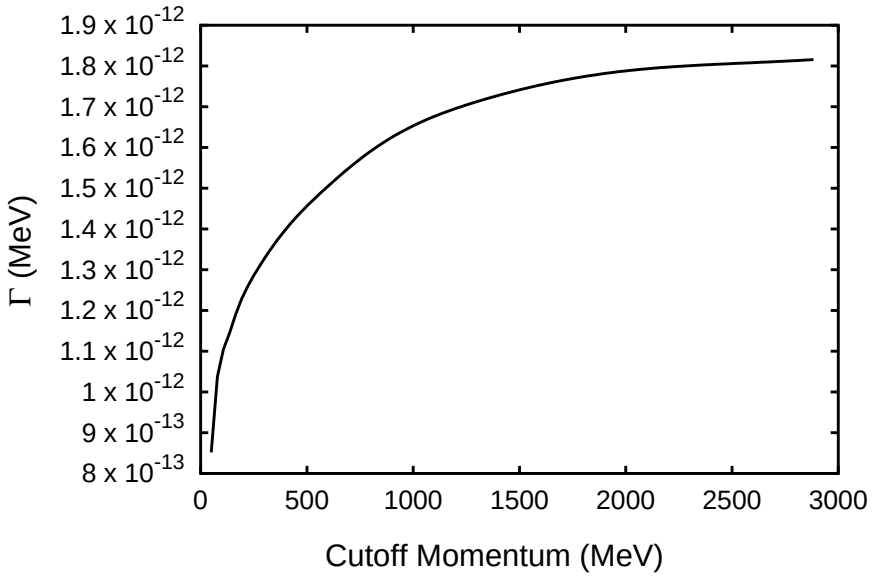

Figure 16: The decay rates $\Gamma(\bar{B}^0 \to D^+\pi^0 e^-\bar{\nu})$ for nonresonant $D^+\pi^0$ as a function of the pion momentum cutoff in the D-frame.

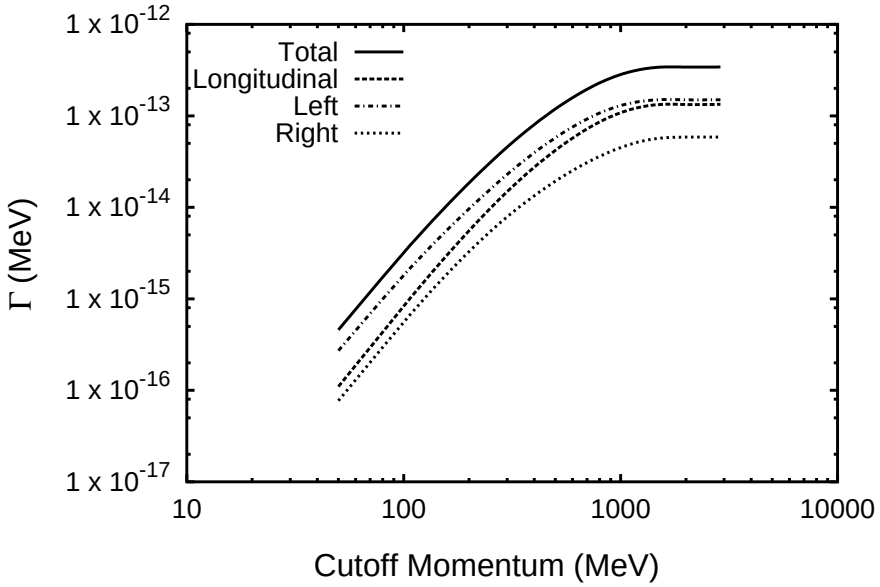

Figure 17: The decay rates $\Gamma(\bar{B}^0 \to D^{*+}\pi^0 e^-\bar{\nu})$ as a function of the pion momentum cutoff in the B-frame.

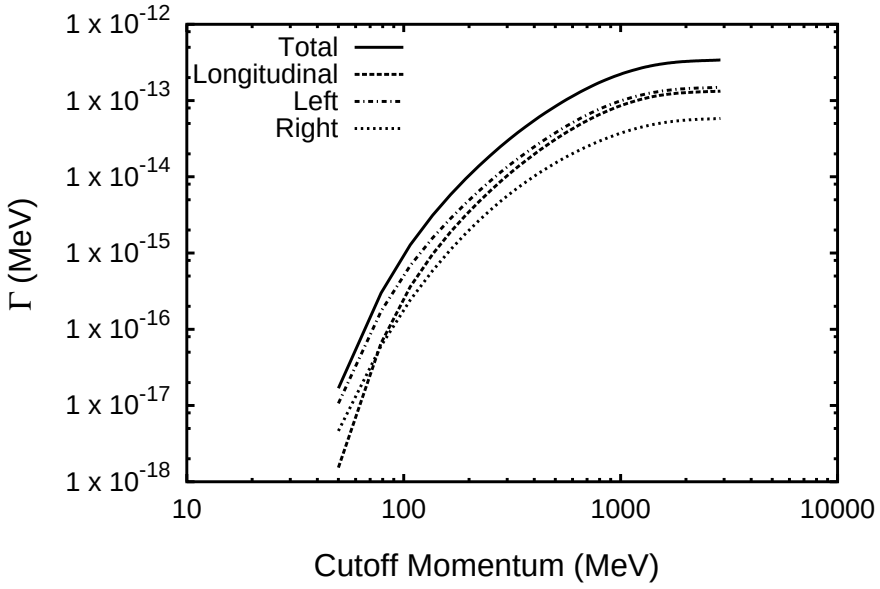

Figure 18: The decay rates $\Gamma(\bar{B}^0 \to D^{*+}\pi^0 e^-\bar{\nu})$ as a function of the pion momentum cutoff in both the B- and D^*-frame.

To get a better idea of how the decay rates depend on the pion momentum cutoffs, we have extrapolated our results beyond the soft pion limit. In Figs. 16-18, we show the various decay rates as a function of the pion momentum cutoff in the B-frame, the D-frame, or both. Since $\bar{B} \to (D\pi)_{\rm nonres}\ell\bar{\nu}$ is dominated by the D^* pole, it is not very sensitive to a change in cutoff. Unfortunately, for $\bar{B} \to D^*\pi\ell\bar{\nu}$ the rates vary rapidly with the cutoff at low pion momenta. This exercise raises an important question: What constitutes a soft pion?

Finally, so far we have completely neglected the contribution from $\bar{B} \to D^{**}\ell\bar{\nu}$, $D^{**} \to D^*\pi$. Theoretically, this is justified since D^{**} and D^* are non-degenerate, so the amplitude vanishes in the soft pion limit. However, this contribution can be important in practice. It certainly deserves further study [36]. In order to compute rates involving an intermediate D^{**} one needs form factors in addition to $\xi(v \cdot v')$. These form factors have not yet been measured experimentally or computed on the lattice. Constituent quark model predictions for the necessary form factors are given in [37].

6 Lattice Gauge Theory – Introduction

Quantum Chromodynamics (QCD) is an asymptotically free theory, so it is possible to calculate short-distance quantities using perturbation theory since the coupling is small. But there are a number of quantities that cannot be computed with perturbation theory, such as the spectrum of hadrons, form factors for hadron interactions, and quark confinement. To truly test whether or not QCD describes reality, its non-perturbative predictions must be analyzed. The desire to study the non-perturbative aspects of QCD led Wilson to formulate lattice QCD in 1974 [38]. In lattice QCD we approximate the universe by a finite number of points arranged on a finite grid. Typically (and in all work described in this dissertation), periodic boundary conditions are used. The space between adjacent points on the grid is denoted a, and we require the theory to give the continuum result as $a \to 0$.

In this dissertation we examine the connection between lattice perturbation theory and Monte Carlo simulations. It is important to be able to compute the coefficients in the pertubative expansion in order to understand the relationship between the bare parameters that are input in a simulation and the physical values that they correspond to. We show that Monte Carlo simulations can be used to compute coefficients in the lattice perturbation theory expansion. This is significant because computing the coefficients using Feynman diagrams is considerably more tedious for the lattice theory than it is for the continuum theory. Specifically, we will use Monte Carlo to compute the 2-loop term in the mass renormalization of a quark by making use of the tree and 1-loop results from lattice perturbation theory.

6.1 Discretizing QCD

In the lattice formulation, we work in Euclidean space to improve the convergence of path integrals. To achieve this, we perform a Wick rotation of the time integral in the action as is done in [39] on p. 180. Performing the Wick rotation and defining $t_E \equiv it$ gives

$$iS = i\int_{-\infty}^{\infty} d^4x\mathcal{L} = i\int_{i\infty}^{-i\infty} dt\int d^3x\mathcal{L}(t,\vec{x}) = \int_{-\infty}^{\infty} dt_E\int d^3x\mathcal{L}(-it_E,\vec{x}) \equiv -S_E. \tag{243}$$

This expression is used to find Euclidean actions from Minkowsky actions. For example, for a scalar field

$$S = \frac{1}{2}\int d^4x\phi[-\partial^2 - m_0^2]\phi \quad \Rightarrow \quad S_E = \frac{1}{2}\int dt_E d^3x\phi[-\partial_E^2 + m_0^2]\phi, \tag{244}$$

where $\partial_E = (\nabla, \partial/\partial t_E)$ (Lorentz index now runs from 1 to 4) and the Euclidean metric is $diag(1,1,1,1)$. For a continuum fermion field, we get

$$S = \int d^4x\bar{\psi}[i\not{\partial} - m]\psi \quad \Rightarrow \quad S_E = \int dt_E d^3x\bar{\psi}[\partial_E\gamma_E + m_0]\psi, \tag{245}$$

where $\gamma_E = (-i\vec{\gamma}, \gamma_0)$. The Euclidean gamma matrix relationships are derived in Appendix C. For the remainder of this dissertation, we will consider only Euclidean actions, so all subscripted E's will be dropped.

To discretize the theory, we convert derivatives into finite difference operators. Care must be taken to ensure that in the limit as the lattice spacing goes to zero, $a \to 0$, our discretized action gives the continuum result. Many discretized actions are possible which have this property. Throughout, we will deal with parameters and fields which have been rescaled by factors of a such that everything is dimensionless. Although a won't appear in our calculations explicitly, it is present implicitly in the β parameter (to be defined later). The lattice theory is a regulated theory with maximum momentum $\sim \pi/a$. The

lattice regulator does not preserve Lorentz invariance, but does preserve gauge invariance.

6.1.1 Link Variables

When a continuum theory contains a continuous global symmetry, we can make it invariant under local symmetry transformations by replacing $\partial_\mu\psi$ with $D_\mu\psi$, where $D_\mu\psi$ is the gauge covariant derivative of the fermion field. This replacement is necessary because under a unitary gauge transformation,

$$\psi(x) \to G(x)\psi(x) \quad \Rightarrow \quad \partial_\mu\psi(x) \to G(x)\partial_\mu\psi(x) + (\partial_\mu G(x))\psi(x) \tag{246}$$

so quantities in the action such as $\bar{\psi}(x)\partial\!\!\!/\psi(x)$ which are invariant under a global transformation are not invariant under a local one. We construct the gauge covariant derivative by adding a gauge boson field, $A(x)$, which transforms in such a way as to cancel the unwanted term that arises from $\partial_\mu\psi(x)$ under a local gauge transformation. Thus, $D_\mu\psi$, transforms like ψ under a local gauge transformation (see [40] for example). The gauge transformation rules are:

$$\psi(x) \to G(x)\psi(x) \qquad D_\mu\psi(x) \to G(x)D_\mu\psi(x) \tag{247}$$

where

$$D_\mu\psi(x) = [\partial_\mu + ig_0A_\mu(x)]\psi(x), \tag{248}$$

and A transforms according to

$$A_\mu(x) \to G(x)A_\mu(x)G^\dagger(x) - \frac{i}{g_0}G(x)\partial_\mu G^\dagger(x). \tag{249}$$

Quantities such as $\bar{\psi}(x)D\!\!\!/\psi(x)$ are invariant under local transformations.

We must modify this approach somewhat for the lattice theory. On the lattice, our derivatives become finite differences, so a local field won't be sufficient

to patch-up our derivative operator in order to make it gauge covariant. We can approximate the derivative of a field by

$$\partial_\mu \psi(n) = \frac{1}{2}[\psi(n+\mu) - \psi(n-\mu)] \tag{250}$$

where $\psi(n+\mu)$ means the field at the lattice site which is one step in the μ'th direction from site n. To make quantities such as $\bar{\psi}(n)\partial_\mu\psi(n)$ invariant under local transformations, we have to introduce a field $U_\mu(n)$, called a "link variable" which transforms in a non-local way (see for example chapters 5 and 6 of [41]):

$$\psi(n) \to G(n)\psi(n) \qquad U_\mu(n) \to G(n)U_\mu(n)G^\dagger(n+\mu). \tag{251}$$

The link field is related to the gauge field that we introduce in the continuum case by

$$U_\mu(n) = P\exp\left\{ig_0 \int_n^{n+\mu} dz_\nu A_\nu(z)\right\} \tag{252}$$

where there is an implicit summation on ν and the line integral is along a path connecting sites n and $n+\mu$ on the lattice. The P means that the A_ν's are ordered along the path of integration. Note that sometimes a different notation is used in the literature: $U_\mu(n) = U_{n,n+\mu}$. From (252) we see that link variables can be thought of as living on lines (links) connecting adjacent lattice sites. Now we can construct a covariant finite difference operator:

$$D_\mu\psi(n) = \frac{1}{2}[U_\mu(n)\psi(n+\mu) - U_\mu^\dagger(n-\mu)\psi(n-\mu)], \tag{253}$$

which transforms like

$$D_\mu\psi(n) \to G(n)D_\mu\psi(n). \tag{254}$$

The link variables can be represented diagramatically as shown in Fig. 19. Note that $U_\mu^\dagger(n) = U_{-\mu}(n+\mu)$.

Figure 19: Diagrammatic representation of link variables

6.1.2 Wilson Fermion Action

Now we are ready to construct the fermion action. From (245), a naive fermion action would be

$$S_F = \sum_n \bar{\psi}(n)[\not{D} + m_0]\psi(n). \tag{255}$$

However, if we transform this to momentum space and invert to find the propagator, we find that it does not produce the continuum behavior in the limit $a \to 0$. The problem is that the denominator of the momentum space propagator is of the form (after putting the a's back in):

$$\sum_\mu \left[\frac{1}{a}\sin(p_\mu a)\right]^2 + m_0^2, \tag{256}$$

If $p_\mu a$ were much smaller than π, we could approximate the sine function by just $p_\mu a$ and we would get the continuum theory in the limit $a \to 0$. But, the largest allowed momentum gives $p_\mu a = \pi$, which corresponds to a zero of the sine function. This is known as the fermion doubling problem. Several techniques have been developed to deal with this problem, and it is still an active area of research. Some of the older techniques are due to Wilson [38], and Kogut and Susskind (staggered fermions) [42]. For a more complete description, see chapter 4 of [41]. We will use Wilson's technique which involves adding a term to the action which removes the extra zeros from the momentum part of the propagator denominator. The extra term is proportional to $\bar{\psi}\Box\psi$, where $\Box$ is the lattice laplacian operator. Naive dimensional analysis shows that this term should vanish linearly with a. However, notice that this term breaks chiral symmetry (regardless of whether or not the fermions have mass) so the Wilson

method is not appropriate for studying spontaneous chiral symmetry breaking on the lattice. Our action is now

$$S_F^{(W)} = S_F - \frac{r}{2}\sum_n \bar{\psi}(n)\left[U_\mu(n)\psi(n+\mu) - 2\psi(n) + U_\mu^\dagger(n-\mu)\psi(n-\mu)\right], \quad (257)$$

where r is the Wilson parameter which we will typically set to 1. We can rewrite this as

$$S_F^{(W)} = \sum_{n,m} \bar{\psi}(n) K(U,n,m)\psi(m) \quad (258)$$

with

$$\begin{aligned} K(U,n,m) &= (m_0 + 4r)\delta_{n,m} \\ &- \frac{1}{2}\sum_\mu \left[(r-\gamma_\mu)U_\mu(n)\delta_{n+\mu,m} + (r+\gamma_\mu)U_\mu^\dagger(n-\mu)\delta_{n-\mu,m}\right] \end{aligned} \quad (259)$$

It is common to describe the quarks with the parameter

$$\kappa \equiv \frac{1}{8r + 2m_0}. \quad (260)$$

6.1.3 Gluon Action

To find a suitable lattice gluon action in terms of link variables we need to look at (252). As $a \to 0$, we can approximate the link variable by

$$U_\mu(n) \approx \exp\{ig_0 A_\mu(n)\} \approx 1 + ig_0 A_\mu(n). \quad (261)$$

To construct the lattice version of the field strength tensor, $F_{\mu\nu}$, we look at the plaquette (see Fig. 20):

$$U_{\mu\nu}(n) \equiv U_\mu(n)U_\nu(n+\mu)U_\mu^\dagger(n+\nu)U_\nu^\dagger(n) \quad (262)$$

which, using (261) and the Baker-Hausdorff formula

$$e^A e^B = e^{A+B+[A,B]/2+\ldots}, \quad (263)$$

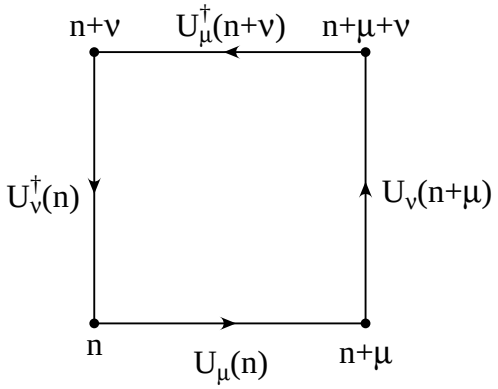

Figure 20: Diagrammatic representation of the plaquette

gives (for small a)

$$U_{\mu\nu}(n) \approx e^{ig_0 F_{\mu\nu}}, \tag{264}$$

where

$$F_{\mu\nu}(n) = \partial^R_\mu A_\nu(n) - \partial^R_\nu A_\mu(n) + ig_0[A_\mu(n), A_\nu(n)], \tag{265}$$

with $\partial^R_\mu A_\nu(n) = A_\nu(n+\mu) - A_\nu(n)$. Now we can write down the gluon action for gauge group $SU(N)$:

$$S_G = \beta \sum_P \left[1 - \frac{1}{2N} \mathrm{Tr}\left\{U_P + U_P^\dagger\right\}\right] \tag{266}$$

where

$$\beta \equiv \frac{2N}{g_0^2}, \tag{267}$$

and the sum is over all plaquettes P. We will be interested in $N = 3$ (QCD). Note that the constant term in the action can be dropped since it will always be canceled out when we compute expectation values of operators. For a more detailed treatment of the gluon action see [41].

6.1.4 Expectation Values

Now that we have the necessary actions, we can compute expectation values of time ordered products of operators using path integral methods. For example,

the quark propagator is given by

$$\begin{aligned} G(x,y) &= \langle 0|T\psi(x)\bar{\psi}(y)|0\rangle \\ &= \frac{1}{Z}\int \mathcal{D}U\mathcal{D}\bar{\psi}\mathcal{D}\psi\,\psi(x)\bar{\psi}(y)\exp\left\{-S_G(U)-S_F^{(W)}(U,\bar{\psi},\psi)\right\}, \end{aligned} \tag{268}$$

where

$$Z \equiv \int \mathcal{D}U\mathcal{D}\bar{\psi}\mathcal{D}\psi\exp\left\{-S_G(U)-S_F^{(W)}(U,\bar{\psi},\psi)\right\}. \tag{269}$$

The integration over fermion fields can be done by using a generating functional (see section 2.2.4 of [43], or 6.7 of [39]),

$$\int \mathcal{D}\bar{\psi}\mathcal{D}\psi\,\psi(x)\bar{\psi}(y)\exp\left\{-S_F^{(W)}(U,\bar{\psi},\psi)\right\} = -\frac{\delta}{\delta\bar{\eta}(x)}\frac{\delta}{\delta\eta(y)}Z_F[U,\eta,\bar{\eta}]\Big|_{\eta=\bar{\eta}=0} \tag{270}$$

where

$$Z_F[U,\eta,\bar{\eta}] \equiv \int \mathcal{D}\bar{\psi}\mathcal{D}\psi\exp\left\{-\int dx\left[\bar{\psi}K(U)\psi+\bar{\eta}\psi+\bar{\psi}\eta\right]\right\}. \tag{271}$$

Defining $\psi_m \equiv -K^{-1}\eta$ and $\bar{\psi}_m \equiv -\bar{\eta}K^{-1}$, we can rewrite this as

$$Z_F[U,\eta,\bar{\eta}] = \int \mathcal{D}\bar{\psi}\mathcal{D}\psi\exp\left\{-\int dx\left[-\bar{\eta}K^{-1}\eta+(\bar{\psi}-\bar{\psi}_m)K(\psi-\psi_m)\right]\right\}, \tag{272}$$

which we integrate to get

$$Z_F[U,\eta,\bar{\eta}] = \exp\left\{\int dx\bar{\eta}K^{-1}(U)\eta\right\}\det\left\{K(U)\right\}. \tag{273}$$

Finally, we put these results into (268) giving

$$G(x,y) = \frac{1}{Z}\int \mathcal{D}U\exp\left\{-S_G(U)\right\}\det\left\{K(U)\right\}K^{-1}(U,x,y) \tag{274}$$

with

$$Z = \int \mathcal{D}U\exp\left\{-S_G(U)\right\}\det\left\{K(U)\right\}. \tag{275}$$

On the lattice, the path integrals become a (large) finite number of integrals and we can interpret (274) as a statistical expectation value with the probability

density given by

$$\frac{1}{Z}\exp\left\{-S_G(U)\right\}\det\left\{K(U)\right\}. \tag{276}$$

Then, Monte Carlo methods can be used to do the computation (for algorithms, see [41]). Often, the "quenched approximation" is made, where $\det\{K(U)\}$ is taken to be a constant. This improves the speed of calculations. All calculations presented in this dissertation were performed in the quenched approximation. To do Monte Carlo simulations we can generate a set of gauge configurations for a particular β and lattice size using Monte Carlo methods and store them. Then, a propagator (or other quantity) can be computed by reading in the gauge configurations and evaluating the expectation value. Generally, generating the gauge configurations requires significantly more computer time than evaluating the expectation value.

6.1.5 Gauge Fixing

Gauge fixing is necessary in perturbation theory to make the gluon propagator well defined. If gauge invariant operators are to be measured in a Monte Carlo simulation, gauge fixing is not needed. However, to examine gauge dependent operators such as the fermion propagator the gauge must be fixed. Since the fundamental gauge fields on the lattice are U_μ instead of A_μ, we must figure out how to translate the familiar gauge conditions from the continuum theory to the lattice. For Landau gauge fixing, the condition is $\partial^\mu A_\mu = 0$. On the lattice, Landau gauge is obtained (for small a) by maximizing the quantity

$$\sum_x \sum_{\mu=1}^{4} \mathrm{Tr}\left\{U_\mu\right\} = \sum_x \sum_\mu \mathrm{Tr}\left\{1 - \frac{1}{2}g_0^2 A_\mu A_\mu + ...\right\} \tag{277}$$

where the term linear in A_μ is dropped because its trace is zero, and the sum over x is over all lattice sites. To see that this gives Landau gauge, we look at the continuum quantity equivalent to the A_μ^2 term. We want to show that the condi-

tion on A_μ which extremizes this term is in fact the Landau condition $\partial^\mu A_\mu = 0$. So we use (249) to write the relevant term after a gauge transformation:

$$X \equiv \mathrm{Tr}\left\{\sum_\mu \int d^4x \left[GA_\mu G^\dagger - \frac{i}{g_0} G\partial_\mu G^\dagger\right]^2\right\} \tag{278}$$

and we find the condition on A_μ which extremizes X for $G = 1$. We substitute $G(x) = \exp(i\alpha_B(x)T^B)$ into (278) and evaluate the functional derivative with respect to $\alpha_B(x)$ at $\alpha(x) = 0$:

$$\left.\frac{\delta X}{\delta \alpha_B(y)}\right|_{\alpha(y)=0} = \mathrm{Tr}\left\{-2\frac{i}{g_0} i\partial_\mu A_\mu T^B\right\} = \frac{1}{g_0}\partial_\mu A_\mu^B(y). \tag{279}$$

So, the gauge which extremizes X is the one where $\partial_\mu A_\mu^B(y) = 0$ for all B and y. In a similar way, we compute Coulomb gauge by maximizing

$$\sum_x \sum_{\mu=1}^{3} \mathrm{Tr}\,\{U_\mu\} \tag{280}$$

where the x sum is over all sites in a particular time slice of the lattice and the Lorentz index is only summed over spatial values. This maximization is done for each time slice separately. Then the quantity analogous to the X in equation (278) contains a three (instead of four) dimensional integral, and we take α_B to be a function of $\vec{x}$ instead of x_μ. Setting the functional derivative to zero gives $\nabla \cdot \vec{A} = 0$ as expected. Note that Coulomb gauge fixing does not completely fix the gauge since a transformation which depends only on time (not $\vec{x}$) does not change the quantity in (280). Axial gauge fixing can be done very efficiently on the lattice since it only involves setting certain link variables to the identity matrix (see section 13.1 of [40]). For a discussion of "Laplacian" gauge fixing and various aspects of lattice gauge fixing, see [45]. For a description of the Fourier acceleration method of performing Landau gauge fixing, see [46].

6.1.6 Relating a to β

We have been leaving the lattice spacing, a, out of the equations so far because quantities have been scaled by factors of a in order to make everything dimensionless. So, how does the lattice spacing enter into the problem? If we consider just the gauge sector of the theory, we see that there is only one adjustable parameter – the bare coupling g_0. It is the choice of the bare coupling that determines the lattice spacing. To see this, we turn the situation around and consider the question: For a given lattice spacing, what is the appropriate choice of the bare coupling to give a good approximation to the continuum result? We denote the appropriate coupling for a particular lattice spacing as $g_0(a)$. The requirement that the lattice theory is a good approximation to the continuum can be written as (for sufficiently small a)

$$\mathcal{Q}(R) = \mathcal{Q}(R, a, g_0(a)) \tag{281}$$

where $\mathcal{Q}(R)$ is some continuum quantity which depends on some physical length R, and $\mathcal{Q}(R, a, g_0(a))$ is the corresponding quantity measured on the lattice. The equality is considered to be true up to order a^n where the value of n depends on the finite lattice spacing errors in the theory. We can write $R = \hat{R}a$ where $\hat{R}$ is a dimensionless quantity which measures a distance in terms of lattice units. The right hand side of (281) can be measured for some value of g_0 and $\hat{R}$ and the left hand side can be used to determine what value of R this corresponds to, which gives us a value for a. Once we know $g_0(a)$ for one value of a, we can in principle compute it for other values of a by using the renormalization group. To see this, take the total derivative of (281) with respect to a:

$$0 = \left[a\frac{\partial}{\partial a} - \beta(g_0)\frac{\partial}{\partial g_0} \right] \mathcal{Q}(R, a, g_0(a)). \tag{282}$$

where

$$\beta(g_0) \equiv -a\frac{dg_0}{da}. \tag{283}$$

If the functional form of $\mathcal{Q}(R, a, g_0(a))$ is known (for example from perturbation theory), we can solve for dg_0/da and integrate to get a as a function of g_0 with the constant of integration determined by the single value of $g_0(a)$ found earlier. An example of this can be found in section 9.2 of [41] where $\mathcal{Q}$ is taken to be the static $q\bar{q}$ potential. Since $\beta(g_0)$ is negative (to lowest order it is $-11g_0^3/16\pi^2$) the $a \to 0$ limit corresponds to $g_0 \to 0$. Because of the correspondence between the lattice spacing and the bare coupling, it is common to describe the lattice spacing for a simulation by quoting the value of $\beta = 6/g_0^2$.

6.2 Lattice Perturbation Theory

Although lattice gauge theory was invented in order to be able to compute quantities which couldn't be analyzed with perturbation theory, it is useful to be able to do perturbative (weak coupling) calculations for the discretized theory. Some quantities should be accurately predicted by perturbation theory, and therefore we can use perturbation theory results to test the Monte Carlo results. Also, when feeding bare parameters into the Monte Carlo simulation, it is desirable to know what renormalized values they correspond to before we run the simulation. Perturbation theory helps us here because it gives an expansion in terms of $\alpha(q^2)$ and we know how α runs as we change the lattice spacing, so renormalized values for the parameters at various lattice spacings can be computed without running a costly simulation. Additionally, perturbation theory is important for computing the coefficients of nonrenormalizable terms which are added to the basic lattice action to correct for finite a errors [47].

We define the Fourier transform on the lattice by:

$$\tilde{f}(k) = \sum_n e^{-ik\cdot n} f(n) \tag{284}$$

where the allowed values of k_μ are $2\pi N_\mu / L_\mu$ where L_μ is the length of the lattice in the μ direction, and N_μ is an integer in the range $[0, L_\mu)$. Note that we could shift the momenta so that they lie in the range $[-\pi, \pi)$ instead of $[0, 2\pi)$. This has the intuitive advantage of associating large $|k|$ with large physical momenta, and it is the proper representation to use when computing the coupling $\alpha(k^2)$ (it doesn't matter which representation you use anywhere else because of periodicity). Note that the sign in the exponent is the opposite of what one would normally expect – this is because the metric is now the identity matrix. The periodic delta function is

$$\delta_{n,m} = \delta_{n-m,0} = \frac{1}{V} \sum_k e^{ik\cdot(n-m)} \tag{285}$$

where $V = L_1 L_2 L_3 L_4$ is the lattice volume. Clearly,

$$f(n) = \frac{1}{V} \sum_k e^{ik\cdot n} \tilde{f}(k). \tag{286}$$

6.2.1 Fermion Propagator

Now we compute the tree-level fermion propagator by finding the Fourier transform of the inverse of the operator K given by equation (259) when there are no interactions (i.e. when $U_\mu = 1$). We start with

$$\sum_m \sum_\beta K_{\alpha\beta}(\ell, m) K^{-1}_{\beta\gamma}(m, n) = \delta_{\ell,n} \delta_{\alpha\gamma} \tag{287}$$

where α, β, and γ are spinor indices. Substituting the Fourier transforms, we have

$$\frac{1}{V^2} \sum_k \sum_p \sum_m \sum_\beta e^{ik\cdot(\ell-m)} e^{ip\cdot(m-n)} \tilde{K}_{\alpha\beta}(k) \tilde{K}^{-1}_{\beta\gamma}(p) = \frac{1}{V} \delta_{\alpha\beta} \sum_q e^{iq\cdot(\ell-n)}. \tag{288}$$

If we substitute (285) into (259), we find

$$K(\ell,m)=\frac{1}{V}\sum_{k}e^{ik\cdot(\ell-m)}\left\{(4r+m_0)+\sum_{\mu=1}^{4}\left[-i\sin(k_\mu)\gamma_\mu-r\cos(k_\mu)\right]\right\} \quad (289)$$

which allows us to read off $\tilde{K}$. Putting this into (288) and doing some algebra (see Appendix C for gamma matrix relationships) gives the momentum space fermion propagator

$$G(p)=\tilde{K}^{-1}(p)=\frac{\left[4r+m_0-r\sum_\mu\cos p_\mu\right]-i\sum_\mu\gamma_\mu\sin p_\mu}{\left[4r+m_0-r\sum_\nu\cos p_\nu\right]^2+\sum_\nu\sin^2 p_\nu}. \quad (290)$$

6.2.2 Gluon Propagator

To derive the gluon propagator, we start by fixing the gauge which is necessary because weak coupling perturbation theory is an expansion about the vacuum and the vacuum is degenerate if the gauge isn't fixed. As in the continuum case, we follow the Faddeev-Popov procedure. The Faddeev-Popov determinant introduces ghosts which won't be relevant to our calculation. The gauge fixing delta function can be converted into an extra term in the action given by (see [41])

$$S_{GF}=\frac{1}{2\xi}\sum_{n,A}\left[\sum_\mu\partial_\mu^L A_\mu^A(n)\right]^2, \quad (291)$$

where $\partial_\mu^L A_\nu(n)=A_\nu(n)-A_\nu(n-\mu)$. For Landau gauge we set $\xi=0$, for Feynman gauge $\xi=1$ and for Fried-Yennie gauge $\xi=3$. The rest of the action, contained in expression (266), can be written as (dropping the constant part):

$$S_G=-\frac{1}{g_0^2}\sum_n\sum_{\mu\nu}\mathrm{Tr}\left\{U_{\mu\nu}(n)\right\}. \quad (292)$$

Using (264), and $F_{\mu\nu}=\sum_A T^A F_{\mu\nu}^A$ with $\mathrm{Tr}\left\{T^A\right\}=0$ and $\mathrm{Tr}\left\{T^AT^B\right\}=\delta_{A,B}/2$:

$$S_G\approx\frac{1}{4}\sum_A\sum_n\sum_{\mu,\nu}F_{\mu\nu}^A F_{\mu\nu}^A. \quad (293)$$

To find the propagator, we look at only the terms quadratic in A_μ. Using (265) we have

$$S_G + S_{GF} = \sum_{n,A} \sum_{\mu,\nu} \left\{ \frac{1}{4} \left[\partial_\mu^R A_\nu^A(n) - \partial_\nu^R A_\mu^A(n) \right]^2 + \frac{1}{2\xi} \partial_\mu^L A_\mu^A(n) \partial_\nu^L A_\nu^A(n) \right\} + ... \tag{294}$$

To proceed, we will need to "integrate" by parts. The identities below will help:

$$\sum_n [\partial_\mu^R f(n)] g(n) = -\sum_n f(n) \partial_\mu^L g(n), \tag{295}$$

$$\sum_n [\partial_\mu^L f(n)] g(n) = -\sum_n f(n) \partial_\mu^R g(n), \tag{296}$$

and

$$\partial_\mu^R \partial_\nu^L = \partial_\nu^L \partial_\mu^R. \tag{297}$$

After working through the algebra and integration by parts, we get

$$S_G + S_{GF} = \frac{1}{2} \sum_{nm} \sum_{AB} \sum_{\mu\nu} A_\mu^A(n) K_{\mu\nu}^{AB}(n,m) A_\nu^B(m) + ... \tag{298}$$

where

$$K_{\mu\nu}^{AB}(n,m) = \delta_{AB} \left\{ -\delta_{\mu\nu} \sum_\alpha \partial_\alpha^L \partial_\alpha^R + \left(1 - \frac{1}{\xi} \right) \partial_\nu^L \partial_\mu^R \right\}. \tag{299}$$

Now we rewrite this in terms of periodic delta functions. For example, we use

$$\partial_\nu^L \partial_\mu^R \to \sum_j (\delta_{n,j} - \delta_{n-\nu,j})(\delta_{j+\mu,m} - \delta_{j,m}) \tag{300}$$

along with (285). We are interested in finding the propagator which is the inverse of the Fourier transform of $K_{\mu\nu}^{AB}(n,m)$, given by:

$$\sum_B \sum_\nu \sum_m K_{\mu\nu}^{AB}(n,m) K_{\nu\beta}^{-1\,BC}(m,\ell) = \delta_{AB} \delta_{\mu\beta} \delta_{n\ell}, \tag{301}$$

which, after some algebra and Fourier transforming, gives

$$\sum_\nu \delta_{AB} \left[\delta_{\mu\nu} \hat{k}^2 - \left(1 - \frac{1}{\xi} \right) \exp\left\{ \frac{i}{2} k \cdot (\mu - \nu) \right\} \hat{k}_\nu \hat{k}_\mu \right] \tilde{K}_{\nu\beta}^{-1\,BC}(k) = \delta_{AC} \delta_{\mu\beta} \tag{302}$$

where

$$\hat{k}_\mu \equiv 2\sin\frac{k_\mu}{2}, \qquad \hat{k}^2 \equiv \sum_\mu \hat{k}_\mu^2. \tag{303}$$

Solving for $\tilde{K}^{-1\,BC}_{\nu\beta}(k)$ we have

$$\tilde{K}^{-1\,BC}_{\nu\beta}(k) = \delta_{BC}\exp\left\{\frac{i}{2}k\cdot(\nu-\beta)\right\}\frac{1}{\hat{k}^2}\left[\delta_{\nu\beta}+(\xi-1)\frac{\hat{k}_\nu\hat{k}_\beta}{\hat{k}^2}\right]. \tag{304}$$

The exponential is just an annoying phase which will be canceled when the propagator is joined to vertices. We can avoid having to carry the phase around and cancel it by using the definition

$$U_\mu(n) \approx 1 + ig_0A_\mu(n+\mu/2) - \frac{1}{2}g_0^2A_\mu^2(n+\mu/2) + ... \tag{305}$$

instead of (261). Then we have

$$G_{\nu\beta}(k) = \tilde{K}^{-1\,BC}_{\nu\beta}(k) \to \delta_{BC}\frac{1}{\hat{k}^2}\left[\delta_{\nu\beta}+(\xi-1)\frac{\hat{k}_\nu\hat{k}_\beta}{\hat{k}^2}\right]. \tag{306}$$

6.2.3 gff Vertex

A vertex with a fermion interacting with a single gluon arises from the U_μ's in (258). Using (305) and keeping only terms linear in A_μ, we have

$$\begin{aligned} S_F^{(1)} &= -\frac{i}{2}g_0\sum_{nm}\sum_{ab}\sum_C\sum_\mu \bar{\psi}^a(n)T^C_{ab}\Big\{\delta_{n+\mu,m}(r-\gamma_\mu)A^C_\mu(n+\mu/2) \\ &\quad -\delta_{n-\mu,m}(r+\gamma_\mu)A^C_\mu(n-\mu/2)\Big\}\psi^b(m). \end{aligned} \tag{307}$$

Now we substitute

$$\bar{\psi}(n) = \frac{1}{V}\sum_k e^{-ik\cdot n}\tilde{\bar{\psi}}(k), \qquad \psi(m) = \frac{1}{V}\sum_p e^{ip\cdot m}\tilde{\psi}(p), \tag{308}$$

and simplify giving

$$\begin{aligned} S_F^{(1)} &= ig_0\frac{1}{V^2}\sum_{ab}\sum_C\sum_\mu\sum_{kp}\tilde{\bar{\psi}}^a(k)T^C_{ab}\left\{\gamma_\mu\tilde{A}^C_\mu(k-p)\cos\left(\frac{p_\mu+k_\mu}{2}\right)\right. \\ &\quad \left. -ir\tilde{A}^C_\mu(k-p)\sin\left(\frac{p_\mu+k_\mu}{2}\right)\right\}\tilde{\psi}^b(p) \end{aligned} \tag{309}$$

which gives us the Feynman rule:

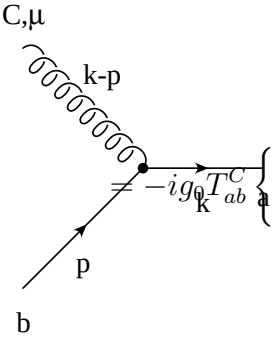

$$= -ig_0 T^C_{ab} \left\{ \gamma_\mu \cos\left(\frac{p_\mu + k_\mu}{2}\right) - ir \sin\left(\frac{p_\mu + k_\mu}{2}\right) \right\}. \tag{310}$$

The minus sign comes from the minus in e^{-S_E}.

6.2.4 ggff Vertex

A vertex with a fermion interacting with two gluons arises from the U_μ's in (258). Note that there is no such vertex in the continuum theory. It occurs here because we had to introduce link variables to make the discretized theory gauge invariant. Later in this dissertation, gauge invariance of the one-loop quark self energy will be demonstrated, and it will be shown that this vertex is necessary in that proof. Using (305) and keeping only terms quadratic in A_μ, we have

$$\begin{aligned} S_F^{(2)} &= \frac{g_0^2}{4} \sum_{nm} \sum_{abf} \sum_{CD} \sum_{\mu} \bar{\psi}^a(n) T^C_{af} T^D_{fb} \Big\{ \delta_{m,n+\mu}(r - \gamma_\mu) A^C_\mu(n + \mu/2) A^D_\mu(n + \mu/2) \\ &\quad + \delta_{m,n-\mu}(r + \gamma_\mu) A^C_\mu(n - \mu/2) A^D_\mu(n - \mu/2) \Big\} \psi^b(m). \end{aligned} \tag{311}$$

Substituting in Fourier transforms as before

$$\begin{aligned} S_F^{(2)} &= -\frac{g_0^2}{4} \frac{1}{V^3} \sum_{kp\ell} \sum_{abf} \sum_{CD} \sum_{\mu} \tilde{\bar{\psi}}^a(k) T^C_{af} T^D_{fb} \tilde{A}^C_\mu(\ell) A^D_\mu(k - p - \ell) \\ &\quad \left\{ i\gamma_\mu \sin\left(\frac{p_\mu + k_\mu}{2}\right) - r \cos\left(\frac{p_\mu + k_\mu}{2}\right) \right\} \tilde{\psi}^b(p), \end{aligned} \tag{312}$$

which gives us the Feynman rule:

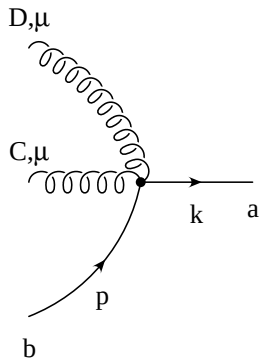

$$= \frac{g_0^2}{2}\{T^C, T^D\}_{ab}\left\{i\gamma_\mu \sin\left(\frac{p_\mu + k_\mu}{2}\right) - r\cos\left(\frac{p_\mu + k_\mu}{2}\right)\right\}. \tag{313}$$

There are other vertices which we do not consider here because they will not be needed for the quark self energy calculation. For a more complete treatment, the reader is referred to [41]. The lattice Feynman rules are summarized in Appendix D.

6.2.5 Running Coupling

For many years, the agreement between Monte Carlo results and lattice perturbation theory was terrible. Once the lattice spacing is made small enough, we expect that quantities which are ultraviolet divergent will be well approximated by leading terms in the perturbation theory expansion. So, the disagreement between Monte Carlo results and perturbative calculations sent the lattice community on a quest to make the lattice spacing smaller. When doing simulations, the lattice must be bigger than the object you are simulating (such as a hadron) so that the calculation isn't sensitive to the boundary conditions. If the lattice spacing is reduced while maintaining a certain minimum physical size for the lattice, the number of points on the lattice must be increased which makes the calculations very expensive.

In 1993, Lepage and Mackenzie [44] pointed out that the disagreement between Monte Carlo results and lattice perturbation theory was due to the fact that lattice perturbation theory wasn't being done in a sensible way. People

had been doing the perturbative calculations by expanding in the bare coupling. When doing continuum calculations, it is normal to express perturbative expansions in terms of a renormalized running coupling rather than the bare coupling, and this procedure works well. Lepage and Mackenzie pointed out that if a bad choice of coupling constants is made, the coefficients in the perturbative expansion become large giving poor convergence. They proposed using a renormalized running coupling for lattice perturbation theory, and presented comparisons of Monte Carlo results with perturbative calculations performed using the bare coupling $\alpha_{\rm lat}$, and running couplings $\alpha_{\overline{\rm ms}}(q)$ and $\alpha_V(q)$. Agreement between the Monte Carlo calculations and perturbative results using running couplings was good even at β's as low as 5.7 while the $\alpha_{\rm lat}$ results disagreed significantly with the Monte Carlo data even at higher β's (smaller a's). They proposed using a coupling which is defined in terms of a physical observable, the heavy quark potential $V(q)$:

$$V(q) = -\frac{C_f 4\pi\alpha_V(q)}{q^2} \tag{314}$$

with no higher-order corrections. To do calculations, we must choose a scale, q^*, such that $\alpha_V(q^*)$ is a good expansion parameter. For a one-loop calculation of a quantity in this scheme:

$$I = \alpha_V(q^*)\int d^4q f(q). \tag{315}$$

Lepage and Mackenzie observed that, although tempting, it is wrong to use

$$\alpha_V(q^*)\int d^4q f(q) \equiv \int d^4q \alpha_V(q) f(q) \tag{316}$$

since the right hand side is singular due to the pole in the coupling constant at $q = \Lambda_V$ that arises from doing an all orders summation of perturbative logarithms. Their solution is to keep only the first two terms in the expansion:

$$\alpha_V(q) = \alpha_V(\mu)[1 + \beta_0 \ln(q^2/\mu^2)\alpha_V(\mu) + ...] \tag{317}$$

where μ is some fixed scale. Then the prescription for setting the scale becomes

$$\alpha_V(q^*) \int d^4q f(q) \equiv \int d^4q \alpha_V(\mu)[1 + \beta_0 \ln(q^2/\mu^2)\alpha_V(\mu)]f(q) \tag{318}$$

which, after expanding $\alpha_V(q^*)$ in terms of $\alpha_V(\mu)$, gives

$$\ln(q^{*2}) \equiv \frac{\int d^4q \ln(q^2) f(q)}{\int d^4q f(q)}. \tag{319}$$

7 Extracting Coefficients from MC

Continuum perturbation theory rapidly becomes tedious as we push calculations to higher and higher orders in α. This is even more significant in lattice perturbation theory since there are more vertices in the Feynman rules and the propagators and vertices are more complicated. Additionally, the sums or integrals over loop momenta are harder to evaluate because the integrands are more complicated. The point of this part of the dissertation is to show that Monte Carlo simulations can be used to extract the next term of a perturbation series. For example, we can calculate some perturbative quantity, $\mathcal{Q}$, at the one-loop level, giving:

$$\mathcal{Q}^{1-\text{loop}} = c_0 + c_1 \alpha_V(q^*). \tag{320}$$

We then measure the same quantity in a Monte Carlo simulation:

$$\mathcal{Q}^{\text{MC}} = c_0 + c_1 \alpha_V(q^*) + c_2 \alpha_V^2(q^*) + c_3 \alpha_V^3(q^*) + ... \tag{321}$$

and we can estimate the two-loop coefficient:

$$c_2 = \left[\mathcal{Q}^{\text{MC}} - \mathcal{Q}^{1-\text{loop}}\right] / \alpha_V^2(q^*) + \mathcal{O}(\alpha_V(q^*)). \tag{322}$$

We make the lattice spacing small so that $\alpha_V(q^*)$ is small. On the other hand, we cannot make the lattice spacing too small because the $c_2 \alpha_V^2(q^*)$ term that we are trying to measure will be smaller than the statistical errors in $\mathcal{Q}^{\text{MC}}$.

7.1 Why is This Useful?

At first glance, it may seem silly to worry about finding the next term in the perturbative expansion when the Monte Carlo simulation gives us the the value of $\mathcal{Q}$ without any approximation involving the coupling. There are (at least) two reasons for wanting to know the perturbative coefficients. One is that the

quantity $\mathcal{Q}$ may be hard to measure in a Monte Carlo simulation at the lattice spacings where simulations are normally done. If we are able to measure it at a much smaller lattice spacing and determine the perturbative coefficients, we can run the coupling to any lattice spacing we want. For example, the mass of a quark is expected to be perturbative since it is logarithmically divergent in the continuum theory. So, in the lattice regulated theory, the largest loop momenta ($\sim \pi/a$), where the running coupling is small, give the dominant contribution to the self energy. When a is small enough, we can measure the mass in a simulation by looking at the propagator for large time separations. If we tried to use this procedure for a moderate value of a we would run into confinement problems. However, when these quarks are combined in a meson, these confinement problems do not occur since the meson is a color singlet. So we can accurately simulate mesons at moderate lattice spacings, but we cannot directly measure the mass of the quarks that compose them. However, we can measure the perturbative coefficients when a is very small and then run the coupling to a more moderate value of a.

A second reason that the perturbative coefficients are useful is in the construction of improved actions. To reduce finite a errors, terms are added to the action. In a classical field theory the coefficients of these terms would be constants. But, in a quantum field theory the couplings in the action are renormalized. So, the coefficients of the correction terms will be expansions in α such that they cancel finite a errors to some order. The correction terms improve the short distance behavior of the theory (i.e. they correct for the space-time points between lattice sites which are missing), so their coefficients should be perturbative. To calculate n correction coefficients, perturbation theory is used to compute n physical quantities $\mathcal{Q}_i$, and the correction coefficients are deter-

mined by requiring that up to some order in a the results match the continuum theory [48]. Again, our method of extracting perturbative results from Monte Carlo simulations proves valuable since it eliminates the need to go through the many tedious calculations with standard perturbative techniques.

7.2 Why This Wasn't Done Before

The procedure outlined above seems so simple that one might be surprised that it wasn't done before. But, recall that lattice perturbation theory results were in gross disagreement with Monte Carlo calculations before Lepage and Mackenzie pointed out that the perturbative calculations should be done with a renormalized running coupling constant [44]. Also, as described in this dissertation, there are surmountable difficulties with the procedure.

7.3 Wilson Quark Mass

7.3.1 Extracting Mass from MC Data

The standard way of extracting masses from Monte Carlo simulations is to look at the propagator with the three-momentum set to zero and the energy Fourier transformed. For a scalar particle in Euclidean space, this gives

$$G(t) = G(t, \vec{p} = 0) = \int_{-\infty}^{\infty} dE e^{iEt} \frac{1}{E^2 + m^2} = \frac{\pi}{m} e^{-mt} \tag{323}$$

which suggests that we measure masses on the lattice using

$$m_{\text{eff}} = \ln \left[G(t)/G(t+1) \right], \tag{324}$$

where the ratio is evaluated for some large value of t to ensure that any excited state contributions will be small. However, we cannot make t too large (i.e. it must be smaller than half of the length of the lattice in the time direction) since the periodic boundary conditions cause the propagator on the lattice to not be

exponential which becomes significant toward the middle of the lattice. When using the procedure for fermions, we consider the propagation of a quark with a particular spin and color (this gives us a single component of the matrix which represents the full propagator). Since we are trying to extract a mass, the hope is that the result from (324) is gauge invariant if we make t large enough. As will be described later, there are some problems with this.

7.3.2 Computing Mass with Perturbation Theory

It is tempting to apply the above method to the calculation of masses in perturbation theory. This would be done by summing insertions of the one-loop off-shell electron self-energy diagram to all orders (see for example section 9.3 of [49]) in order to get the self energy into the denominator of the propagator where it could shift the pole (renormalize the mass). Then, this momentum space propagator would be used to compute $G(t)$, giving m_{eff}. This calculation involves a sum over the four components of the loop momentum, matrix inversion, and another sum for the Fourier transform. While this procedure is appealing since it closely parallels the technique used for the Monte Carlo simulation, it is not a good approach because it includes some (but not all) of the higher loop result, and these higher order terms are not gauge invariant because they do not include all diagrams which are relevant at that order. Also, because of the presence of higher order terms, if we define the perturbative coefficient, c_1, using

$$m_{\text{eff}}^{1-\text{loop}} = c_0 + c_1 \alpha_V(q^*), \tag{325}$$

and we compute m_{eff} at two different β's and extract c_1 from each, we will find that the c_1's are slightly different because the c_1 defined in this way is equal to a constant plus higher order (gauge dependent) terms in α.

Tree Level Mass Instead, we find the one-loop correction to the mass directly from the on-shell self energy diagram. This gives a constant (β independent) result which is gauge invariant. To begin, we find the tree-level mass by locating the pole of the tree-level propagator in Eq. (290). Looking at the denominator of the propagator with $\vec{p} = 0$, $p_4 = E$, and $r = 1$, we have

$$(1 + m_0 - \cos E)^2 + \sin^2 E = 0, \tag{326}$$

which is rearranged to give

$$\cos E = \frac{1 + (m_0 + 1)^2}{2(m_0 + 1)}. \tag{327}$$

Now we use

$$\cos E = \frac{1}{2}(e^{iE} + e^{-iE}) = \frac{1}{2}\left(x + \frac{1}{x}\right), \tag{328}$$

where $x \equiv \exp(iE)$. Substituting this into (327) and solving for x gives:

$$x = \frac{1}{2}\left[\frac{1 + (m_0 + 1)^2}{(m_0 + 1)} \pm \sqrt{\left(\frac{1 + (m_0 + 1)^2}{m_0 + 1}\right)^2 - 4}\right]. \tag{329}$$

The upper sign gives $x = 1 + m_0$ and the lower sign gives $x = 1/(1 + m_0)$. So, the poles are at

$$E = \pm\, i \ln(1 + m_0). \tag{330}$$

The fact that the poles are located at purely imaginary energies is due to our Wick rotation described Sec. 6.1. Since we changed the time variable to $t_E = it$, but use an energy variable defined by the Fourier transform (284), our energy variable has a factor of i relative to the Minkowsky energy, i.e. $E_E = iE_M$. So, the pole at $E = i \ln(1 + m_0)$ tells us that the tree-level mass of a quark is

$$m^{\text{tree}} = \ln(1 + m_0). \tag{331}$$

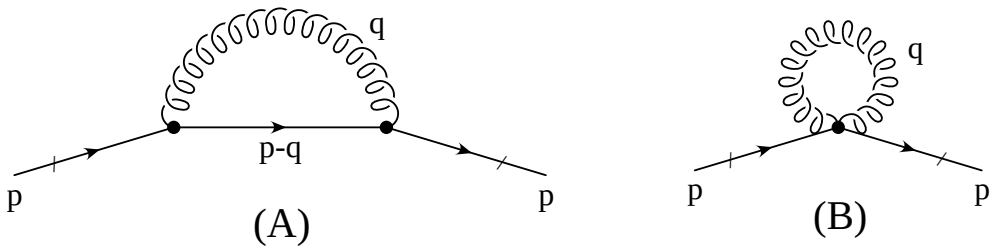

Figure 21: Diagrams contributing the the 1-loop quark self energy.

1-Loop Self Energy Now we compute the 1-loop correction to the mass from the truncated self energy diagrams shown in Fig. 21 using the Feynman rules in Appendix D. Note that diagram B does not arise in the continuum theory, but is present in the lattice theory to ensure gauge invariance. The self energy is given by the sum of the two diagrams:

$$\Sigma(p) = \Sigma_A(p) + \Sigma_B(p). \tag{332}$$

The first diagram gives:

$$\Sigma_A(p) = (-ig_0)^2 \frac{1}{V} \sum_q \sum_E \sum_b T^E_{cb} \mathcal{V}^{(1)}_\nu(p - q/2) G(p-q) T^E_{ba} \mathcal{V}^{(1)}_\mu(p-q/2) G_{\mu\nu}(q), \tag{333}$$

where $G(p-q)$ is the intermediate fermion propagator given by (290), $G_{\mu\nu}(q)$ is the gluon propagator (306), and

$$\mathcal{V}^{(1)}_\mu(\ell) = \gamma_\mu \cos(\ell_\mu) - ir \sin(\ell_\mu) \tag{334}$$

is from the vertex (310). We can do the sum over gluon colors:

$$\sum_E (T^E T^E)_{ca} = \frac{1}{2} \sum_E \{T^E, T^E\}_{ac} = \frac{1}{2} \sum_E \left\{ \frac{1}{3} \delta_{EE} \delta_{ca} + \sum_F d_{EEF} T^F_{ac} \right\} = \frac{4}{3} \delta_{ca} \tag{335}$$

where d_{EEF} is given in Eq. 11-23 of [50] (also given in the footnote on p. 201 of [41], but d_{448} is wrong), and we have used $\sum_E d_{EEF} = 0$. Putting this into

(333), we have

$$\Sigma_A(p) = -g_0^2 \frac{4}{3}\frac{1}{V}\delta_{ca} \sum_q \sum_{\mu\nu} \mathcal{V}_\nu^{(1)}(p - q/2) G(p-q) \mathcal{V}_\mu^{(1)}(p - q/2) G_{\mu\nu}(q). \quad (336)$$

For the second diagram, we have

$$\begin{aligned} \Sigma_B(p) &= \frac{1}{2}\frac{g_0^2}{2}\frac{1}{V}\sum_q \sum_E \{T^E, T^E\}_{ca} \mathcal{V}_\mu^{(2)}(p) G_{\mu\mu}(q) \\ &= \frac{1}{2} g_0^2 \frac{4}{3}\frac{1}{V}\delta_{ca} \sum_\mu \mathcal{V}_\mu^{(2)}(p) \sum_q G_{\mu\mu}(q), \end{aligned} \quad (337)$$

where the $1/2$ is a symmetry factor and

$$\mathcal{V}_\mu^{(2)}(p) = i\gamma_\mu \sin p_\mu - r \cos p_\mu \quad (338)$$

from (313).

Now we must figure out how to extract the 1-loop correction to the mass from the self energy. To do this, we look at the propagator with $\vec{p} = 0$ and the energy close to im^{tree} (i.e. close to the tree-level pole). First, we examine the tree-level propagator (290). In the neighborhood of $E = im^{\text{tree}}$ we write it as

$$G(p) = \frac{N}{[E - im^{\text{tree}}] \cdot \partial D/\partial E|_{E=im^{\text{tree}}}} + \text{finite} \quad (339)$$

where N is the numerator of (290) and D is the denominator of (290). We have used "finite" to denote parts that remain finite as $E \to im^{\text{tree}}$ which won't concern us. Evaluating this expression and throwing away the finite parts, we get

$$G(p) \sim \frac{-iZ_\psi P^+}{E - im^{\text{tree}}} \quad (340)$$

where P^+ is given by

$$P^+ \equiv \frac{1}{2}(1 + \gamma_4) \quad (341)$$

and Z_ψ is a tree-level wavefunction renormalization (see [51]):

$$Z_\psi = \frac{1}{1 + m_0}. \quad (342)$$

At the 1-loop level our propagator becomes:

$$\begin{aligned} G(p) + G(p)\Sigma(p)G(p) &= G(p)\frac{1}{1-\Sigma(p)G(p)} + \mathcal{O}(\alpha^2) \\ &\sim -iZ_\psi P^+ \frac{1}{E - im^{\text{tree}} + iZ_\psi \Sigma P^+}. \end{aligned} \tag{343}$$

When $p = (\vec{0}, im^{\text{tree}})$

$$\Sigma(p) = \Sigma^+ P^+ + \Sigma^- P^- \tag{344}$$

where $P^- \equiv (1-\gamma_4)/2$ and Σ^+ and Σ^- are real numbers. This enables us to write

$$\frac{1}{E - im^{\text{tree}} + iZ_\psi \Sigma P^+} = \frac{1}{E - im^{\text{tree}} + iZ_\psi \Sigma^+} P^+ + \frac{1}{E - im^{\text{tree}}} P^-. \tag{345}$$

Putting this into the 1-loop propagator (343) gives (in the neighborhood of the quark pole):

$$\frac{-iZ_\psi P^+}{E - im^{\text{tree}} + iZ_\psi \Sigma^+}. \tag{346}$$

We read off the 1-loop mass from the location of the pole:

$$m^{1-\text{loop}} = m^{\text{tree}} - Z_\psi \Sigma^+. \tag{347}$$

Note that we have evaluated the self energy at m^{tree} rather than at the renormalized mass. This was done to ensure that our result was truly $\mathcal{O}(\alpha)$ and did not include any higher order contributions.

7.3.3 Proof of Gauge Invariance

If our calculations are to have any meaning at all, $m^{1-\text{loop}}$ must be gauge invariant – otherwise we can get any value we want for $m^{1-\text{loop}}$ by choosing an appropriate value of the gauge parameter ξ. While the proof is simple for the continuum theory, it can be quite messy for the lattice theory if it is not organized correctly. Bodwin and Kovacs found an elegant way of handling Ward identities on the lattice which involves re-writing the vertices in terms of the

inverse of the fermion propagator [53]. We will use their technique here. To prove gauge invariance, it is sufficient to show that the $\hat{q}_\mu \hat{q}_\nu$ part of the gluon propagator (306) gives zero contribution to the fermion self energy when the fermion is on shell. This is sufficient because it shows that we get the same mass regardless of the value of the gauge parameter ξ. We define

$$X_A \equiv -\sum_{\mu\nu} \mathcal{V}_\nu^{(1)}(p - q/2) G(p-q) \mathcal{V}_\mu^{(1)}(p - q/2) \hat{q}_\mu \hat{q}_\nu \tag{348}$$

and

$$X_B \equiv \frac{1}{2} \sum_\mu \mathcal{V}_\mu^{(2)}(p) \hat{q}_\mu \hat{q}_\mu. \tag{349}$$

To demonstrate gauge invariance, we must show that (see (336) and (337))

$$\sum_q \bar{u}(p)[X_A(q) + X_B(q)]u(p) = 0. \tag{350}$$

Following [53], we define (note that our γ's are different by a factor of i)

$$\nabla_\mu(p) \equiv 2\sin^2(p_\mu/2) + i\gamma_\mu \sin p_\mu \tag{351}$$

and notice that

$$\nabla_\mu(p) - \nabla_\mu(p-q) = \hat{q}_\mu\{i\gamma_\mu \cos(p_\mu - q_\mu/2) + \sin(p_\mu - q_\mu/2)\} \tag{352}$$

and

$$\begin{aligned} \nabla_\mu(p+\ell_1+\ell_2) - \nabla_\mu(p+\ell_1) - \nabla_\mu(p+\ell_2) + \nabla_\mu(p) = \\ \hat{\ell}_{1\mu}\hat{\ell}_{2\mu}\left\{-i\gamma_\mu \sin\left(\frac{p_\mu + k_\mu}{2}\right) + \cos\left(\frac{p_\mu + k_\mu}{2}\right)\right\} \end{aligned} \tag{353}$$

where $k = p + \ell_1 + \ell_2$. We can relate $\nabla_\mu(p)$ to the fermion propagator:

$$G(p) = \frac{1}{m_0 + \sum_\mu \nabla_\mu(p)}. \tag{354}$$

Combining (352), (354) and (334) gives

$$\sum_\mu \mathcal{V}_\mu^{(1)}(p - q/2)\hat{q}_\mu = i[G^{-1}(p-q) - G^{-1}(p)] \tag{355}$$

and (353), (354) and (338) gives (with $\ell_1 = q$ and $\ell_2 = -q$)

$$\sum_\mu \mathcal{V}^{(2)}_\mu(p)\hat{q}_\mu\hat{q}_\mu = 2G^{-1}(p) - G^{-1}(p+q) - G^{-1}(p-q). \tag{356}$$

Putting these relations into (348) and (349) gives

$$X_A = \left[G^{-1}(p-q) - G^{-1}(p)\right] G(p-q) \left[G^{-1}(p-q) - G^{-1}(p)\right] \tag{357}$$

and

$$X_B = \frac{1}{2}\left[2G^{-1}(p) - G^{-1}(p+q) - G^{-1}(p-q)\right]. \tag{358}$$

To show that gauge invariance is satisfied (350), we need to evaluate X_A and X_B between on-shell spinors. The Dirac equation is

$$G^{-1}(p)u(p) = 0. \tag{359}$$

Using this, we see that $\bar{u}(p)X_Au(p) = \bar{u}(p)X_Bu(p) = 0$ for $q = 0$. For $q \neq 0$

$$\bar{u}(p)X_Au(p) = \bar{u}(p)G^{-1}(p-q)u(p) \tag{360}$$

and

$$\bar{u}(p)X_Bu(p) = -\frac{1}{2}\bar{u}(p)\left[G^{-1}(p+q) + G^{-1}(p-q)\right]u(p) \tag{361}$$

so we have

$$\bar{u}(p)\left[X_A(q) + X_B(q) + X_A(-q) + X_B(-q)\right]u(p) = 0 \tag{362}$$

and (350) is satisfied. A similar proof can be done for the continuum theory. For the continuum case $G^{-1}(p-q) = G^{-1}(p) - \not{q}$, so $\bar{u}(p)\left[X_A(q) + X_A(-q)\right]u(p) = 0$. For the lattice case, $G^{-1}(p-q)$ is not linear in q so diagram A is not independently gauge invariant and the self energy is not gauge invariant without the contribution from diagram B. In our proof, we made no assumptions about the denominator of the gluon propagator except that it was even in q_μ, so we find that the on-shell self energy is gauge invariant regardless of whether or not the gluon has a mass.

7.4 Difficulties and Subtleties

7.4.1 Tunneling

Several difficulties arise when using Monte Carlo simulations to determine the perturbative coefficients for the quark mass renormalization. The first problem, which affects the extraction of all perturbative coefficients (not just mass renormalizations) is tunneling. Examination of the gluon action (266) and the definition of the plaquette (262) reveals that there is an extra symmetry in the theory (when there are no quarks). It is referred to as the "center symmetry" because it involves elements of the center of SU(3) (i.e. those elements that commute with all elements of SU(3)), Z(3). These elements are 1,$e^{2\pi i/3}$, and $e^{4\pi i/3}$. The gluon action is invariant under

$$U_\mu(n) \to zU_\mu(n) \quad \text{for a particular } \mu \in \{1,2,3,4\} \text{ and } z \in \mathrm{Z}(3), \tag{363}$$

where the transformation is performed on all link variables in the μ plane. For example, if we choose $\mu = 4$, the transformation is performed on links $U_4(n)$ where $n = (n_1, n_2, n_3, n_4)$ for all n_1, n_2, n_3, and a particular value of n_4. Note that this is not a gauge transformation (see Eq. (251)). For all plaquettes in the action which are affected by the transformation, there is a factor of z and $z^\dagger$. Since the z's commute with the U_μ's (i.e. they commute with elements of SU(3)), the z and $z^\dagger$ can be brought together to give 1, leaving the gluon action (but not the fermion action) unchanged by the center transformation.

This extra symmetry causes the minimum of the gluon action to be degenerate. Perturbation theory is an expansion about a single minimum, so we expect to have problems if the system tunnels between the various minima. Additionally, the quark action is not invariant under the center symmetry, so the propagator will be affected by the tunneling. The Polyakov Loop (also called the Wilson line) allows us to detect tunneling between the degenerate ground states.

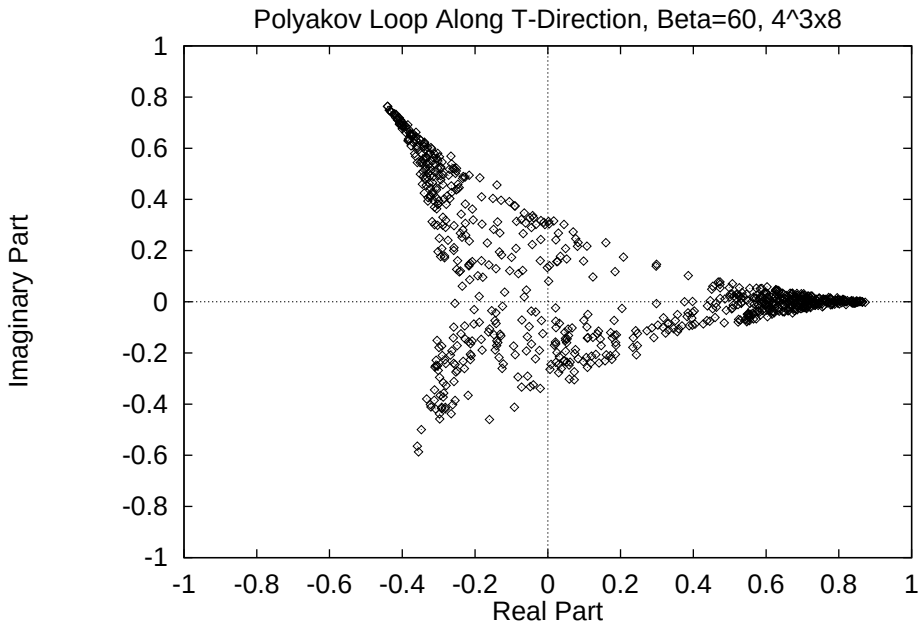

Figure 22: Average value of Polyakov Loop along the time direction showing tunneling. 795 configurations of a $4^3 \times 8$ lattice at $\beta = 60$ (dataset tp6) are shown.

A Polyakov Loop is simply the trace of the product of the link variables along a single direction from one end of the lattice to the other. Because of the periodic boundary conditions, the Polyakov Loop is a closed loop and therefore is gauge invariant. But, it only cuts through a plane which is perpendicular to it once (unlike a plaquette which goes through the plane twice – once in each direction). So a center symmetry transformation causes a Polyakov loop perpendicular to the plane to change in value by a factor of $e^{2\pi i/3}$ or $e^{4\pi i/3}$. Polyakov loops are commonly used to study deconfinement transitions in finite temperature field theory – see sections 18.3 and 19.1 of [41].

We detect tunneling by watching the average value of the Polyakov Loop along each direction to see when it changes significantly. An example is shown in Fig. 22. At the beginning of the simulation shown, the expectation value of the Polyakov Loop is a positive real number as shown in Fig. 23. After about

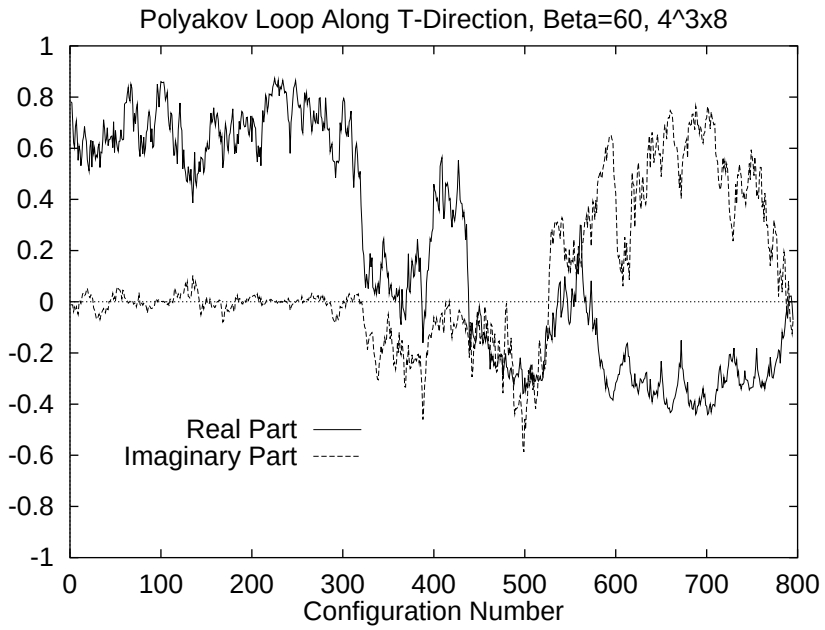

Figure 23: Average value of Polyakov Loop along the time direction as a function of configuration number for a $4^3 \times 8$ lattice at $\beta = 60$ (dataset tp6).

300 configurations, the system begins to tunnel toward the minimum located at $e^{4\pi i/3}$ times the original minimum. After a total of 580 configurations it has tunneled to the minimum located at $e^{2\pi i/3}$ times the original minimum. We think that domains are being formed during the tunneling process which causes the "continuous" transition from one minimum to another. Within each domain, the plaquettes should be close to the perturbation theory values, and perturbation theory should work. In the regions between domains perturbation theory is not expected to accurately describe the system. Since the quark propagator is not invariant under the center symmetry transformation, it will have different values in different domains, so the tunneling presents a major problem to the measurement of quark propagators. Quantities which are invariant under the center symmetry, such as Wilson loops, have less of a problem (as long as they are small) since they have the same value in different domains, and are thus

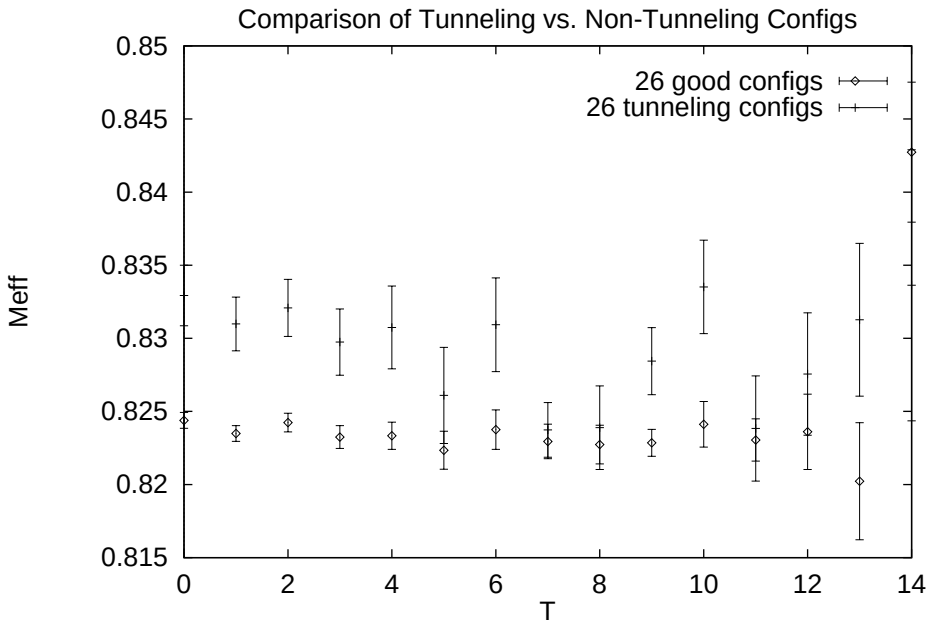

Figure 24: Comparison of m_{eff} for tunneling and non-tunneling configurations in Axial-Coulomb gauge on a $24^3 \times 32$ lattice at $\beta = 16$ for Wilson quarks with $\kappa = 0.100$ (dataset HQ14). Errorbars were computed with the bootstrap method.

only affected by the regions between domains. In Fig. 24 we show plots of m_{eff} as computed from (324) for an equal number of configurations with and without tunneling. The configurations which were in the process of tunneling show significantly more noise.

To cope with the problem of tunneling, we stopped the calculation when there were signs of tunneling and then started the calculation over with a new seed for the gauge field generator. Using this method, we were able to generate enough configurations without including configurations which had tunneling. Another possible approach would be to add a small term to the gluon action which would break the center symmetry (like applying a small magnetic field to a material) and extrapolating it away.

One might think that problems could be avoided by examining meson prop-

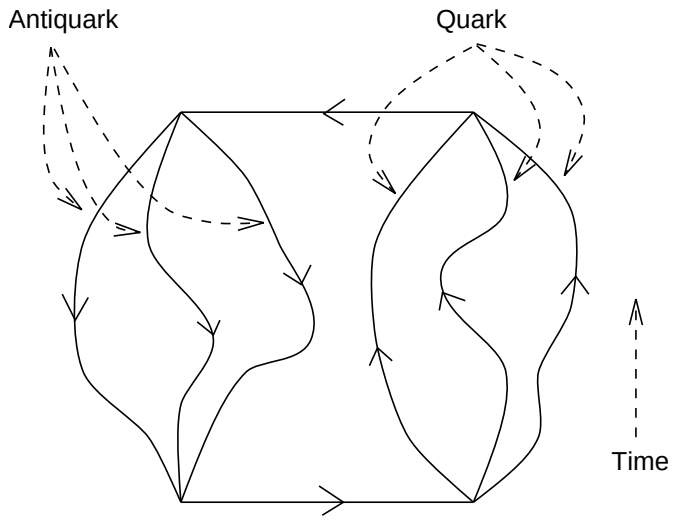

Figure 25: Some link variable paths contributing to a meson propagator.

agators in the Monte Carlo simulation instead of quark propagators. Such an idea is inspired by the fact that gauge invariant meson propagators can be constructed. To understand this better, we look back at the quark propagator after performing the path integral (274). The quark propagator can be interpreted as follows (see the appendix to chapter 14 in [40] for details). The $K^{-1}(U, x, y)$ part can be written as a sum over all paths connecting x and y that involve a product of link operators along the path. The $\det\{K(U)\}$ part can be written as a sum over closed loops which involves a product of link operators around the loop (our simulation used the quenched approximation, so these loops were dropped). So, if we construct a meson operator with two quark fields connected by link variables to make it gauge invariant (see for example section 7.2 of [41]), the meson propagator can be seen to be related to a sum over closed loops of products of link variables around the loop – see Fig. 25. But, a product of link variables around a closed loop is gauge invariant. Tunneling will give an extra factor of $e^{2\pi i/3}$ or $e^{4\pi i/3}$ to the quark propagator if the paths connecting the two ends of the propagator pass through the plane which has tunneled. So one might

hope that a meson wouldn't have problems since the antiquark would pick up the complex conjugate factor. But, if domains are formed some of the paths for the quark propagator will pass through a particular domain and some will not, so the phases will not cancel even for a meson. Thus mesons don't solve the tunneling problem.

7.4.2 Choosing a Gauge – Infrared Problems

Since the quark's mass is a physical quantity, it should be gauge invariant and one would naively think that we could perform the Monte Carlo simulation with any gauge. However, our method of extracting the mass won't work with some gauges because of infrared problems. For example, consider the result of a continuum Feynman gauge calculation of the electron self energy (in Minkowsky space) given in Eq. 8.42 of [54]. The infrared singularity gives rise to a term proportional to $\ln((m^2-p^2)/m^2)$. When infrared singularities are summed to all orders, the result is the 1-loop singularity exponentiated (see for example [55]). So, the propagator is really of the form

$$\frac{\not{p}+m}{p^2-m^2}\exp\left\{a\ln((m^2-p^2)/m^2)\right\} \propto \frac{1}{(p^2-m^2)^{1-a}} \tag{364}$$

where a is a (gauge dependent) constant. We see that a gauge with infrared problems will have a branch cut in the propagator rather than a simple pole. Because of this, our procedure for extracting m_{eff} using (324) won't work in gauges that have infrared singularities. To see this, we consider instead of equation (323):

$$G_a(t) = \int_{-\infty}^{\infty} dE e^{iEt}\frac{1}{(E^2+m^2)^{1-a}} = \int_{-\infty}^{\infty} dE \frac{\cos(Et)}{(E^2+m^2)^{1-a}}. \tag{365}$$

This integral can be done, giving

$$G_a(t) = \frac{2^a\sqrt{2\pi}}{\Gamma(1-a)}\left(\frac{m}{t}\right)^{a-\frac{1}{2}} \mathrm{K}_{\frac{1}{2}-a}(mt), \tag{366}$$

where $\mathrm{K}_\nu(z)$ is the modified Bessel Function of the second kind. For fixed ν and large z (see Eq. 9.7.2 of [56]),

$$\mathrm{K}_\nu(z) \sim \sqrt{\frac{\pi}{2z}} e^{-z} \left\{ 1 + \frac{4\nu^2 - 1}{8z} + \ldots \right\}. \tag{367}$$

This gives us

$$G_a(t) \sim \frac{2^a \pi}{\Gamma(1-a)} \frac{m^{a-1}}{t^a} e^{-mt} \left\{ 1 + \frac{4(\frac{1}{2} - a)^2 - 1}{8mt} + \ldots \right\} \tag{368}$$

Notice that for $a \neq 0$, m_{eff} will depend on t and a, which shows that we shouldn't expect m_{eff} to be a useful (gauge independent) quantity for gauges with infrared singularities. For $a = 0$, we get the expected result

$$G_0(t) = \frac{\pi}{m} e^{-mt}. \tag{369}$$

Infrared problems make Landau and Axial gauges useless for extracting masses from quark propagators. Coulomb gauge has desirable infrared properties, but as described in Sec. 6.1, Coulomb gauge fixing doesn't completely fix the gauge. Our solution to this problem was to first do Axial gauge fixing, and then do Coulomb gauge fixing on the result. We refer to the resulting gauge as Axial-Coulomb gauge. In Fig. 26 we compare Monte Carlo results to perturbation theory at $\beta = 60$. At this lattice spacing, $\alpha \approx 0.008$, so 1-loop perturbation theory and Monte Carlo should be in excellent agreement. We find that Axial-Coulomb gauge works well while Landau and Axial gauges fail terribly. The slope of the m_{eff} curve for Landau gauge depends on the volume of the lattice. Generally, as the volume is increased the slope decreases, but beyond a volume of $20^3 \times 32$ the slope seems to stop changing. In Fig. 27 we do a similar comparison for NRQCD quarks. Again, Axial-Coulomb gauge is the only acceptable gauge. Note that for NRQCD quarks the tree-level result is just zero. Axial-Coulomb gauge is free of infrared problems as long as the

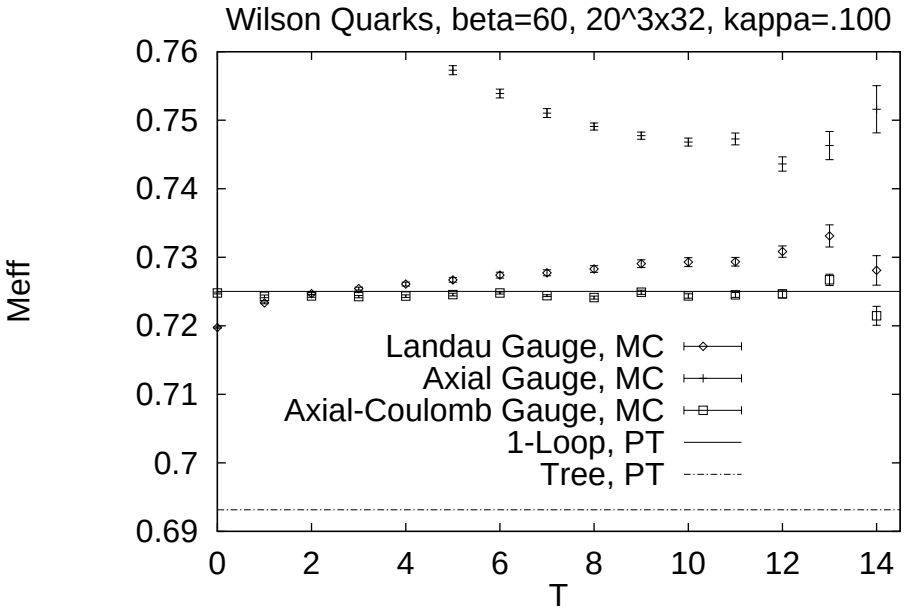

Figure 26: Comparison of $m_{\rm eff}$ Monte Carlo calculation in various gauges to perturbation theory results for a Wilson quark.

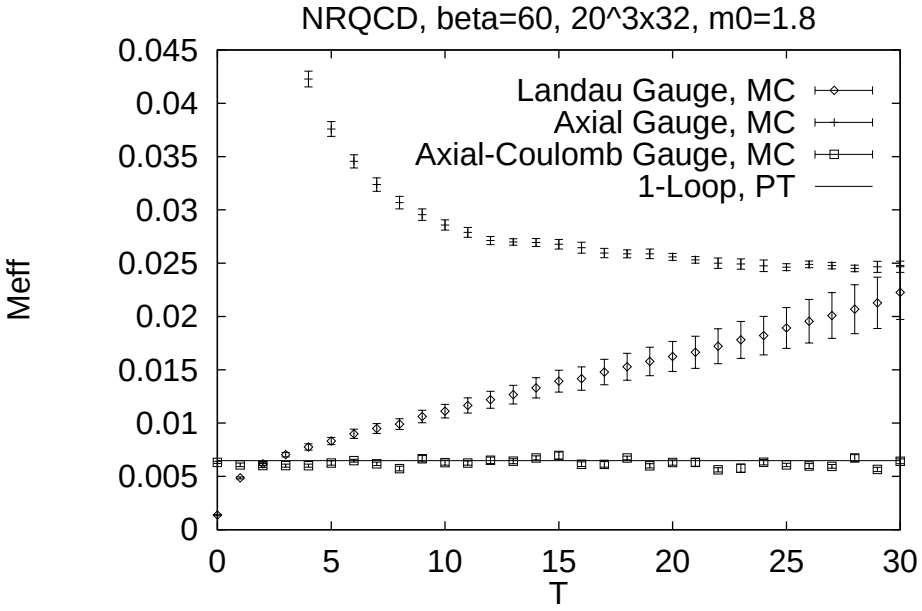

Figure 27: Comparison of $m_{\rm eff}$ Monte Carlo calculation in various gauges to perturbation theory results for a NRQCD quark.

three momentum of the quark is zero since the divergence in Coulomb gauge is multiplied by $\vec{p}^2$. When $\vec{p} \neq 0$ it has problems similar to Landau gauge.

7.4.3 Zero Mode

Problems arise in the lattice perturbation theory calculation as well. Examining the gluon propagator (306), we see that it is infinite when the gluon momentum is zero. This is problematic because for a finite lattice the self energy calculation involves a sum over gluon momenta. The sum can be replaced by an integral if we take the lattice volume to infinity while keeping the lattice spacing fixed. This introduces a systematic error since the Monte Carlo calculation is done on a finite lattice. The complexity of the integrand forces us to evaluate it numerically, so again the gluon propagator gives problems at zero momentum. This can be overcome by giving the gluon a non-zero mass and then extrapolating to zero gluon mass. The gluon is given a mass by modifying its propagator by replacing the overall factor of $1/\hat{q}^2$ with $1/(\hat{q}^2 + \lambda^2)$ and replacing the $(\xi - 1)\hat{q}_\mu \hat{q}_\nu / \hat{q}^2$ term with $(\xi - 1)\hat{q}_\mu \hat{q}_\nu / (\hat{q}^2 + \xi\lambda^2)$ (see Eq. 3-149 of [50]). Morningstar gives a procedure in [57] which improves the convergence to the infinite volume limit. The integral is written as a sum just as it would be for a finite volume calculation. But, this sum is pictured as a trapezoid rule approximation to the integral (keeping in mind the periodicity of the integrand so the endpoint terms that would be multiplied by 1/2 can be replaced by a single term with no 1/2). A change of variables that maintains the periodicity of the integrand is performed to improve the convergence of the sum to the value of the integral:

$$q'_\mu = q_\mu - \alpha \sin(q_\mu) \tag{370}$$

where optimal convergence is obtained by using the α which satisfies

$$\alpha = \operatorname{sech}(u) \qquad \text{where} \qquad \lambda = u - \tanh(u) \tag{371}$$

and λ is the gluon mass. This brings in a Jacobian factor: $\prod_\mu(1-\alpha\cos q_\mu)$. Adding a gluon mass isn't enough to tame the numerical problems for the diagram in figure 21A since the intermediate fermion propagator is on shell when the gluon momentum is zero. To avoid this problem, the contour for the q_4 integration is deformed for this diagram. Instead of going along the real line from $-\pi$ to π, it goes along the three line segments: $-\pi \to -\pi+i\lambda/2 \to \pi+i\lambda/2 \to \pi$. The periodicity of the integrand causes the contributions from the the two segments parallel to the imaginary axis to cancel. Note that the original sum was exactly gauge invariant because gauge dependent terms with momentum q canceled against those with momentum $-q$ as shown in Sec. 7.3. Now that our q_4 sum is from $-\pi+i\lambda/2$ to $\pi+i\lambda/2$ we no longer have this exact cancellation and our result will only be gauge invariant to the extent that the sum correctly approximates the contour integral that it replaces. We tested this and found that there is no sign of gauge dependence as long as a reasonable number of terms are included in the sum.

The calculation of the scale for the coupling, q^*, has problems because of the logarithm in (319). We can use the gluon mass to regulate the logarithm:

$$\ln(q^2) \to \ln(q^2+\lambda^2). \tag{372}$$

But this is not periodic in q_4, so the contour deformation that we did for the diagram in figure 21A isn't correct unless we keep the contributions from the segments parallel to the imaginary axis. An alternative proposed in [58] is to replace q_4^2 with a [2/2] Padé approximant in $\exp(-iq_4)$ to make the integrand periodic in q_4 so that the contribution from the segments of the contour parallel to the imaginary axis will cancel. We dropped the segments parallel to the imaginary axis without making this substitution and later verified that this did not affect our results within the accuracy we required after the extrapolation

$\lambda \to 0$ (results with $\lambda \neq 0$ were affected and were not gauge invariant – using the Padé approximant is a much better approach). Another way to maintain periodicity of the integrand is to use $\ln(\hat{q}^2 + \lambda^2)$.

The zero mode also obscures the analysis of the Monte Carlo data. We run the Monte Carlo calculations with large β to give a small lattice spacing a. The smallest non-zero momentum on the lattice is $2\pi/La$ where L is the number of lattice sites along the longest side of the lattice. By making a small we make the smallest non-zero momentum large which removes non-perturbative low energy effects. However, there are zero momentum gluons on the lattice. The mass is UV divergent, so we expect the high momentum modes to dominate in the calculation, but we must keep in mind that the coupling grows as the gluon momentum goes to zero. The zero mode is especially problematic for gauges that have infrared problems since quantities computed in such gauges are very sensitive to the low energy gluons.

7.5 Results

7.5.1 Perturbation Theory

Wilson Fermions The perturbation theory calculations were performed for several values of the tree-level mass. For each calculation the gluon masses used were: 0.10, 0.20, 0.30, 0.35, 0.40, 0.45, 0.50, 0.55, 0.60, 0.65, 0.70, and 0.80. Rational function extrapolation was used to find the $\lambda \to 0$ results. The sums used to approximate the integrals contained 28^4 points. The calculation was attempted for $\kappa = 0.125$ (i.e. $m^{\text{tree}} = 0$) but could not be extrapolated to $\lambda \to 0$ because the results (even c_1) were not monotonic in λ. So we obtained results for $\kappa = 0.125$ by performing an extrapolation in the tree-level mass. We calculate

Table 2: Infinite volume perturbation theory results for Wilson quark mass. The uncertainty in q^* and c_1 is due to the extrapolation to zero gluon mass. Values with an asterisk next to them (ie. $\kappa = .125$ values) were obtained by extrapolating the other values – the second uncertainty is the estimated extrapolation error.

κ	q^*	$\alpha_V(q^*), \beta = 16$	$\alpha_V(q^*), \beta = 20$	c_0	c_1
0.067	1.99(1)	0.03607(1)	0.027652(7)	1.49575	2.82(1)
0.087	2.11(1)	0.03594(1)	0.027573(7)	1.01056	3.32(1)
0.100	2.20(1)	0.03584(1)	0.027518(7)	0.69315	3.83(1)
0.108	2.28(5)	0.03575(5)	0.02747(3)	0.48835	4.25(1)
0.115	2.31(1)	0.03573(1)	0.027450(7)	0.29849	4.71(1)
0.118	2.34(1)	0.03569(1)	0.027431(7)	0.21292	4.94(1)
0.125	2.42(1)(2)*	0.03562(3)	0.02739(2)	0.00000	5.52(1)(1)*

the parameters in:

$$m = c_0 + c_1\alpha_V(q^*) + c_2\alpha_V^2(q^*) + ... \tag{373}$$

We get c_0 from the tree-level mass (331), c_1 from the 1-loop result (347), and q^* from (319). The results are shown in Table 2.

We calculate α_V from Eq. 8 in [44]:

$$\alpha_V^{-1}(q) = \beta_0 \ln(q^2/\Lambda_V^2) + \beta_1/\beta_0 \ln\ln(q^2/\Lambda_V^2) + \mathcal{O}(\alpha_V) \tag{374}$$

where $\beta_0 = 11/4\pi$ and $\beta_1 = 102/16\pi^2$ (for zero quark flavors). We determine Λ_V for each lattice spacing (each value of β) by using the known relationship between the logarithm of the plaquette and α_V. This relationship is given by Eq. 20 in [44]:

$$-\ln\left\langle \frac{1}{3}\mathrm{Tr}\left\{U_{\mathrm{plaq}}\right\}\right\rangle = \frac{4\pi}{3}\alpha_V(3.41)\left\{1 - (1.19 + 0.017n_f)\alpha_V + \mathcal{O}(\alpha_V^2)\right\}, \tag{375}$$

where the number of quarks, n_f, is zero in our case. We measure the plaquette during the simulation and then solve this equation for $\alpha_V(3.41)$. This value is used in (374) to solve for Λ_V with an iterative procedure. Results are shown in Table 3.

Table 3: Measured values of the 1×1 Wilson loop $W_{11} = \left\langle \frac{1}{3}\mathrm{Tr}\left\{U_{\mathrm{plaq}}\right\}\right\rangle$ and corresponding values of Λ_V for various β's.

β	W_{11}	$a\Lambda_V$
7	0.6715	0.045
9	0.7564	0.0041
12	0.8225	0.00012
16	0.8694	1.1×10^{-6}
20	0.8966	9.8×10^{-9}
60	0.9663	2.9×10^{-29}

NRQCD Fermions Nonrelativistic QCD (NRQCD) is an effective field theory which approximates full QCD by a systematic expansion in powers of the velocity of the quarks. NRQCD can be more efficient than the full theory and has been successfully used in lattice simulations of the ψ and Υ families of mesons. The reader is referred to [51] and [59] for more details. In NRQCD the energy of a quark is given by:

$$E = c_1^A \alpha_V(q_A^*) + c_2^A \alpha_V^2(q_A^*) + ... + \frac{\hat{p}^2}{2M} + \mathcal{O}(\hat{p}^4) \tag{376}$$

where

$$M = M_0 \left[1 + c_1^B \alpha_V(q_B^*) + c_2^B \alpha_V^2(q_B^*) + ...\right]. \tag{377}$$

The perturbation theory values for c_A, q_A^*, c_B, and q_B^* were computed by Morningstar [60] and are given in Table 4.

7.5.2 Monte Carlo

Wilson Fermions We used the Monte Carlo measurements of m_{eff} in two ways. The first was to extract c_1 and q^* and test to see if they agreed with the known perturbation theory results. This was done by measuring m_{eff} at two different lattice spacings and using

$$m_{\mathrm{eff}}(\beta = 16) \;\; = \;\; c_0 + c_1 \alpha_V(q^*, \beta = 16) + \mathcal{O}(\alpha^2)$$

Table 4: Infinite volume perturbation theory results for NRQCD quark energy. Values were computed with tadpole improvement and $\delta H = 0$.

M_0	n	c_1^A	q_A^*	c_1^B	q_B^*	$\alpha_V(q_A^*), \beta = 16$	$\alpha_V(q_A^*), \beta = 20$
8.0	1	1.0019	0.77	0.0319	0.02	0.03845	0.02902
6.0	1	.9791	0.74	0.0990	0.34	0.03856	0.02908
5.0	1	.9609	0.72	0.1514	0.54	0.03863	0.02912
4.0	1	.9337	0.69	0.2278	0.73	0.03874	0.02918
1.8	2	.7669	0.45	0.6385	1.02	0.03994	0.02985
0.8	4	.3880	0.03	1.2155	1.00	0.04969	0.03492
0.6	4	.1606	0.00	1.4702	0.99	?	?

$$m_{\rm eff}(\beta = 20) \quad = \quad c_0 + c_1 \alpha_V(q^*, \beta = 20) + \mathcal{O}(\alpha^2). \tag{378}$$

We neglect the $\mathcal{O}(\alpha^2)$ terms and solve for the ratio $\alpha_V(q^*, \beta = 16)/\alpha_V(q^*, \beta = 20)$ in terms of the measured values of $m_{\rm eff}$ and the known value of c_0. We then employ a combination of the Newton-Raphson and bisection methods (see the rtsafe() function in [61]) to solve for q^* using (374) and the known values of Λ_V from Table 3. Once we know q^* we compute c_1 from (378). In order to account for the uncertainty in $m_{\rm eff}$, $\delta m_{\rm eff}$, we generated samples from a gaussian distribution with mean $m_{\rm eff}$ and standard deviation $\delta m_{\rm eff}$ at each β and used the samples to generate distributions for the values of c_1 and q^* by using the procedure above to compute c_1 and q^* for each sample. The distribution of c_1 was fairly symmetric as shown in Fig. 28 but that of q^* was highly skewed as shown in Fig. 29.

In Table 5 we show intervals for the values of c_1 and q^* at the 68% and 90% confidence level. These values should be compared to the perturbation theory calculations in Table 2. We see that values for c_1 are fairly precisely determined but values for q^* are not. The values for c_1 computed by Monte Carlo are slightly too small for small values of κ, but the agreement with perturbation theory is good for larger values of κ (small mass). For q^* the Monte Carlo values are too

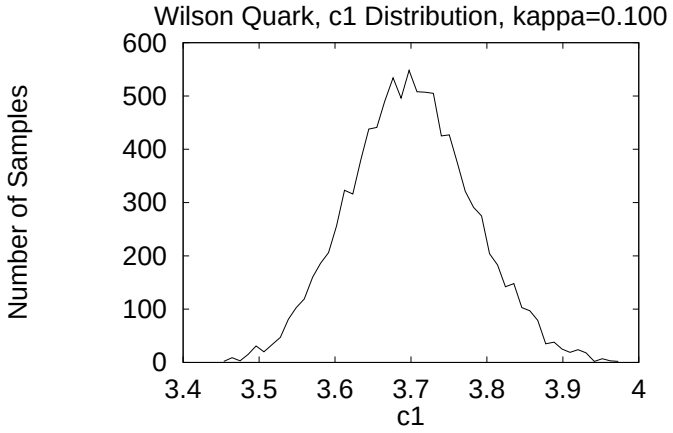

Figure 28: Example of c_1 distribution for $\kappa = 0.100$. 10,000 samples total.

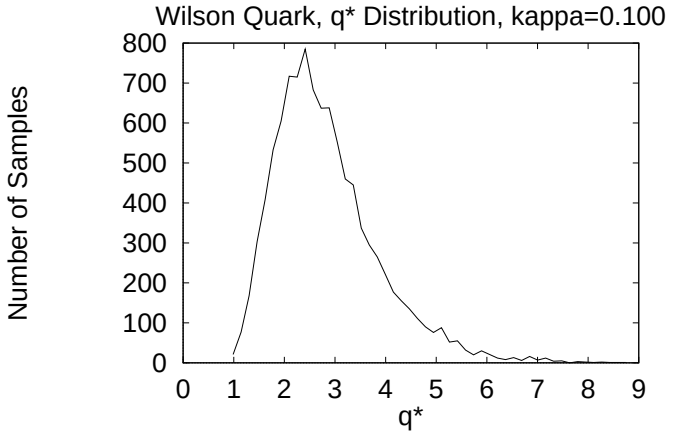

Figure 29: Example of q^* distribution for $\kappa = 0.100$. 10,000 samples total

Table 5: Values for c_1 and q^* for Wilson quarks at 68% and 90% confidence levels from Monte Carlo measurements at $\beta = 16$ (239 configurations) and $\beta = 20$ (234 configurations) on a $24^3 \times 32$ lattice.

κ	c_1 (68%)	c_1 (90%)	q^* (68%)	q^* (90%)
0.067	2.59-2.74	2.54-2.80	0.95-2.30	0.72-3.15
0.087	3.10-3.26	3.05-3.32	1.42-3.08	1.11-4.05
0.100	3.62-3.78	3.57-3.84	1.88-3.77	1.51-4.80
0.108	4.06-4.23	4.01-4.29	2.40-4.56	1.95-5.70
0.115	4.57-4.74	4.52-4.80	3.13-5.69	2.59-6.99
0.118	4.85-5.02	4.79-5.08	3.63-6.48	3.02-7.91

Table 6: Monte Carlo results for 2-loop Wilson quark mass at $\beta = 16$ (239 configurations) and $\beta = 20$ (234 configurations) on a $24^3 \times 32$ lattice. The uncertainties in c_2 are from the uncertainty in $m^{\rm MC}$, c_1, and the $\mathcal{O}(\alpha^3)$ term. Values with an asterisk next to them (i.e. $\kappa = .125$ values) were obtained by extrapolating the other values (excluding $\kappa = .118$) – the second uncertainty is the estimated extrapolation error.

κ	$m^{\rm MC}$, $\beta = 16$	c_2, $\beta = 16$	$m^{\rm MC}$, $\beta = 20$	c_2, $\beta = 20$
0.067	1.5938(2)	-2.9(7)	1.5705(5)	-4.2±1.2
0.087	1.1250(2)	-3.8(7)	1.0984(5)	-5.0±1.2
0.100	0.8241(2)	-4.8(7)	0.7940(5)	-5.9±1.2
0.108	0.6331(2)	-5.6(7)	0.6002(5)	-6.4±1.2
0.115	0.4588(2)	-6.3(7)	0.4227(5)	-6.8±1.2
0.118	0.3811(2)	-6.4(7)	0.3436(5)	-6.5±1.2
0.125	0.1914(3)	-7.7(7)(1)*	0.1503(5)	-7.0±1.2±.6*

large for large κ and are in reasonable agreement with perturbation theory for small κ. Note that we have neglected α^2 contribution in (378) which we expect to cause an error of order 5-10% in c_1 (since $\alpha \approx .03$). With this in mind, the agreement between Monte Carlo and perturbation theory values of c_1 is very good.

In our second analysis of the Monte Carlo data we assume c_1 and q^* are known from perturbation theory and we use the Monte Carlo data to compute the 2-loop coefficient, c_2, using (322). We do this for both values of β and compare the results for consistency. The results are shown in Table 6. The agreement between the values of c_2 measured at different β's is reasonable.

NRQCD Fermions We perform the same analysis for NRQCD fermions with zero momentum. The values of c_1^A and q_A^* are shown in Table 7. Again, q^* is not very well determined. The uncertainty in c_1^A is larger (as a percentage) than the uncertainty in c_1 for Wilson quarks, but the absolute uncertainties are about the same. When sampling values for $m_{\rm eff}$ to compute the distribution of

Table 7: Values for c_1^A and q_A^* for NRQCD quarks at 68% and 90% confidence levels from Monte Carlo measurements at $\beta = 16$ (239 configurations) and $\beta = 20$ (234 configurations) on a $24^3 \times 32$ lattice.

M_0	n	c_1^A (68%)	c_1^A (90%)	q_A^* (68%)	q_A^* (90%)
8.0	1	0.766-0.995	0.705-1.078	0.03-1.02	0.01-3.46
6.0	1	0.748-0.975	0.688-1.058	0.03-0.99	0.01-3.44
5.0	1	0.734-0.960	0.674-1.042	0.03-0.97	0.01-3.36
4.0	1	0.713-0.937	0.653-1.018	0.03-0.93	0.01-3.35
1.8	2	0.581-0.793	0.527-0.872	0.02-0.72	0.006-3.00
0.8	4	0.294-0.464	0.255-0.532	0.002-0.27	0.0007-1.91
0.6	4	0.150-0.274	0.134-0.329	0.0004-0.09	0.0002-1.11

Table 8: Monte Carlo results for 2-loop NRQCD quarks at $\beta = 16$ (239 configurations) and $\beta = 20$ (234 configurations) on a $24^3 \times 32$ lattice. The uncertainties in c_2^A are due to uncertainties in $m^{\rm MC}$ and the $\mathcal{O}(\alpha^3)$ term. No values are given for c_2^A when $M_0 = 0.6$ because the q_A^* is not known.

M_0	n	$m^{\rm MC}, \beta = 16$	$c_2^A, \beta = 16$	$m^{\rm MC}, \beta = 20$	$c_2^A, \beta = 20$
8.0	1	0.0376(2)	-0.65±.2	0.0275±.001	-1.81±1.2
6.0	1	0.0370(2)	-0.57±.2	0.0270±.001	-1.70±1.2
5.0	1	0.0364(2)	-0.50±.2	0.0266±.001	-1.60±1.2
4.0	1	0.0356(2)	-0.40±.2	0.0260±.001	-1.46±1.2
1.8	2	0.0307(2)	0.02±.2	0.0222±.001	-0.79±1.2
0.8	4	0.0193(2)	-0.004±.2	0.0134±.001	-0.13±1.2
0.6	4	0.0124(2)	?	0.0081±.001	?

c_1^A and q_A^* about 3-10% of the samples had to be discarded because values of c_1^A and q_A^* could not be found that would generate the appropriate $m_{\rm eff}$'s. This could cause some systematic error in the results. This was not a problem for the Wilson quarks. Comparison with the results from perturbation theory in Table 4 shows good agreement (recall that $\mathcal{O}(\alpha^2)$ terms should introduce a systematic error of about 5% for c_1^A). It is interesting to note that the Monte Carlo data confirms the perturbation theory prediction that q_A^* is very small when M_0 is small. This leads us to the conclusion that the perturbative results cannot be

used on a lattice with realistic lattice spacing for quarks with small M_0 since the renormalization is not dominated by high momenta.

Extraction of the 2-loop coefficient, c_2, from the Monte Carlo data is shown in Table 8. The agreement between the values of c_2^A extracted from $\beta = 16$ and $\beta = 20$ data is reasonable.

7.6 Conclusions

We find that we are able to succesfully extract the 1-loop coefficient and q^* for the quark mass renormalization from Monte Carlo data given only the tree level result for both Wilson quarks and NRQCD quarks. We also find that by using the lattice perturbation theory results for the 1-loop coefficient and q^* we are able to extract the 2-loop coefficient from the Monte Carlodata with consistent results. This technique is important because the coefficients in the perturbative expansion are difficult to compute using Feynman rules.

A Kinematics in Various Frames

In this appendix we present some of the properties of various four-momenta in the three coordinate systems mentioned in Sec. 5 (the B-, M-, and L-frames). Many of the results can be found in the literature [25, 28, 29].

In the center of mass system of $D(D^*)\pi$ (the M-frame), we have

$$\begin{aligned} p &= |\,\vec{p}\,| = |\,\vec{q}\,| \\ &= \frac{1}{2}\sqrt{s_M}\beta\ , \end{aligned} \tag{379}$$

$$L = |\,\vec{L}\,| = \frac{X}{\sqrt{s_M}}\ , \tag{380}$$

where

$$X = \sqrt{(P\cdot L)^2 - s_M s_L}, \tag{381}$$

and

$$\beta = \frac{1}{s_M}\sqrt{s_M^2 - 2s_M\,(m^2+m_\pi^2) + (m^2-m_\pi^2)^2}\ . \tag{382}$$

In the M-frame, the components of the four-vectors P^μ and L^μ as well as the linear polarization vectors $e^\mu_{1,2,3}$ are given in Table 9. The values of $|\,\vec{p}\,|$ and $P\cdot L$ are given by (379) and (142), respectively. The three linear polarization vectors of D^* in the M-frame as indicated in Fig. 5 are denoted by e^μ_1, e^μ_2, and e^μ_3. Their components in the M-frame are listed in Table 9.

At times it is useful to know the Lorentz transformations that connect the different reference frames. A simple calculation gives the parameters

$$\beta_{ML} = \frac{X}{P\cdot L}\ , \tag{383}$$

Table 9: Components of various four-vectors in the center-of-mass frame of $D(D^*)\pi$ (the M-Frame).

a^μ	a^x	a^y	a^z	a^0
p^μ	$p\sin\theta$	0	$p\cos\theta$	$\frac{1}{2\sqrt{s_M}}(s_M - m_\pi^2 + m^2)$
L^μ	0	0	$-L$	$\frac{1}{\sqrt{s_M}}P\cdot L$
e_1^μ	$\cos\theta$	0	$-\sin\theta$	0
e_2^μ	0	1	0	0
e_3^μ	$\frac{p^0}{m}\sin\theta$	0	$\frac{p^0}{m}\cos\theta$	$\frac{p}{m}$

$$\beta_{MB} = \frac{X}{P\cdot L + s_M} \quad . \tag{384}$$

If a_L^μ and a_M^μ are components of the same four-vector in the L-frame and the M-frame, respectively, they are related by the Lorentz transformations

$$a_L^z = \gamma_{ML}\left(a_M^z + \beta_{ML}a_M^0\right) \quad , \tag{385}$$

$$a_L^0 = \gamma_{ML}\left(a_M^0 + \beta_{ML}a_M^z\right) \quad . \tag{386}$$

Similar equations hold using β_{MB} to relate a_B^μ and a_M^μ, the components of a vector in the B and M frames.

From Q^μ and P^μ we can construct another four-momentum which is orthogonal to P^μ:

$$Q'_\mu = Q_\mu - \frac{m^2 - m_\pi^2}{s_M}P_\mu \tag{387}$$

with (see (140))

$$Q'\cdot P = 0 \quad . \tag{388}$$

Table 10: Components of various four-vectors in the rest frame of the lepton pair (the L-Frame).

a^μ	a^x	a^y	a^z	a^0
L^μ	0	0	0	$\sqrt{s_L}$
P^μ	0	0	$X/\sqrt{s_L}$	$P\cdot L/\sqrt{s_L}$
Q'^μ	$\sqrt{s_M}\beta\sin\theta$	0	$P\cdot L\beta\cos\theta/\sqrt{s_L}$	$X\beta\cos\theta/\sqrt{s_L}$
p_ℓ^μ	$\frac{1}{2}\sqrt{s_L}\sin\theta_\ell\cos\phi$	$-\frac{1}{2}\sqrt{s_L}\sin\theta_\ell\sin\phi$	$-\frac{1}{2}\sqrt{s_L}\cos\theta_\ell$	$\frac{1}{2}\sqrt{s_L}$

Now, we are ready to list the components of various four-vectors in different frames of reference. In the L-frame, the components of various four-vectors are listed in Table 10.

The components of P_B and p_ν can be found from the quantities given above in the Tables. Furthermore, with the help of a Lorentz transformation we can determine the components of all the four-vectors in another coordinate system.

B Relating Rates to D^* Width

In this appendix we derive a linear relation between the semileptonic decay rates with a soft pion emission and the inverse of the D^* width. In what follows, the $D^*D\pi$ coupling constant f which appears in the pion emission vertices is held fixed, while the width Γ_{D^*} is considered to be a free parameter in the D^* propagator.

We emphasize that our numerical work does not make the approximation presented below. The purpose of this appendix is to understand the regularities exhibited in the numerical results of Figs. 9-12.

Consider the Feynman diagram with the D^* pole contributing to $\bar{B} \to D\pi\ell\bar{\nu}$ (Fig. 3b). The matrix element can be written as

$$M(\bar{B} \to D\pi\ell\bar{\nu}) = \sum_{\lambda} M[D^*(\lambda) \to D\pi] \frac{1}{P^2 - m^2 + im\Gamma_{D^*}} M[\bar{B} \to D^*(\lambda)\ell\bar{\nu}], \tag{389}$$

where λ denotes the polarization of D^*, and P and m are the 4-momentum and mass of D^*, respectively. For example,

$$M[D^*(\lambda) \to D\pi^a] = u^*(D^*)\frac{1}{2}\tau^a u(D)\sqrt{m_D m}\,\frac{f}{f_\pi}\,\varepsilon(\lambda)\cdot q, \tag{390}$$

where q is the pion momentum. The decay rate for $\bar{B} \to D\pi\ell\bar{\nu}$ due to the D^* pole is

$$\begin{aligned}
\Gamma_{\mathrm{D^*\,pole}}(\bar{B} \to D\pi\ell\bar{\nu}) &= \frac{1}{2m_B}\frac{1}{2\pi}\sum_{\lambda}\int ds_M |M[\bar{B} \to D^*(\lambda)\ell\bar{\nu}]|^2 (2\pi)^4 \\
&\times \delta^4(P_B - p_\ell - p_\nu - P)\frac{d^3p_\ell}{(2\pi)^3 2E_\ell}\,\frac{d^3p_\nu}{(2\pi)^3 2E_\nu}\,\frac{d^3P}{(2\pi)^3 2E_P} \\
&\times \frac{1}{(s_M - m^2)^2 + m^2\Gamma_{D^*}^2}\int |M[D^*(\lambda) \to D\pi]|^2 \\
&\times (2\pi)^4\delta^4(P - q - p)\frac{d^3p}{(2\pi)^3 2E_p}\,\frac{d^3q}{(2\pi)^3 2E_q}.
\end{aligned} \tag{391}$$

This equation follows from inserting the factor

$$1 = \int ds_M \, \frac{d^3P}{2E_P} \delta^4(P - q - p), \quad E_P \equiv \sqrt{\vec{P}^2 + s_M}, \tag{392}$$

and the observation that one of the double sums over D^* polarizations after squaring (389) is eliminated when we carry out the integration over the directions of $\vec{q}$. Making use of the standard formula for a decay width, we find

$$\Gamma_{\mathrm{D^* \, pole}}(\bar{B} \to D\pi\ell\bar{\nu}) = \frac{1}{\pi} \int ds_M \frac{\sqrt{s_M}\,\Gamma(\bar{B} \to D^*\ell\bar{\nu}, s_M)\Gamma(D^* \to D\pi, s_M)}{(s_M - m^2)^2 + m^2\Gamma_{D^*}^2}. \tag{393}$$

To obtain (393), we have used the fact that the width of the decay $D^* \to D\pi$ is independent of the D^* polarization. The argument s_M appears in the numerator of the integrand of (393) because the widths are those appropriate for D^* with a mass $\sqrt{s_M}$.

Let us introduce the new variables

$$s_M = m^2 + xm\Gamma_{D^*}, \tag{394}$$

$$F(s_M) = \sqrt{s_M}\,\Gamma(\bar{B} \to D^*\ell\bar{\nu}, s_M)\Gamma(D^* \to D\pi, s_M). \tag{395}$$

(393) now becomes

$$\Gamma_{\mathrm{D^* \, pole}}(\bar{B} \to D\pi\ell\bar{\nu}) = \frac{1}{m\Gamma_{D^*}} \frac{1}{\pi} \int dx \frac{1}{x^2 + 1} F[m^2 + xm\Gamma_{D^*}]. \tag{396}$$

When the width Γ_{D^*} is small, the integrand can be expanded in a Taylor series. The leading term is

$$\Gamma_{\mathrm{D^* \, pole}}(\bar{B} \to D\pi\ell\bar{\nu}) = \frac{F(m^2)}{m\Gamma_{D^*}} \frac{1}{\pi} \int dx \frac{1}{x^2 + 1} + \cdots. \tag{397}$$

If the range of s_M is not restricted, after the x-integration we obtain

$$\Gamma_{\mathrm{D}^*\,\mathrm{pole}}(\bar{B}\to D\pi\ell\bar{\nu}) = \Gamma(\bar{B}\to D^*\ell\bar{\nu})\,\frac{\Gamma(D^*\to D\pi)}{\Gamma_{D^*}} + \cdots, \tag{398}$$

where (395) has been used. This is a well-known result in the theory of resonances. In practice, experimental cuts are imposed on the range of s_M. Suppose the cut is

$$|\sqrt{s_M} - m| < N\Gamma_{D^*}, \tag{399}$$

which corresponds to

$$-2N + N^2\frac{\Gamma_{D^*}}{m} < x < 2N + N^2\frac{\Gamma_{D^*}}{m}, \tag{400}$$

then the region (399) or (400) is the resonant contribution and outside this region is the nonresonant contribution. Finally,

$$\Gamma[\bar{B}\to(D\pi)_{\mathrm{res}} + \ell\bar{\nu}] = \left(\frac{2}{\pi}\tan^{-1}2N\right)\frac{1}{\Gamma_{D^*}}\cdot\frac{F(m^2)}{m} + A, \tag{401}$$

$$\Gamma[\bar{B}\to(D\pi)_{\mathrm{nonres}} + \ell\bar{\nu}] = \left(1 - \frac{2}{\pi}\tan^{-1}2N\right)\frac{1}{\Gamma_{D^*}}\cdot\frac{F(m^2)}{m} + A'. \tag{402}$$

The constant terms A and A' which are independent of Γ_{D^*} may arise from the nonleading contributions of $\Gamma_{\mathrm{D}^*\,\mathrm{pole}}$, the B^*-pole contributions, and the interference terms between the B^*-pole and D^*-pole contributions. The constants A and A' are generally very different for resonant and nonresonant contributions.

The definition (226) for resonant contributions corresponds to $N = 3$ and for this choice we have

$$\Gamma[\bar{B}\to(D\pi)_{\mathrm{res}} + \ell\bar{\nu}] = 0.895\,\frac{1}{\Gamma_{D^*}}\cdot\frac{F(m^2)}{m} + A, \tag{403}$$

$$\Gamma[\bar{B}\to(D\pi)_{\mathrm{nonres}} + \ell\bar{\nu}] = 0.105\,\frac{1}{\Gamma_{D^*}}\cdot\frac{F(m^2)}{m} + A'. \tag{404}$$

These linear relations are confirmed by the numerical results shown in Figs. 9-12 for $\bar{B}^0 \to D^+\pi^0 e^-\bar{\nu}_e$, $\bar{B}^0 \to D^0\pi^+ e^-\bar{\nu}_e$, and $B^- \to D^0\pi^0 e^-\bar{\nu}_e$. The ratio of slopes of the two linear relations is

$$\frac{(\text{slope})_{\text{res}}}{(\text{slope})_{\text{nonres}}} = \frac{0.895}{0.105} = 8.52 \quad , \tag{405}$$

which agrees with the slopes in Figs. 9-12, as can easily be verified. The decays $B^- \to D^+\pi^- e^-\bar{\nu}_e$ deserve special attention. First of all, $B^- \to (D^+\pi^-)_{\text{res}} e^-\bar{\nu}_e$ is kinematically forbidden if $\Gamma_{D^{*0}} \leq 0.4$ MeV, since $m(D^+\pi^-)$ always falls outside the resonant condition (226). For $\Gamma_{D^{*0}}$ between 0.4 and 1 MeV, the phase space is so restricted that the decay rates for $B^- \to (D^+\pi^-)_{\text{res}} e^-\bar{\nu}_e$ are completely negligible. Furthermore, the decay rate for $B^- \to (D^+\pi^-)_{\text{nonres}} e^-\bar{\nu}_e$ is found to be rather small and independent of Γ_{D^*} as seen in Fig. 12. This behavior can be understood by the following considerations. We notice that the leading term in the approximation (397) vanishes since there is no phase space for the decay $D^{*0} \to D^+\pi^-$ (see the mass values given in (221)). In addition, from (221) we have

$$P^2 = (p+q)^2 \geq (m_{D^+} + m_{\pi^-})^2, \tag{406}$$

or

$$P^2 - m_{D^{*0}}^2 \geq 7500 \text{ MeV}^2, \tag{407}$$

as compared with

$$200.7 \text{ MeV}^2 \leq m_{D^{*0}}\Gamma_{D^{*0}} \leq 2007 \text{ MeV}^2, \tag{408}$$

for 0.1 MeV $\leq \Gamma_{D^{*0}} \leq 1$ MeV. We conclude that in the denominator of the D^* propagator of (389), the imaginary part is always small and hence it can be neglected. The result is therefore independent of $\Gamma_{D^{*0}}$. Moreover, the denominator

of the D^* propagator is never very small and the phase space near its minimum (406) is very limited. As a consequence, the decay rate is substantially reduced.

The definition (226) for resonant contributions is reasonable, but somewhat arbitrary. However, the decay rate for resonant contributions is rather insensitive to the definition. As N varies from $N = 2$ to $N = \infty$, the slope in (403) changes by -5.7% and $+11.7\%$, respectively. On the other hand, the nonresonant contributions are very sensitive to the experimental cuts.

Finally, Figs. 9-12 show that the straight lines for the resonant contributions for both charged and neutral $\bar{B}$ mesons pass through the origin. We conclude that $A \approx 0$. This is to be expected since the cut (226) gives rise to a very small phase space contributing to the constant A.

C Euclidean Gamma Matrix Relations

The Euclidean gamma matrices are related to the Minkowsky gamma matrices by

$$\gamma_4 = \gamma_M^0 \quad , \quad \gamma_j = -i\gamma_M^j, \tag{409}$$

where the subscript M refers to Minkowsky (normal) gamma matrices. From this relation and the definition $\gamma_5 \equiv \gamma_1\gamma_2\gamma_3\gamma_4$ we find that $\gamma^5 = -\gamma_M^5$. We will also make use of the definition $\sigma_{\mu\nu} \equiv \frac{i}{2}[\gamma_\mu, \gamma_\nu]$, and the anticommutation relation $\{\gamma_\mu, \gamma_\nu\} = 2\delta_{\mu\nu}$.

C.1 Traces

Using the relationship between Euclidean and Minkowsky gamma matrices, we can easily obtain traces of Euclidean gammas from the Minkowsky relations published in Mandl and Shaw [49] (beware of the sign error in their equation A.21)

$$\mathrm{Tr}\{\gamma_\mu\gamma_\nu\} = 4\delta_{\mu\nu}, \tag{410}$$

$$\mathrm{Tr}\{\gamma_{\mu_1}\gamma_{\mu_2}\gamma_{\mu_3}\gamma_{\mu_4}\} = 4(\delta_{\mu_1\mu_2}\delta_{\mu_3\mu_4} - \delta_{\mu_1\mu_3}\delta_{\mu_2\mu_4} + \delta_{\mu_1\mu_4}\delta_{\mu_2\mu_3}), \tag{411}$$

$$\mathrm{Tr}\{\gamma_5\gamma_{\mu_1}\gamma_{\mu_2}\gamma_{\mu_3}\gamma_{\mu_4}\} = -4\epsilon_{\mu_1\mu_2\mu_3\mu_4}, \tag{412}$$

where $\epsilon_{4123} = +1$. Using (411) we find

$$\mathrm{Tr}\{\sigma_{\mu\nu}\sigma_{\alpha\beta}\} = 4(\delta_{\mu\alpha}\delta_{\nu\beta} - \delta_{\mu\beta}\delta_{\nu\alpha}). \tag{413}$$

C.2 Matrix Expansion

Any 4×4 matrix can be written as a linear combination of 1, γ_μ, $\sigma_{\mu\nu}$, γ_5, and $\gamma_5\gamma_\mu$. These 16 matrices are particularly convenient since the trace of the product of any two of them is only non-zero if they are equal, which makes it

easy to extract the coefficients when expanding a 4×4 matrix in terms of these 16 matrices. For any 4×4 matrix, X, we can write

$$X = x^0 + x_\mu \gamma_\mu + x_{\mu\nu}\sigma_{\mu\nu} + x^5\gamma_5 + x^5_\mu \gamma_5\gamma_\mu \tag{414}$$

where the coefficients are given by

$$\begin{aligned} x^0 &= \frac{1}{4}\mathrm{Tr}\{X\}, & (415)\\ x_\mu &= \frac{1}{4}\mathrm{Tr}\{X\gamma_\mu\}, & (416)\\ x_{\mu\nu} &= \frac{1}{8}\mathrm{Tr}\{X\sigma_{\mu\nu}\}, & (417)\\ x^5 &= \frac{1}{4}\mathrm{Tr}\{X\gamma_5\}, & (418)\\ x^5_\mu &= \frac{1}{4}\mathrm{Tr}\{X\gamma_\mu\gamma_5\}. & (419) \end{aligned}$$

Note that in (417) we have a 1/8 instead of 1/4 because in (414) we sum over both μ and ν which double counts since $\sigma_{\mu\nu}$ and $\sigma_{\nu\mu}$ are not independent.

Using (414) we can now write several common products of gamma matrices in terms of 1, γ_μ, $\sigma_{\mu\nu}$, γ_5, and $\gamma_5\gamma_\mu$ by simply evaluating the appropriate traces:

$$\gamma_\mu\gamma_\nu = \delta_{\mu\nu} - i\sigma_{\mu\nu}, \tag{420}$$

$$\gamma_\mu\gamma_\nu\gamma_\lambda = (\delta_{\mu\nu}\delta_{\lambda\alpha} - \delta_{\mu\lambda}\delta_{\nu\alpha} + \delta_{\mu\alpha}\delta_{\nu\lambda})\gamma_\alpha - \epsilon_{\mu\nu\lambda\alpha}\gamma_5\gamma_\alpha, \tag{421}$$

$$\gamma_5\gamma_\alpha\gamma_\beta = -\frac{1}{2}i\epsilon_{\alpha\beta\mu\nu}\sigma_{\mu\nu} + \delta_{\alpha\beta}\gamma_5. \tag{422}$$

We can derive an expression for four gamma matrices by multiplying (421) by γ_β and then making use of (420) and (422):

$$\gamma_\mu\gamma_\nu\gamma_\lambda\gamma_\beta = (\delta_{\mu\nu}\delta_{\lambda\alpha} - \delta_{\mu\lambda}\delta_{\nu\alpha} + \delta_{\mu\alpha}\delta_{\nu\lambda})(\delta_{\alpha\beta} - i\sigma_{\alpha\beta}) - \epsilon_{\mu\nu\lambda\beta}\gamma_5 + \frac{1}{2}i\epsilon_{\mu\nu\lambda\alpha}\epsilon_{\alpha\beta\kappa\gamma}\sigma_{\kappa\gamma}. \tag{423}$$

To compute $\gamma_\mu\sigma_{\nu\lambda}$ we write $\sigma_{\nu\lambda} = i\gamma_\nu\gamma_\lambda$, use (421), and then antisymmetrize with respect to $\nu\lambda$. Note that the antisymmetrization gets rid of a term symmetric in $\nu\lambda$. Although this term contains $\delta_{\nu\lambda}$, and thus is zero, it is important

to get rid of it at this stage since the relationship we are deriving may be used at an intermediate stage of a calculation where it is possible to have ν and λ be the same. We get

$$\gamma_\mu \sigma_{\nu\lambda} = i\left[(\delta_{\mu\nu}\delta_{\lambda\alpha} - \delta_{\mu\lambda}\delta_{\nu\alpha})\gamma_\alpha - \epsilon_{\mu\nu\lambda\alpha}\gamma_5\gamma_\alpha\right], \tag{424}$$

and

$$\sigma_{\nu\lambda}\gamma_\mu = i\left[(\delta_{\nu\alpha}\delta_{\lambda\mu} - \delta_{\nu\mu}\delta_{\lambda\alpha})\gamma_\alpha - \epsilon_{\nu\lambda\mu\alpha}\gamma_5\gamma_\alpha\right]. \tag{425}$$

We use a similar approach to compute $\gamma_5\gamma_\mu\sigma_{\lambda\beta}$. After writing $\sigma_{\lambda\beta}$ as $i\gamma_\lambda\gamma_\beta$, we can either use (422) with the identity

$$\epsilon_{\mu\lambda\kappa\gamma}\epsilon_{\kappa\gamma\beta\alpha} = 2(\delta_{\mu\beta}\delta_{\lambda\alpha} - \delta_{\mu\alpha}\delta_{\lambda\beta}), \tag{426}$$

or we can use (421). We get

$$\gamma_5\gamma_\mu\sigma_{\lambda\beta} = i(\delta_{\mu\lambda}\delta_{\alpha\beta} - \delta_{\mu\beta}\delta_{\lambda\alpha})\gamma_5\gamma_\alpha - i\epsilon_{\mu\lambda\beta\alpha}\gamma_\alpha, \tag{427}$$

$$\sigma_{\mu\nu}\gamma_5\gamma_\lambda = i(\delta_{\mu\alpha}\delta_{\nu\lambda} - \delta_{\mu\lambda}\delta_{\nu\alpha})\gamma_5\gamma_\alpha - i\epsilon_{\mu\nu\lambda\alpha}\gamma_\alpha. \tag{428}$$

We derive an expression for $\sigma_{\mu\nu}\sigma_{\lambda\beta}$ by using (423) and then antisymmetrizing with respect to $\mu\nu$ and $\lambda\beta$:

$$\begin{aligned}\sigma_{\mu\nu}\sigma_{\lambda\beta} &= \epsilon_{\mu\nu\lambda\beta}\gamma_5 + (\delta_{\mu\lambda}\delta_{\nu\beta} - \delta_{\mu\beta}\delta_{\nu\lambda}) \\ &\quad + \frac{1}{2}i(\delta_{\nu\lambda}\delta_{\mu\kappa}\delta_{\beta\alpha} - \delta_{\mu\lambda}\delta_{\nu\kappa}\delta_{\beta\alpha} + \delta_{\mu\beta}\delta_{\nu\kappa}\delta_{\lambda\alpha} - \delta_{\nu\beta}\delta_{\mu\kappa}\delta_{\lambda\alpha})\sigma_{\kappa\alpha} \\ &\quad + \frac{1}{4}i(\epsilon_{\mu\nu\beta\xi}\epsilon_{\xi\lambda\kappa\alpha} - \epsilon_{\mu\nu\lambda\xi}\epsilon_{\xi\beta\kappa\alpha})\sigma_{\kappa\alpha}.\end{aligned} \tag{429}$$

Table 11: Multiplication Rules for the 16 Independent Euclidean 4×4 Matrices

	γ_λ	$\sigma_{\lambda\beta}$	γ_5	$\gamma_5\gamma_\lambda$
γ_μ	$\delta_{\mu\lambda} - i\delta_{\mu\kappa}\delta_{\lambda\alpha}\sigma_{\kappa\alpha}$	$i(\delta_{\mu\lambda}\delta_{\beta\alpha} - \delta_{\mu\beta}\delta_{\lambda\alpha})\gamma_\alpha - i\epsilon_{\mu\lambda\beta\alpha}\gamma_5\gamma_\alpha$	$-\delta_{\mu\alpha}\gamma_5\gamma_\alpha$	$\frac{1}{2}i\epsilon_{\mu\lambda\kappa\alpha}\sigma_{\kappa\alpha} - \delta_{\mu\lambda}\gamma_5$
$\sigma_{\mu\nu}$	$i(\delta_{\mu\alpha}\delta_{\nu\lambda} - \delta_{\mu\lambda}\delta_{\nu\alpha})\gamma_\alpha - i\epsilon_{\mu\nu\lambda\alpha}\gamma_5\gamma_\alpha$	See (429)	$\frac{1}{2}\epsilon_{\mu\nu\kappa\alpha}\sigma_{\kappa\alpha}$	$i(\delta_{\mu\alpha}\delta_{\nu\lambda} - \delta_{\mu\lambda}\delta_{\nu\alpha})\gamma_5\gamma_\alpha - i\epsilon_{\mu\nu\lambda\alpha}\gamma_\alpha$
γ_5	$\delta_{\lambda\alpha}\gamma_5\gamma_\alpha$	$\frac{1}{2}\epsilon_{\lambda\beta\kappa\alpha}\sigma_{\kappa\alpha}$	1	$\delta_{\lambda\alpha}\gamma_\alpha$
$\gamma_5\gamma_\mu$	$-\frac{1}{2}i\epsilon_{\mu\lambda\kappa\alpha}\sigma_{\kappa\alpha} + \delta_{\mu\lambda}\gamma_5$	$i(\delta_{\mu\lambda}\delta_{\beta\alpha} - \delta_{\mu\beta}\delta_{\lambda\alpha})\gamma_5\gamma_\alpha - i\epsilon_{\mu\lambda\beta\alpha}\gamma_\alpha$	$-\delta_{\mu\alpha}\gamma_\alpha$	$-\delta_{\mu\lambda} + i\delta_{\mu\kappa}\delta_{\lambda\alpha}\sigma_{\kappa\alpha}$

D Lattice Feynman Rules

In this appendix we summarize the lattice Feynman rules for Wilson fermions derived in section 6.2. There are vertices which have not been included here because they were not needed for the fermion self energy calculation. Expressions for some of the other vertices are given in [41].

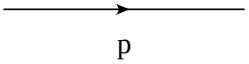

$$= \frac{\left[m_0 + 2r\sum_\mu \sin^2(k_\mu/2)\right] - i\sum_\mu \gamma_\mu \sin k_\mu}{\left[m_0 + 2r\sum_\nu \sin^2(k_\nu/2)\right]^2 + \sum_\nu \sin^2 k_\nu} \tag{430}$$

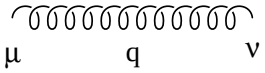

$$= \frac{1}{\hat{q}^2}\left\{\delta_{\mu\nu} + (\xi - 1)\frac{\hat{q}_\mu \hat{q}_\nu}{\hat{q}^2}\right\} \tag{431}$$

Where $\hat{q}_\mu \equiv 2\sin(q_\mu/2)$.

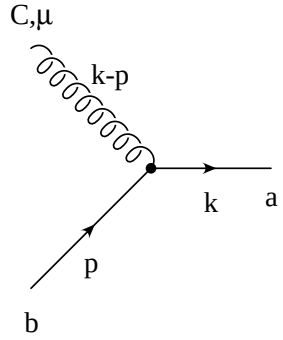

$$= -ig_0 T^C_{ab}\left\{\gamma_\mu \cos\left(\frac{p_\mu + k_\mu}{2}\right) - ir\sin\left(\frac{p_\mu + k_\mu}{2}\right)\right\} \tag{432}$$

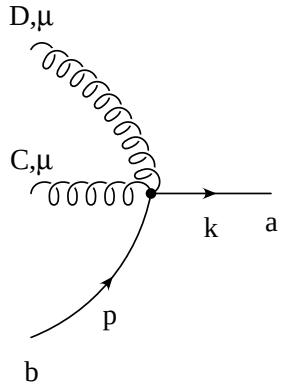

$$= \frac{g_0^2}{2}\{T^C, T^D\}_{ab}\left\{i\gamma_\mu \sin\left(\frac{p_\mu + k_\mu}{2}\right) - r\cos\left(\frac{p_\mu + k_\mu}{2}\right)\right\} \tag{433}$$

For finite volume, loops give a sum over loop momenta: $\frac{1}{V}\sum_k$. For infinite volume, loops give an integral: $(2\pi)^{-4}\int_{-\pi/2}^{\pi/2} d^4k$. Symmetry factors are calcu-

lated in the same way as in the continuum theory. Fermions bring in factors of -1 in the same way as in the continuum.

References

[1] N. Isgur and M. Wise, Phys. Lett. B **232**, 113 (1989); **237**, 527 (1990).

[2] M. Neubert, Physics Reports, **245**, 259 (1994).

[3] M. Wise, Lectures presented at the Lake Louise Winter Institute, February 1991, CALT-68-1721.

[4] T.M. Yan, Lectures given for P661 at Cornell, Fall 1992.

[5] T. Mannel, W. Roberts, and Z. Ryzak, Nucl. Phys. **B368**, 204 (1992).

[6] J. Soto and R. Tzani, Barcelona preprint UB-ECM-PF-92/15 (1992).

[7] A. Falk, Nucl. Phys. **B378**, 79 (1992).

[8] T.M. Yan, H.Y. Cheng, C.Y. Cheung, G.L. Lin , Y.C. Lin and H.L. Yu, Phys. Rev. D **46**, 1148 (1992); see also T.M. Yan, Chin. J. Phys. (Taipei) **30**, 509 (1992).

[9] Argus Collaboration, Zeitschrift fur Physic **C57**, 533 (1993).

[10] M. Luke, Phys. Lett. B **252**, 447 (1990).

[11] M. Neubert, *Proceedings of the XXX*$^{\rm th}$ *Rencontres de Moriond "Electroweak Interactions and Unified Theories"*, Les Arcs, France, 1995, hep-ph/9505238.

[12] R. Haag, Phys. Rev. **112**, 669 (1958).

[13] S. Coleman, J. Wess, and B. Zumino, Phys. Rev. **177**, 2239 (1969).

[14] C. G. Callen, S. Coleman, J. Wess, and B. Zumino, Phys. Rev. **177**, 2247 (1969).

[15] J. F. Donoghue, E. Golowich, B. R. Holstein, *Dynamics of the Standard Model*, Cambridge University Press (1992).

[16] H. Leutwyler, Lectures given at the Workshop "Hadrons 1994", Gramado, RS, Brazil, BUTP-94/13, hep-ph/9406283.

[17] A. Manohar, UCSD/PTH 93-12, hep-ph/9305298.

[18] H. Georgi, *Weak Interactions and Modern Particle Theory*, Addison-Wesley (1984).

[19] H.Y. Cheng, C.Y. Cheung, W. Dimm, G.L. Lin, Y.C. Lin, T.M. Yan, and H.L. Yu, Phys. Rev. D **48**, 3204 (1993).

[20] Particle Data Group, Phys. Rev. D **45**, S1 (1992).

[21] The ARGUS Collaboration, H. Albrecht *et al.*, Z. Phys. **C57**, 533 (1993).

[22] The CLEO Collaboration, R. Fulton *et al.*, Phys. Rev. **43**, 651 (1992); The CLEO Collaboration, S. Hernandez *et al.*, ibid **D45**, 2212 (1992).

[23] H.Y. Cheng, C.Y. Cheung, G.L. Lin, Y.C. Lin, T.M. Yan, and H.L. Yu, Phys. Rev. D **47**, 1030 (1993).

[24] The CLEO Collaboration, F. Butler *et al.*, Phys. Rev. Lett. **69**, 2041 (1992).

[25] Clarence L.Y. Lee, Ming Lu, and Mark B. Wise, Phys. Rev. D **46**, 5040 (1992).

[26] Clarence L.Y. Lee, Phys. Rev. D **48**, 2121 (1993).

[27] G. Kramer and W.F. Palmer, DESY 92-130 (1992); G. Köpp, G. Kramer, W. Palmer, and G. Schuler, Z. Phys. **C48**, 327 (1990).

[28] A. Pais and S.B. Treiman, Phys. Rev. **168**, 1858 (1968); see also, N. Cabibbo and A. Maksymowicz, Phys. Rev. **137**, B438 (1965).

[29] G.L.Kane, K. Stowe, and W.B. Rolnick, Nucl. Phys. **B152**, 390 (1979).

[30] P. Nyborg and O. Skjeggestad, in *Kinematics and Multiparticle Systems*, Proceedings of the International School of Elementary Particle Physics, Herceg-Novi, Yugoslavia, 1965, edited by M. Nikolić. Pages 55-57 are especially useful for computing single particle energy spectra.

[31] N. Cabibbo, Phys. Rev. Lett. **10**, 531 (1963); M. Kobayashi and K. Maskawa, Prog. Theor. Phys. **49**, 652 (1993).

[32] The value of the B^* mass used here is from the 1990 edition of PDG [Phys. Lett. B **239**, S1 (1990)]. We have checked our results using its new value in 1992 PDG, $m_{B^*} = 5324.6$ MeV. The differences for $\bar{B} \to D\pi\ell\bar{\nu}$ are negligible and those for $\bar{B} \to D^*\pi\ell\bar{\nu}$ are less than 1%.

[33] G. Burdman, Phys. Lett. **B284**, 133 (1992).

[34] For a review of the experimental status of V_{cb}, see Persis S. Drell and J. Richie Patterson, CLNS 92/1177, to appear in *Proceedings of the XXVI International Conference on High Energy Physics*, Dallas, August 1992.

[35] We have benefited from conversations with Prof. P. Drell on the general question of how to define resonant and nonresonant contributions.

[36] P. Bialas, K. Zalewski, and J.G. Körner, TPJU-19/92, MZ-TH/92-53 (1992); Ming Lu, M.B. Wise, and N. Isgur, Phys. Rev. D **45**, 1553 (1992).

[37] T. Suzuki, T. Ito, S. Sawada, Nagoya preprint DPNU-93-35, AUE-04-93 (1993).

[38] K.G. Wilson, Phys. Rev. D **10**, 2445 (1974).

[39] L. Ryder, *Quantum Field Theory*, Cambridge University Press (1985).

[40] K. Huang, *Quarks, Leptons, & Gauge Fields*, 2nd ed., World Scientific, Singapore (1992).

[41] H. J. Rothe, *Lattice Gauge Theories: An Introduction*, World Scientific, Singapore (1992).

[42] J. Kogut and L. Susskind, Phys. Rev. D **11**, 395 (1975).

[43] T. Muta, *Foundations of Quantum Chromodynamics*, World Scientific, Singapore (1987).

[44] G. P. Lepage and P. B. Mackenzie, Phys. Rev. D **48**, 2250 (1993).

[45] J.C. Vink and U-J Wiese, Phys. Lett. B **289**, 122 (1992).

[46] C. T. H. Davies, G. G. Batrouni, G. R. Katz, A. S. Kronfeld, G. P. Lepage, K. G. Wilson, P. Rossi, and B. Svetitsky, Phys. Rev. D **37**, 1581 (1988).

[47] M. Alford, W. Dimm, G. P. Lepage, G. Hockney, P. B. Mackenzie, *Lattice '94 Conference Proceedings*, Bielefeld, Germany, 1994.

[48] G. P. Lepage, *Proceedings of the 1993 TASI School*, edited by S. Raby et al.

[49] F. Mandl and G. Shaw, *Quantum Field Theory*, Wiley, New York (1984).

[50] C. Itzykson and J.B. Zuber, *Quantum Field Theory*, McGraw Hill, New York (1980).

[51] G. Peter Lepage, Nuc. Phys. B **26**, 45 (1992).

[52] M. Creutz, *Quarks, Gluons, and Lattices*, Cambridge University Press, New York (1983).

[53] G. Bodwin and E. Kovacs, Phys. Rev. D **35**, 3198 (1987).

[54] J. D. Bjorken and S. D. Drell, *Relativistic Quantum Mechanics*, McGraw-Hill, New York (1964).

[55] G. Grammer, Jr. and D. R. Yennie, Phys. Rev. D **8**, 4332 (1973).

[56] M. Abramowitz and I. Stegun, *Handbook of Mathematical Functions*, Dover, New York (1972).

[57] C. J. Morningstar, Phys. Rev. D **48**, 2265 (1993).

[58] C. J. Morningstar, Phys. Rev. D **50**, 5902 (1994).

[59] G. P. Lepage, L. Magnea, C. Nakhleh, U. Magnea, K. Hornbostel, Cornell preprint, CLNS 92/1136, OHSTPY-HEP-T-92-001 (1992).

[60] Private communication from C. Morningstar to G. P. Lepage.

[61] W. Press, S. Teukolsky, W. Vettering, B. Flannery, *Numerical Recipes in C*, Cambridge University Press (1992).